A study on the propagation of harmonics in a Power System

MSc Thesis submitted to the Technical University of Delft in partial fulfilment of the requirements for the degree of **MASTER OF SCIENCE** in Electrical Power Engineering

by

SANUJ VIJAY WARGIYA

4795881

Graduation Committee Members
Department of Electrical Engineering, Mathematics and Computer Science

Responsible full professor	: Prof. ir. P.T.M. Vaessen, DCE&S
Daily supervisors	: Dr. ir. B Gholizad, DCE&S
	Dr. ir. M.G. Niasar, DCE&S
External Committee member	: Dr. S.H. Tindemans, IEPG
Submission	: September 19, 2020

Preface

This master thesis dissertation is written as a final project for the study program: MSc in Electrical Power Engineering at the Technical University of Delft. The work is based on the successful model designing, simulation results and the literature survey analysis. The project was carried out between the months of January-August in the year 2020.

Parts of the section: Introduction 1 and Theory 2 have been used from the applicable sources with due recognition in terms of a reference. The case studies in the section 2.5 have been used as a part of the literature survey and had been summarised according to the needs of this thesis.

The section regarding the Wind turbine modeling 3 consists of designing a control strategy governing the Wind turbine model. A standard strategy for current control has been used and referenced in detail. The design of the LCL filter has been taken from standard wind turbine - grid connection topology.

The modified IEEE-13 node feeder in section 4 was modelled in line with the standard IEEE-13 node feeder.

The reader of this dissertation is assumed to have sufficient knowledge of power system designing, wind turbine modeling and harmonic distortion analysis. Knowledge of MAT-LAB/Simulink is a plus but not essential to understand the simulation blocks mentioned in the appendix and the MATLAB code.

Acknowledgement

This master thesis has been performed at the research group of DC Energy Storage and Conversion of the department of Electrical Engineering, Mathematics and Computer Science at the Technical University of Delft.

Firstly, I would like to express my deep sense of gratitude to my guide Professor Ir Peter Vaessen, for his indispensable inspiration and encouragement for this project. I feel fortunate to have had the privilege to work under his guidance.

I am indebted to my daily supervisors Dr Ir Babak Gholizad and Dr Ir Mohamad Ghaffarian Niasar for their continuous support, guidance and regular feedback throughout the thesis. I am extremely grateful for their time and belief in me.

I would like to thank Dr Simon Tindemans for accepting to be a part of my thesis Assessment Committee.

I would also like to thank my fellow colleagues from the DCE&S group. I had a wonderful time inside and outside the university. I am glad I had the opportunity to be a member of one of the most competitive and remarkable research groups in Netherlands.

Furthermore, I would like to thank my friends for their cherished company (in-person and online) and spirited motivation. Friendly talks, especially during the latter half of the thesis, helped a lot in maintaining the work-like motivation.

Due to the COVID-19 pandemic, everyone was forced to work from home this year. More than half of my thesis work was performed at home. During these unforeseen circumstances, I would like to thank my daily supervisors for scheduling regular skype meetings to ensure the smooth progress of the thesis. I would also like to thank my housemates and my family for their cooperation and support during this difficult time.

Finally, special gratitude to my grandfather Prof. Ir. Umashanker Vijaywargiya. He has been a role model for me, always guiding me throughout my life. I would also like to profoundly thank my mother Dr. Manisha Vijaywargiya for all the sacrifices she has made for me and for always supporting me in the pursuit of my dreams.

Sanuj Vijay Wargiya

Abstract

There has been a rapid development in the growth of Wind power generation in the last decade. This has led to the wind power becoming a major contributor to the modern electrical grids. For the grids that are still based on conventional sources of energy, integrating wind power causes serious impact on their performance. While the Wind farm must ensure the quality of power it supplies to the grid, the wind farm should itself remain resistant from the small disturbances coming from the grid. The power electronic converters used in the integration process are often responsible for the disturbance. These disturbances include, among other issues, the generation of certain harmonics based on the high frequency converter switching. This affects the power quality and performance of the entire system. Certain harmonics are often amplified by resonating impedance. This phenomenon of harmonic resonance has been identified as a major cause of several grid failures.

In this master thesis, a study is carried out to investigate the generation and propagation of harmonics in a wind farm network. A modified IEEE-13 node feeder has been considered as a network accommodating a wind farm. The suggestive wind farm consists of 10 wind turbines, with each turbine connected at a different node of the modified IEEE-13 node feeder. These wind turbines are connected with the grid using an IGBT converter and an LCL filter. The switching topology and the filter tuning has been discussed in detail. All the components comprising a wind turbine including cables, Voltage Source Converters (VSCs), transformers, filters and control system have been included.

The modeling is carried out in MATLAB/Simulink with the necessary data taken from the literature survey. A control system governing the switching of the IGBT converter has been developed. It consists of a power control and a current control scheme. A dq transformation scheme has been selected for the current control of the wind farm. A Phase Locked Loop (PLL) is used to synchronize the converter with the grid and a Pulse Width Modulator (PWM) is used to generate gate pulses, controlling the switching of the IGBT switches.

The simulations have been carried out for 5 cases: the base case, de-tuned control system, disconnection of a part of the grid, wind speed dynamics and finally, a combination of all the above contingency cases termed as "the worst case scenario". Each case is designed to represent the impacts inside a real offshore wind farm. A quantitative and qualitative analysis has been carried out for the harmonic distortions at different buses of the wind farm network under each case.

Results from the simulations show the harmonic orders that are common across the frequency spectrum in different cases. The base case provided relatively low voltage harmonics, but with more disturbances in the network, higher harmonic content was observed. The harmonic order corresponding (or nearest) to the switching frequency of the IGBT converter and the resonant frequency of the network, contributed the most for the Total Harmonic Distortion (THD).

Contents

List of Figures

List of Tables

1   Introduction

The past few decades has seen the environmental crisis becoming a significant factor for the way in which the modern day manufacturing industries operate. The world is striving towards a carbon-neutral sustainable society. Hence, the renewable energy resources like wind, solar, hydro, geothermal, bio-gas etc. are being utilised at higher rates than ever. With the fast pace of depletion of fossil fuels, and the rising global temperatures, the need to efficiently and economically utilise the renewable resources become even more dire. The following pie chart shows the world energy generation with source type:
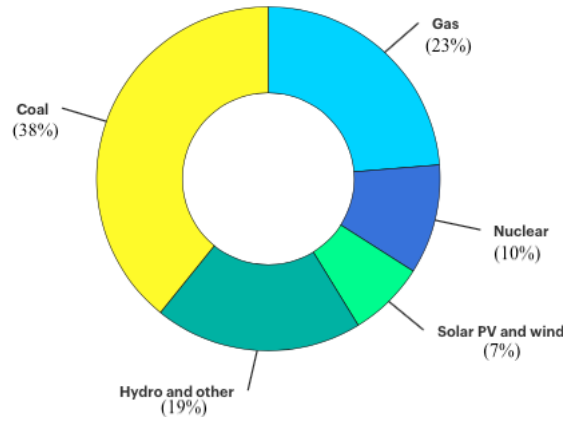
Figure 1: Worldwide energy generation 2019
[1]

As seen from figure(1), the clean energy sources make up almost 26% of the modern day electricity generation. Although this has increased from 19% in 2013 [3], the dependence on the conventional sources remain fairly high. Nevertheless, the focus of the industries is changing rapidly towards the non-conventional sources. This change is directly affecting the already established power system network [3], as new sources would have different requirements, additional demands and criteria before being successfully integrated into the existing network.

The requirements of a modern day power system are ever changing. Depending upon the demand, the system's configuration also keeps on varying. Power electronic controllers such as Static Compensators (STATCOMs), Unified Power Flow Controllers (UPFCs), Convertible Static Controllers (CSCs), and others are continuously being applied in power systems to provide flexible operation of the system and to increase the effective utilization of existing transmission grid [4]. It has been well established that the integration of these converters lead to the injection of harmonics in the grid. The presence of any non-linear element in the power system results in harmonics. Non-linear elements include transformers, power-electronic components, non-linear load, and converters. Harmonics cause a periodic voltage distortion, which if exceed a certain level, has harmful effects on individual equipment as well as the network components, in the form of amplification of harmonic levels, reduction in efficiency of network components. This can be in the form of ageing of the insulation of electrical plant equipment, malfunctioning of system devices etc. [5].

In this thesis, the propagation of such harmonics are explored within a grid connected wind farm.

1.1 Wind Power

Wind power penetration in the electric power system has increased rapidly over the past 20 years, with the total capacity of installed wind farm worldwide rising to 591 GW in 2018 [1]. According to The European Wind Energy Association (EWEA), the installed wind power capacity in Europe is expected to increase to 217 GW by the end of 2020 [6]. The following graph shows the worldwide variation in the wind power generation in past two decades.
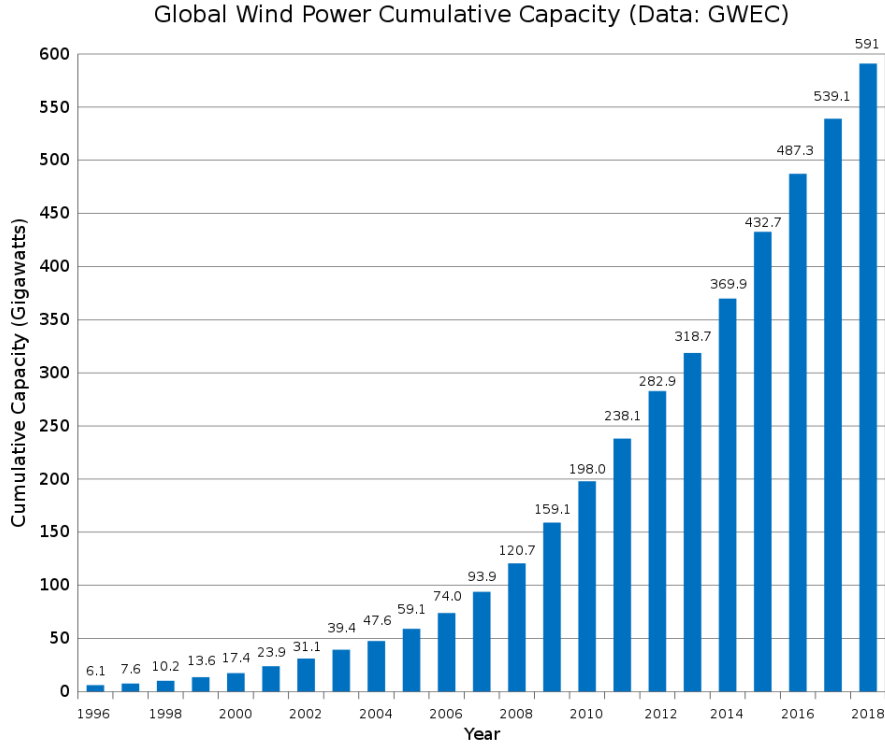
Figure 2: Wind power Capacity worldwide [1]

It can be seen from the figure (2), the wind power capacity increased by a factor of almost 100 in two decades. This growing trend in wind power had accounted for a share of almost 5 % of the total electrical energy production [1].

Therefore, as the dependence on wind power increases, it becomes crucial to understand the critical challenges posed by their implementation on the existing power system network. In this thesis, we deal with the harmonic propagation related issues generated by a wind farm connected to a grid. It has to be noted that, if the switching frequency of the wind turbine converter is close to the harmonic frequency and the resonance frequency of the system, the phenomenon known as harmonic resonance might occur and produce more disturbance in the system. The harmonic propagation is analysed on a system level (wind farm) and the results are compared with a previous component level (cable accessories and joints) study. This study would help us to understand which harmonic contents are more likely to create significant disturbance.

1.2 Primary challenge

Harmonic resonance is a major concern for the power systems with an increased use of harmonic-producing loads such as motors, generators, drives, power electronic converters, electric arc furnaces etc. [7]. It is caused by the energy exchange between the capacitive elements and inductive elements in a system. Since a power system could consist of numerous inductive and capacitive elements, the phenomenon of harmonic resonance can become quite complex. The problems associated with harmonic resonance include - harmonic related heating, equipment failure, blown up fuses etc. [7] .

Generally, the inductive reactance of a power system at power frequency is quite less compared to the capacitive reactance, so the harmonic resonance does not take place [8] [9]. However, when a system contains a harmonic component, the impedance will change and the LC resonance will occur [10]. For a power system, the resonance frequency can be calculated as :

$$f = \frac{1}{2\pi} \cdot \sqrt{\frac{1}{LC}}, \tag{1}$$

where, L is the inductance and C is the capacitance of the system.
This could lead to the distortion of voltage and current waveform, even damaging the power system and its components, thereby disturbing the normal system operation [10].

On a component level, the vast cables network associated with the offshore wind farm face tremendous harmonics related issues. Possible harmonics occurring at the various points of a cable (especially joints and termination) are a matter of concern. It includes the possibility of the magnification of harmonics in voltage waveforms from the grid due to the large capacitance of long AC cables [11]. These high frequency harmonics can distort the electric field distribution around the cable and lead to cable failures and defects .

1.3 Research Questions

The following research questions are addressed in this thesis:

1. How do the VSC-generated harmonics propagate within a modelled power system network?

2. Which harmonic orders are capable of causing significant damage to the power system under various operating conditions?

3. What are the effects of harmonic resonance on the order and magnitude of harmonics inside the power system network?

1.4 Thesis Layout

This thesis has the following layout:

- **Chapter** 1 introduces the present-day needs and dependence of the world energy sector on wind generation. It also outlines the main challenges faced during the effective integration of wind power generation into the grid.

- **Chapter** 2 analyses the theoretical aspects, including a brief description of harmonics, resonance and harmonics resonance. This section also discusses some case studies, highlighting the hazards of harmonic resonance in real grids.

- **Chapters** 3 and 4 discusses the wind farm modeling. It consists of a brief description of all the important wind turbine components. It discusses the control strategy used in

designing the control system. It also presents a brief description of the IEEE-13 bus node feeder, and discusses the load flow results of the modified feeder network. In addition, this section also contains the frequency scans of the system and converter side of the turbine to identify the resonating frequencies.

- **Chapters** 5 and 6 details the results obtained from different scenarios, and the inference from them. It also discusses the impact of these harmonics on a cable accessory.

- **Chapters** 7 and 8 summarizes the most important findings of this master thesis dissertation and briefly discusses the future work that can be done to further expand the results of this thesis.

- Appendices A and B show the parameter data - load flow, turbine data, transformer data, and all the models developed and utilized during the simulation of the wind farm to study harmonics and its propagation under several scenarios.

2 Theory

In this section, the relevant background regarding harmonic resonance phenomenon is discussed. The concept of harmonic distortion is explained, along with the magnification of harmonics due to various sources. The resonance phenomenon is also discussed along with its effects on harmonic propagation. Finally, examples are given of the effects of harmonic resonance in real life.

2.1 Resonance

Resonance analysis is an important aspect in the design and operation of grid-connected wind farms [5]. There are two types of resonances, namely - series resonance and parallel resonance. The next section discusses them in brief:

The following figure gives the parallel and series circuits juxtaposed to each other:
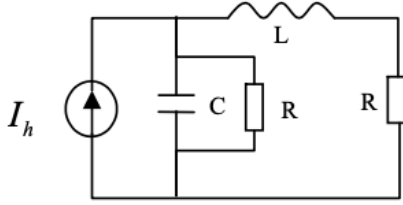
Figure 3: Parallel resonance circuit
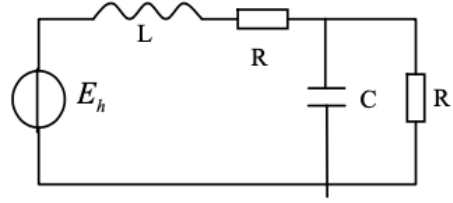
Figure 4: Series resonance circuit

The parallel resonance circuit shown in figure (3) is associated with high impedance at resonant frequency, resulting in voltage distortion and high harmonic currents [2]. The resonant frequency associated with extremely high (infinite) impedance is given by equation(1). Since the current source is the origin for harmonics in the circuit, high harmonic voltage occurs and the harmonic current will be amplified tending to infinity. Although a real (non-zero) resistance would mean the impedance would not reach infinity. This resistance helps in determining the impedance and amplification near the resonant frequency [5].

The series resonance, on the other hand, is associated with low impedance at resonant frequency leading to high current and a high voltage distortion even at locations where there is no or little harmonic emission. The resonance frequency is the same as given by equation(1).

A simple way to determine if a capacitor resonates with its supply system is by computing the ratio $h_{res} = \sqrt{\frac{S_{s.c.}}{S_{cap}}}$, where $S_{s.c.}$ is the short circuit power in MVA and S_{cap} is the capacitor power in MVA. This method is useful only for finding harmonic resonant frequencies but it cannot determine the harmonic order or the harmonic impedance.

For determining the harmonic orders, a simple RLC system is assumed in resonance. The system capacitor and inductor forms a tank circuit, resulting in amplified currents of resonant frequency in the tank circuit. The amplification factor is given by the system X/R ratio times the harmonic order [12]. Thus for a given spectrum of currents, harmonic order can be determined.

2.2 Harmonic Distortion

The presence of nonlinear loads are the main cause of Harmonic distortions in the network. Nonlinear loads, a vast majority of which are loads with power electronic devices, draw current

in a non-sinusoidal manner [13]. As these devices are being used with increased frequency by the consumers, the presence of distortions in current and voltage waveforms has become a common notion today.

Harmonic analysis is conventionally based on the Fourier transform, which is a way of expressing a signal as a weighted sum of sine and cosine waves. It can be shown that any arbitrary discretely sampled signal can be described completely by the sum of a finite number of sine and cosine components whose frequencies are 0, 1 ,2 ,3 ... n/2 times the frequency f=1/n△x, where △x is the interval between adjacent x-axis values and n is the total number of points. The Fourier transform is simply the set of amplitudes of those sine and cosine components [14].

Mathematically, a Fourier series of a periodic function x(t) is expressed as:

$$x(t) = a_0 + \sum_{n=1}^{\infty} (a_n cos(\frac{2\pi nt}{T}) + b_n sin(\frac{2\pi nt}{T})) \tag{2}$$

Where, a_0 = average value of the function x(t), a_n and b_n are coeffecients of the series besides being the rectangular components of nth order harmonics.

The following figure (5) represents a distorted sinusoidal wave with fundamental, 5th and 7th order harmonic components:
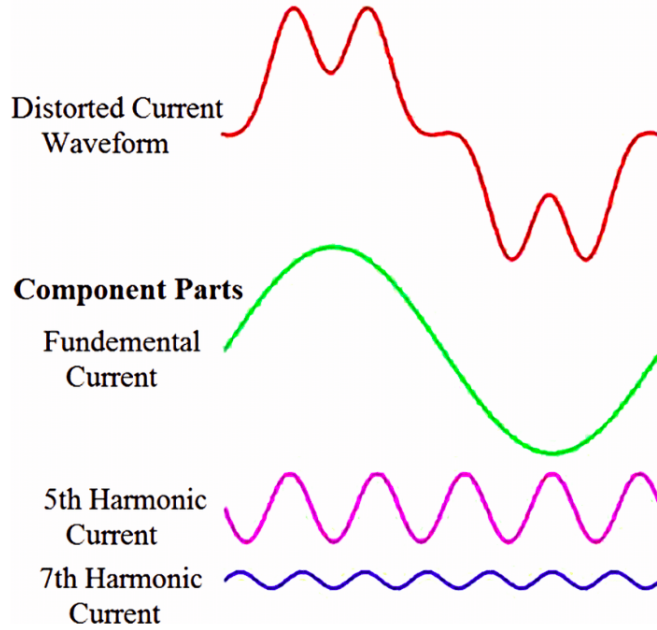
Figure 5: Harmonic plot with superposition of fundamental, 5th and 7th order harmonics

The above figure (5) shows an example of a signal with fundamental, fifth and seventh harmonic order.

The Total Harmonic Distortion (THD) is a measurement that represents the total amount of harmonic content in a signal [13]. It is measured as a percentage of the fundamental component of the signal as shown below:

$$THD = 100 \cdot \sqrt{\sum_{n=2}^{\infty} H_n^2} \tag{3}$$

where, $H_n = \frac{b_n}{b_1}$

We note that there is no role of a_n in the calculation of THD as the cosine and sine functions are periodic in nature. The Fourier transformation as shown in equation (2) leads to eventual cancelling of all the cosine coefficients (a_n) and thus only the sine coefficients (b_n) participate in the THD equation.

To find the order of harmonic which might be responsible for the most disturbances, one can employ the following technique mentioned below:

The following figure (6) shows a prototype model of a grid connected windfarm:
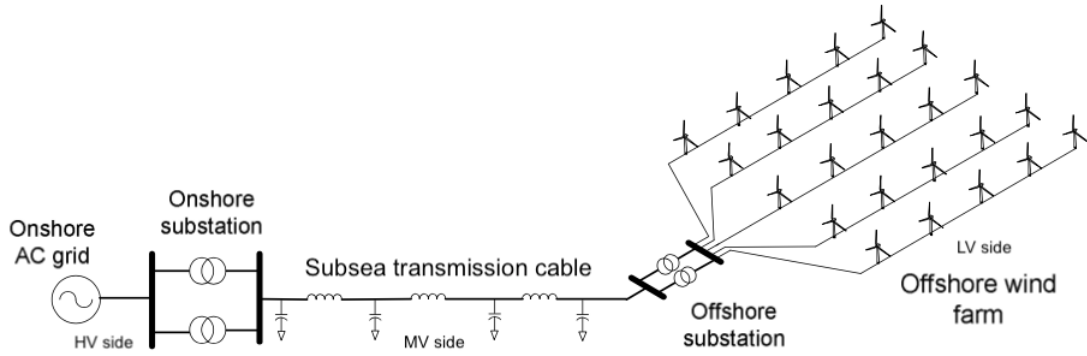
Figure 6: Grid connected windfarm [2]

A method for calculating the harmonic order of series and parallel resonance is by shifting all the impedance from HV (High Voltage) and LV (Low Voltage) side of the grid to the MV side. This simplifies the model for a more efficient MATLAB/Simulink programming as well. The series resonance occurred due to harmonic voltage source of the main grid causing voltage distortions at the MV (Medium Voltage) side. The parallel resonance, on the other hand, occurrs due to each wind turbine current source.

Note: In figure (6), the LV side is referred to as the converter side of an individual wind turbine.

To determine the harmonic order (h) during series resonances, an analysis of sensitivities of the voltage ratio: $\frac{U_{MV}}{U_{HV}}(h)$ and $\frac{U_{LV}}{U_{HV}}(h)$ is required. It can be simplified mathematically as [2] [15]:

$$\frac{U_{LV}}{U_{HV}}(h) = \frac{U_{LV}}{U_{AB}}(h) \cdot \frac{U_{AB}}{U_{MV}}(h) \cdot \frac{U_{MV}}{U_{HV}}(h) \tag{4}$$

where, U_{LV}, U_{MV}, U_{HV} are the voltage level at the low voltage side, medium voltage side and high voltage side respectively and U_{AB} is the voltage level at the offshore substation in figure (6).

For parallel resonance the harmonic order (h) could be realised by analyzing the sensitivities of the current ratio: $\frac{I_{cap}}{I_{MV}}(h)$ and $\frac{I_{fil}}{I_{LV}}(h)$. The current distortion caused by parallel resonance is proposed as:

$$\frac{I_{fil}}{I_{LV}}(h) = \frac{Z_{LV}(h)}{Z_{fil}^*(h)/n} \tag{5}$$

17

where, I_{fil} and I_{LV} are the currents at the converter side filter and low voltage side respectively, and, Z_{LV} and Z_{fil} are the impedance at the low voltage side and at the converter side filter respectively in the figure (6)

The number of wind turbines inside the offshore wind farm shown in figure(6), have a very slight impact on the order of harmonics, but it significantly increases the magnitude of harmonics and resonances [2].

2.3 Harmonic Resonance

The harmonics propagating throughout a power system network have a huge dependence on harmonic resonance [16]. Resonance, in a system, arise due to the interaction between the capacitive and inductive elements of a system and is excited by the current injection in other non-linear components [17]. In other words, harmonic resonance occurs when the natural frequency of the system corresponds to the frequency of the harmonic current source [7]. However, not all the resonances result in harmonic resonance. Harmonic resonance occurs only at certain harmonic levels [8]. A resonance condition is referred as a harmonic resonance when it occurs at a nonlinear load-generated harmonics [16].

Therefore, the following conditions are to be met for stimulating a harmonic resonance [18] [17]:

1. The system inductive and capacitive reactances match with each other at some frequencies.

2. A harmonic source within the system matches with one or more of the system resonant frequencies.

The condition generally takes place when a capacitive element is connected in parallel to a combination of inductive and resisitive elements. This is carried out for power factor improvement, voltage support, and reactive power compensation [16] [17].

The system natural frequency is a function of the reactance of the system and the amount of power factor correction factors connected to the system [7]. Therefore, adding shunt capacitor can give rise to harmonic resonance. This would naturally increase the impedance of the system. Load-generated harmonics are amplified manifolds due to this phenomenon. The amplification of harmonics result in serious effects on the equipment power loss via heating, harmonic torque generation, improper operation of protective devices, de-rating of electrical equipment, damage to the shunt capacitors due to overloading, and can lead to shutdowns [16].

When the harmonic resonance occurs, the total effective impedance can be very high (parallel resonance). The parallel resonance occurs when the reactance X_c cancels the Thevenin equivalent impedance Z_{th}. The frequency at the instance is given by [2]:

$$f_{res} = \frac{1}{2\pi}\sqrt{\frac{1}{L_{th} \cdot C} - \frac{R_{th}^2}{4L_{th}^2}} \approx \frac{1}{2\pi}\sqrt{\frac{1}{L_{th} \cdot C}} \tag{6}$$

The voltage and current at different buses can be given by equations (4) and (5).

2.4 Filtering

The previous section showed how currents and voltages will experience a frequency dependant impedance. In this section, we look at the use of filters in a system with a Voltage Source

Converter (VSC) based DC-AC converter. The harmonic spectrum of the output voltage of the converter consists of two parts: fundamental frequency harmonics (low frequencies) and switching harmonics (high frequencies) [19]. Additional power losses and malfunctions in the grid components can be caused by the presence of harmonics and reactive power in the grid. A filter is needed for reducing and preferably removing high frequency content in the output voltage waveforms, allowing only low frequencies to pass through. Conventionally, passive filters consisting of tuned L–C components have been widely used to suppress harmonics because of their low initial cost and high efficiency [20]. The most widely used filter configurations are based on LC and LCL filter topologies.

For grid-connected operation, an LCL filter is highly recommended [4] [19] [21] [22]. It is preferred over LC filter, especially in grid-connected cases, because of the presence of a second inductance, which shields the filter response to the variations in grid parameters. Using lower value of grid side inductance would lead to reduced output current ripple. However, excessive lowering of inverter side inductance is not desirable since it would lead to higher current ripples through the power electronic devices.
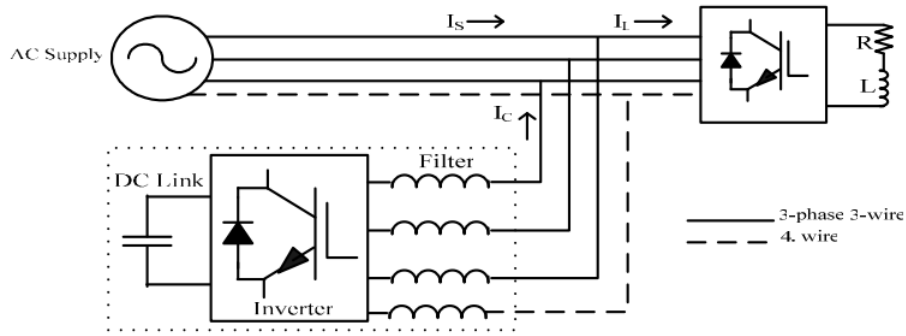
Figure 7: Filter topology

Figure 7 represents the physical location of LCL filter to shield the filter response against the grid variations. For the filter topology shown above, the Power converters require passive low-pass filters which are capable of effectively reducing the voltage ripples. In contrast to signal filters, the components of power filters must carry large currents or withstand large voltages. The following table (1) demonstrates various passive filters as per the suitability of power converters:
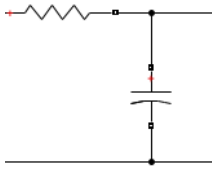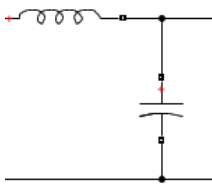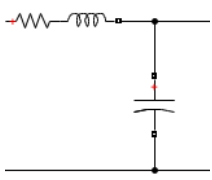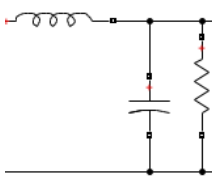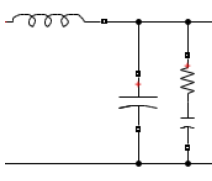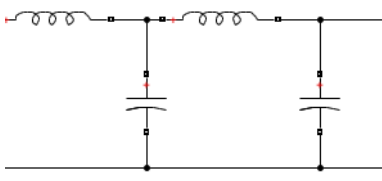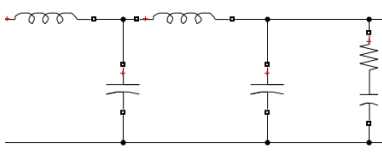
Filter topology	Comments
	For signal filters simple RC circuits are commonly used. They offer an attenuation of only 20 dB/decade. The full current flows through the resistor, which causes high losses.
	With an LC structure we get 40 dB/decade, but there is a large resonance.
	Series damping in order to overcome the resonance problem: the full current flows through the resistor. If the parasitic resistance of the inductor is large enough, this might be ok.
	Parallel damping in order to overcome the resonance problem: the full voltage is across the resistor, which causes high losses.
	Parallel RC damping in order to overcome the resonance problem: the resonance can be damped effectively and the losses are reasonable
	Two LC stages offer an attenuation of 80 dB/decade, but the resonance issue remains.
	Parallel RC damping in the second stage in order to overcome the resonance problem: losses are low.

Table 1: Suitable filter topologies

2.5 Case studies

To further formulate and understand the general problem statement of this master thesis, four case studies are mentioned from the literature survey. These cases are concisely discussed in this section. They show the origins of the problem and their consequences in real life scenarios.

2.5.1 Case I:

In [12], Lemieux documented a case of failure of a 13.8 kV switchgear and the consequential power grid failure in a pulp and paper mill in Kitimat, Canada. The failure was touted as the result of occasional occurrence of 5th harmonic voltage waveform which subsequently lead to harmonic resonance. For the power factor correction measures, capacitor banks were used which were responsible for the system's natural frequency of 300-400 Hz (5th or 7th harmonic). During resonant condition, harmonic current measurements were done at the main 13.8 kV circuit breaker, the capacitor banks, and the transformer. It was observed that the 5th order harmonic current was approximately 3% of the total system current. Presence of higher order harmonic currents were also detected. It took 4 minutes to achieve the harmonic resonance, as the power system tuned to 5th harmonic current, before the 13.8 kV circuit breaker failure. The total resonant harmonic current through the breaker was found to be 38 % of the system resonant current, which resulted in an overcurrent stress through the breaker. Thus, they concluded that the observed 5th harmonic current along with the 4 minute time correlation of the switching of the power system with respect to the failure, the harmonic resonance was the most likely cause of the failure of the 13.8 kV circuit breaker. To solve the recurrence of these harmonics, the inrush current at the breaker was to be limited by additional reactance between the capacitor banks and the bus. These reactors were tuned and sized to serve the purpose economically. They were able to de-tune the mill natural frequency below the 5th order harmonic and limit the currents through the breaker.

2.5.2 Case II:

In [7], Eghtedarpour et al. studied a real case of power system harmonic resonance that resulted in the failure of 20 kV capacitor bank fuses at a substation in Fars power grid, Iran. The possibility of harmonic resonance was considered due to the high load (steel factory) connected to the substation. They carried out harmonic measurement investigations and analysed the load current harmonics along with the system impedance frequency characteristic. They were able to determine the voltage harmonic distortion and corresponding capacitor current. Their results showed that the capacitor installation has caused a parallel resonance between the 5th and 6th harmonics and due to a relatively high 5th order harmonic current, the voltage distortion on the 5th harmonic has been occurred. With the small capacitor impedance, the voltage harmonics result in large capacitor current which cause thermal instability to the fuse. They calculated the current distortion limits which suggested that the operation of steel factory contained the large 5th harmonic distortions, over the range of limits resulting in the eventual fuse failure. They proposed a method to mitigate this problem by modifying the system impedance frequency characteristics. This was done by resizing the capacitor according to the current harmonic distortion limits. They used a factor called the Fuse Harmonic Loss Factor (FHLF) to determine different electrical and thermal parameters inside the fuse. The FHLF was computed as a function of frequency and was used to calculate the total power loss of the fuse for different load current harmonics. The results showed that even at the standard harmonic distortion limits, there will be a blown capacitor fuse. They concluded that during the installation of capacitors it

is required to consider the load harmonic distortion besides the system frequency characteristic.

In the above two cases it is documented that the harmonic resonance pose a serious threat when the grid is connected to heavy loads like mills and factories. The next two cases deal with the harmonic resonance effects on grid connected wind farms.

2.5.3 Case III:

In [23], Yin et al. have documented a case study of the effects of harmonic resonance on a wind farm connected to an ERCOT (Electric Reliability Council of Texas) grid. There was a failure of a 579.5 MW wind farm connected to the ERCOT grid following the switching of a 12 MVAR capacitor bank at one of its phases. The phase (4B) along with its 46 wind turbines tripped simultaneously. Initial investigations suggested the presence of high harmonic levels just before the tripping. The authors carried out root cause analysis involving wind farm modeling, comprehensive frequency scans and sensitivity studies. The model benchmarking along with harmonic load flow studies were performed, keeping the main focus on 8th and 9th order voltage harmonics. The study also aimed to identify the presence of any harmful higher order harmonic. The voltage harmonic studies aligned with the load flow results indicating the presence of harmonic resonance as the root cause of the failure. During the sensitivity studies, the worst case scenario for the prospective future failures were analysed. Several grid operating conditions and their combinations were modelled. These cases included a comparison of a strong grid against a weak grid. Generally, the parallel combination of inductive and capacitive reactance dominate the harmonic impedance, but for a weak grid the inductive reactance increases, thereby decreasing the harmonic impedance. They also found that increasing the number of wind turbines in the network would increase the harmonic impedance, leading to the worst case scenario, with all the turbines in function. Their mitigation strategies mainly focussed on capacitor detuning, however they acknowledged that other strategies like filter tuning and reactor detuning as other possible harmonic mitigation approaches.

2.5.4 Case IV:

In [24] and [25], Badrzadeh et al. proposed a methodology for conducting harmonic resonance analysis in a grid connected wind power plant. They have analyzed turbines with back-to-back power electronic converters which can inject harmonics using the PWM switching strategy. They characterized the VSC harmonics by the converter switching at the balanced steady state condition as characteristic harmonics. Further these characteristic harmonics contained no low order harmonics, but higher order harmonic components (10 kHz). Low order harmonics were produced due to the interaction of wind turbine generator with the source power system. A third type of harmonics discussed was zero sequence triplen harmonics which could appear due to asymmetry in the grid voltage. They simulated these harmonics during resonance and non-resonance conditions. During non-resonance the harmonic distortion at various buses was found within limits without using filters. During resonance, however, amplification of harmonic currents and voltages occurred. Harmonic currents flow from harmonic generating sources to the lowest impedance path provided by reactive power compensation capacitors. These capacitors shift the resonance frequency to lower frequencies. When these frequencies matched with harmonics, a parallel harmonic resonance occurred exceeding the limit of harmonic distortion. This issue was solved by using suitable number of mechanically switched capacitors. They concluded that when the wind turbine generator injected the harmonic currents, if the resonance point is close to the harmonic frequency then harmonic voltage amplification occurred. The shifting of resonance frequency by capacitors solved the purpose.

Case study I and II show the extent of damage from the occurrence of harmonic resonance in grids connected to high loads (paper mill and steel factory respectively). Case study III is the direct study of a wind farm failure, which is taken into account for this thesis. Case study IV provides for the mitigation techniques and recommendations for harmonic-resonance related issues, some of which are employed in this thesis.

2.6 Acceptable Harmonic Limits (IEEE Standard)

A standard limit for acceptable harmonics in the grid is used in order to mitigate the risk of excess harmonics and thereby providing sufficient time for operators to take protective measures to safeguard the most vulnerable links of the grid. These limits are published and maintained by IEEE and it serves as a guide for operators involved in the maintenance of electrical equipment in the grid. The IEEE's regulations have been criticized for not being precise enough for large wind farms. This follows since different models for calculating the harmonics yield different results, and the specified method in the standards is not always the most precise [26] [27].

Bus voltage at PCC	Individual harmonic (%)	Total Harmonic Distortion THD (%)
$V \leq 1kV$	5.0	8.0
$1 \text{ kV} < V \leq 69kV$	3.0	5.0
$69 \text{ kV} < V \leq 161kV$	1.5	2.5
$161 \text{ kV} < V$	1.0	1.5

Table 2: Voltage distortion acceptable limit

The standard limit is the amount of acceptable harmonic content at the point of common coupling (PCC). For this thesis the bus 632 of the modified IEEE-13 bus system has been chosen as the PCC as it connects the offshore network of wind turbines with the onshore grid.

Since the model would lie in a range of voltages between 1 kV and 69 KV, the following maximum current harmonic distortion limits are standardized:

I_{SC}/I_L	$3 \leq n < 11$	$11 \leq n < 17$	$17 \leq n < 23$	$23 \leq n < 35$	$35 \leq n \leq 50$
<20	4	2	1.5	0.6	0.3
20-50	7	3.5	2.5	1	0.5
50-100	10	4.5	4	1.5	0.7
100-1000	12	5.5	5	2	1
>1000	15	7	6	2.5	1.4

Table 3: Current distortion acceptable limit

The above tables (2) and (3) show the maximum voltage and current distortion for low voltage and high voltage systems, respectively. 'n' is the specific harmonic order, I_L is the load current and I_{SC} is the maximum short circuit current at PCC. Grid connected systems have low system impedance and high short circuit current [27]. Systems with higher short circuit current levels can employ classical protection schemes, which are well defined and tested.

3 Wind Turbine Modeling

In order to study the harmonic propagation in a wind farm network, we need to design wind turbines which constitute this network. The most important elements to consider for modelling a wind farm include wind turbine generator side model, transformers, filters, converters and transmission network components such as HVAC/HVDC transmission cables. [11].

These elements are discussed below:

3.1 Transmission lines/Subsea cables

Short to medium length cables can be modelled as pi equivalents whereas, longer cables can be modelled as a series combination of these pi equivalents [11].
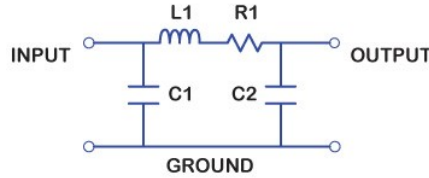
Figure 8: Pi section representing short cables

For connecting offshore windfarms to the shore, generally large cables are required as can be represented by a series combination of multiple pi equivalents [18]. The longer cable length also helps in dynamic modelling of the network which complies with different frequency harmonics and transients [11]. The reactive power also increases with length of the cables.

3.2 Wind turbine generators

There are two main subsystems of a wind energy system - a wind turbine system and an electrical generator. The electrical generator provides a means of energy conversion from the wind turbine, as a mechanical prime mover to an electrical load [28]. There are a number of suitable generators for a wind turbine. The squirrel cage induction generator has been the most historically used. The induction generator with wound-rotor and the field-excited synchronous generator are also very popular [29]. Recently, new generator types such as permanent magnet and doubly-fed induction generators have been developed for potential use in wind turbine applications.

Following is a brief description of the various types of the electrical generators used in wind turbine system:

3.2.1 Induction Generators

The induction or asynchronous generators are currently the most predominant commercial wind turbine generators [28]. They have several advantages including the flexible asynchronous operation, especially at fluctuating wind speeds. The following diagram (9) shows a wind turbine system based on an induction generator:
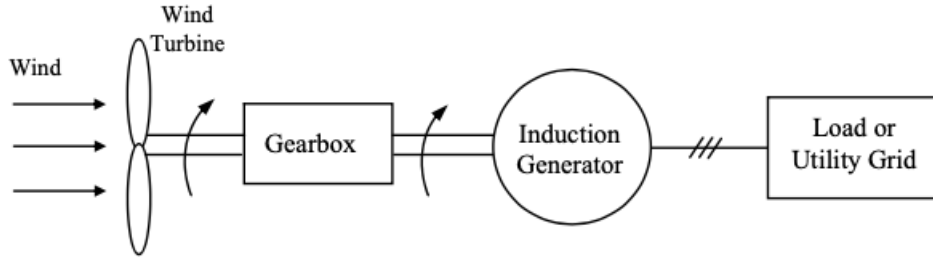
Figure 9: Wind turbine system based on induction generator

Some of the important induction generators used as wind turbine generators are mentioned below:

1. **Squirrel-Cage Induction Generators**:
   The Squirrel-Cage Induction Generator has been the most widely used wind turbine generator [29]. Their main advantage lies in low cost, robustness and simplicity of use [30] [31]. However, these generators are difficult to control with limited range of speed variation.

2. **Doubly-fed Induction Generators**:
   Doubly-fed Induction Generators are relatively new variation of asynchronous generators than Squirrel-Cage generators. The need of the modern grid for good quality power, with reduced noise (both electrical and mechanical) has led to the introduction of DFIGs [31]. The DFIGs also provide a robust control system for a large range of speed variation. However, it requires a combination of expensive power electronic converters to connect with the grid [29]. Also it has complex control strategies. Therefore, it is not recommended as the primary wind turbine generator by this thesis.

3.2.2 Synchronous generators

Synchronous generator is considered the workhorse of the electrical power supply industry [28]. They have high efficiency as well as are suitable for parallel operation of multiple turbines. They are also economically feasible and hence put them in a strong position for wind turbine generators. The following diagram (10) shows a wind turbine system based on an synchronous generator:

Figure 10: Wind turbine system based on synchronous generator
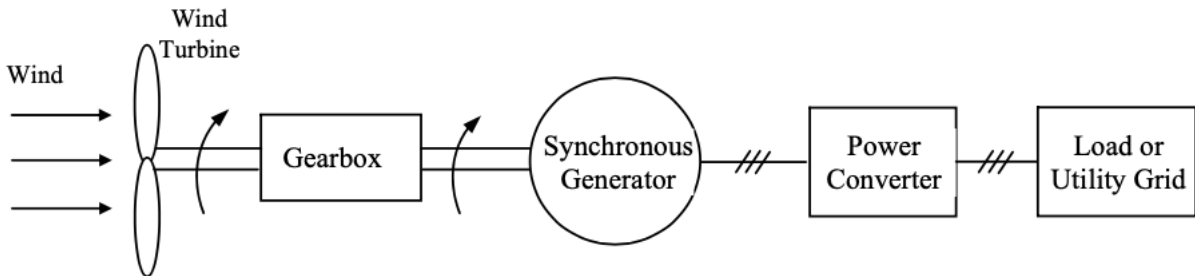
Some of the important synchronous generators used as wind turbine generators are mentioned below:

1. **Electrically Excited Synchronous Generators**: The Electrically Excited Synchronous Generators work quite like the induction generators carrying a 3-phase winding. Their output speed and voltage are fully controlled by converters, independent of grid characteristics

[29]. They are the most used type generators in large sized wind turbines [30]. They save the cost for using the permanent magnets. However, they need to have continuous excitation in their rotor windings using a DC source or a DC rectifier. Expensive power electronic components and the requirement of intensive cooling are among other drawbacks of these generators [29]. Also since they have larger size, their transportation and maintenance becomes difficult.

2. **Permanent Magnet Synchronous Generators**: One of the most exciting upcoming generators are the PM Synchronous generators. They utilise permanent magnets in place of a rotor. Hence, no need for external excitation as the permanent magnets takes care of that. They have several advantages over electrically excited machines. They have a smaller rotor and hence compact size, less weight, less mechanical components and better thermal characteristics [29]. The various other advantages of these generators are discussed in [28] [29] [30] [31]. The cost of permanent magnets as well as maintenance from demagnetization are some of the drawbacks of permanent magnets. However, in recent years with improvements in the PM performance and the general cost reduction, they become a viable choice of wind turbine generators. Hence, in this thesis a Permanent Magnet Synchronous Generator is recommended to be the source for the wind energy generation.

As this thesis deals with the grid side harmonics, the design of the generator and the AC to DC converter is not modelled. It assumes a DC voltage as the source connected to the grid via the IGBT DC-AC converter and the LCL filter.

3.3 Converter side modelling

The DC voltage source is taken as the output of the generator-converter system. This DC voltage becomes the input to the DC to AC converter side model since the modern day turbines are connected to the grid using the VSC [32]. The following figure (11) depicts a schematic of the converter side model:
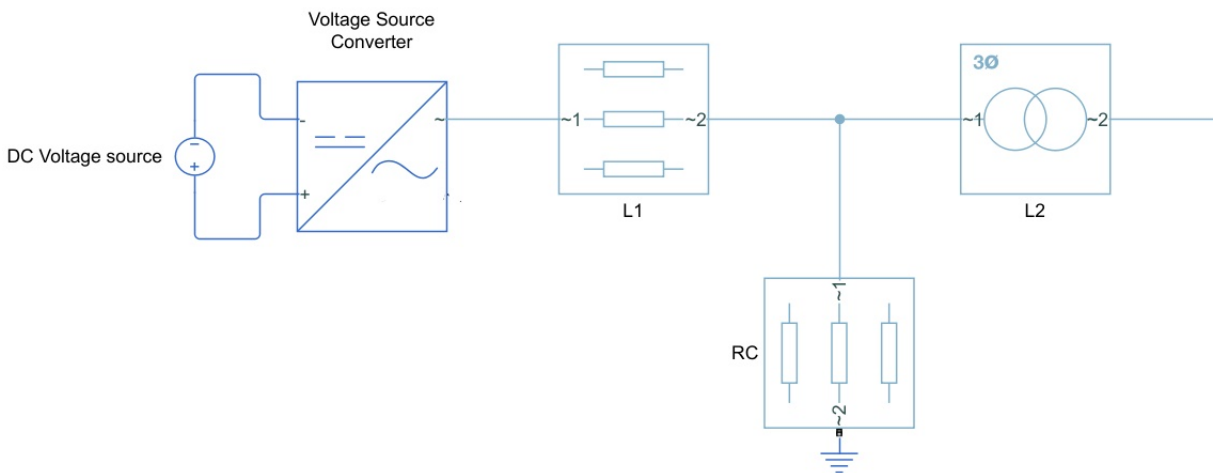

Figure 11: Converter side Model

In the above figure, the V_DC refers to the DC voltage source, which is connected to a VSC. The driving signal to the VSC is provided by the control system. The connection to the grid

is completed via a 3 phase Y-D transformer, which also provides a grid side inductance to the filter. Each block parameter is discussed in detail in the further sections.

3.3.1 Transformers

Every turbine in the wind farm is equipped with a step-up transformer, which enhances the turbine generator output voltage from a few hundred volts to the generating substation side MV levels. There are several factors that influence the performance of these transformers including variable loading, non-sinusoidal loads, transformer sizing, voltage variation, low voltage (LV) fault ride through, protection and fire behavior, step-up duty, switching surges and transient over-voltages, loss evaluation and gassing [33]. In a power system grid, an average of 1-2% of Total Harmonic Distortion is common at the point of generation [33] [34]. More over non-linear loads like switching devices, rotating machines, variable frequency drives and power electronic converters further distort the voltage and current waveform. These cumulative distortions repeat after every cycle, adding peaks that ride on the voltage and current waveforms and occur at other than the fundamental frequency of 50 Hz. Eddy currents and stray losses are some of the defects arising from high harmonic content. [34]. Though harmonic filtering is not specifically a function of the generation side transformer, electrostatic shields located between the primary and secondary windings act as a filter to prevent the transfer of dangerous harmonics onto the collector bus [33]. In this thesis, we have considered a 3-phase 3-winding star-delta transformer which is shown below:
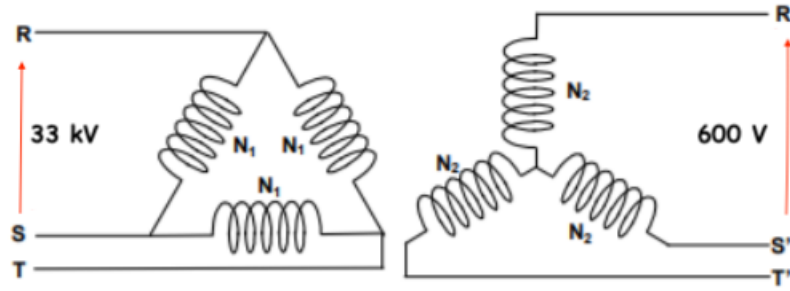
Figure 12: 3 Phase Y-D transformer

The wind turbine generators are generally connected to the grid via star-delta connected transformer. The use of delta winding at the high voltage side avoids transfer of zero-sequence triplen harmonic components under balanced operating conditions [25]. The zero sequence current can only flow when the neutral point is connected.

The parameters are selected as per the load flow calculations. The converter side transformer is used as a part (L_2) of the LCL filter which is discussed in the next section.

3.3.2 LCL filter

The LCL filter consists of a converter side inductor (L_1), a compensating capacitive element and a grid side inductor (L_2). As mentioned in the last section the grid side inductor will be the transformer.

The inductance and capacitance elements are calculated from the literature survey based on real values of operational wind farms. The selection of converter side inductor (L_1) is done on the basis of limiting the current ripple from the converter to less than 10% [22]. The current ripple from the converter is given by equation (7):

$$\triangle i_{max} = \frac{(Vdc - D \cdot Vdc)D}{2L_1 \cdot f_{sw}} \tag{7}$$

where, D= duty cycle of the VSC converter. It corresponds to the fraction of the complete cycle in which the upper switches of the complementary pair of switches at each phase is open [22]. It can be seen that the highest amount of current ripple will result when D=0.5. The switching frequency is f_{sw} and Vdc is the DC voltage. The following figure gives a switching topology of a VSC converter, LCL filter and a DC voltage source:
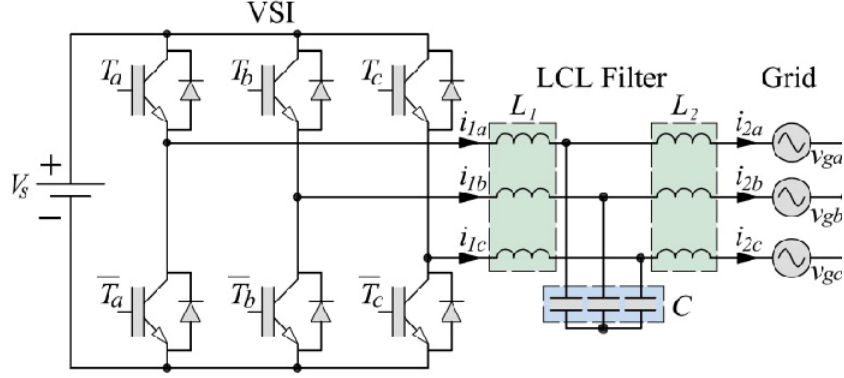
Figure 13: VSC switching topology, LCL filter and DC voltage source

If I_{base} is the amount of base grid current injected from the converter, the the current ripple can be calculated by the equation (8):

$$\triangle i_{max} = 0.1 \cdot \sqrt{2}I_{base} \tag{8}$$

Combining equations (7) and (8), and substituting the value of D, the equation for converter side inductance can be obtained as:

$$L_1 = \frac{Vdc}{1.13I_{base} \cdot f_{sw}} \tag{9}$$

The selection of grid side inductance, which is a transformer, is much more complex. A great deal of significant perspectives need to be mulled over, for example, the winding ratio and the size and saturation of the transformer etc. [21]. The inductance L_2 can vary with all these parameters. The selection of transformer has been done with an extensive literature survey.

With the values of the LCL filter known, the resonant frequency of the filter can be calculated easily. To dampen resonance in the converter side, a small resistance is added to the shunt branch of the LCL filter. The resonant frequency is given by the equation (10).

$$f_{res} = \frac{1}{2\pi}\sqrt{\frac{L_1 + L_2}{L_1 \cdot L_2 \cdot C_f}} \tag{10}$$

3.4 Control System

The control system has been designed such that it consist of a power balance control as well as current control.

Designing the control system broadly consists of three parts [35]:

1. Obtaining the converter current and voltage. This means that the output current and voltage of the converter have to be measured.

2. Generating the reference signal. The control system has to be designed in such a way that the converter will produce the desired current. In a wind turbine converter, this is done by controlling the reference current.

3. Generating a gate signal. The switches of the IGBT converter needs to be controlled in order to generate the desired current.

The following figure (14) shows the control topology used in the modeling of the control system:
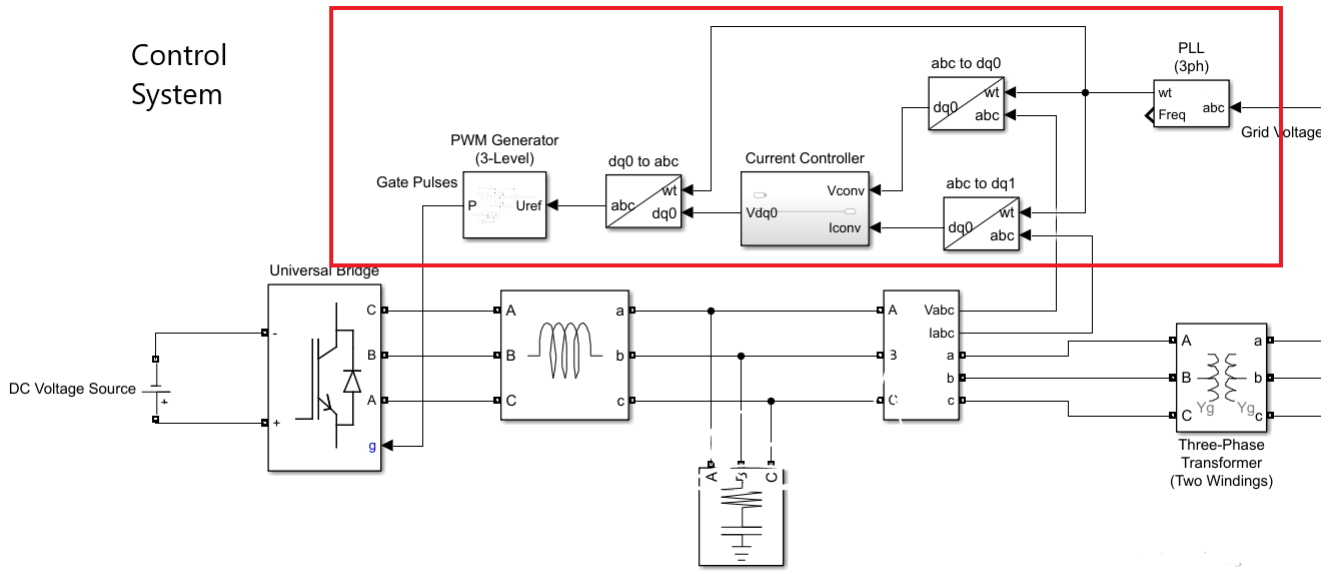

Figure 14: Control System topology

The input to the control system are the voltage and current from the IGBT converter and the grid. The converter current and voltage are converted from ABC components to DQ0. This conversion is carried out to be in line with the common norm of wind farms where DQ0 components are the reference frame [11] [18] [36]. The DQ0 components of converter voltage and current then pass through the current controller. The topology of current controller will be discussed in section 3.4.3. On the other hand, the grid voltage is used to generate the reference current in DQ0 frame. The converter voltage and current are compared with the reference components in the current controller. Output from the current controller is converted back to the ABC component and serve as the input to the Pulse Width Modulator (PWM). The topology of PWM is discussed in the section 3.4.2. The PWM generates a signal which is closest possible resemblance to the reference voltage and provide the gate pulses to the IGBT converter. These gate pulses act as the output of the control system.

3.4.1 Reference Current generator

The current controller uses a rotating DQ0 reference frame synchronized with the grid voltage at the converter side of the transformer. The reference current generator is therefore modelled using the voltage and current from the grid as input. The active and reactive power per phase

is measured and compared with a reference. Since the DC-side of the converter is represented by an ideal DC source, the reference active and reactive power can be set as desired [37]. The following figure (15) shows the reference current generator scheme used in this thesis:
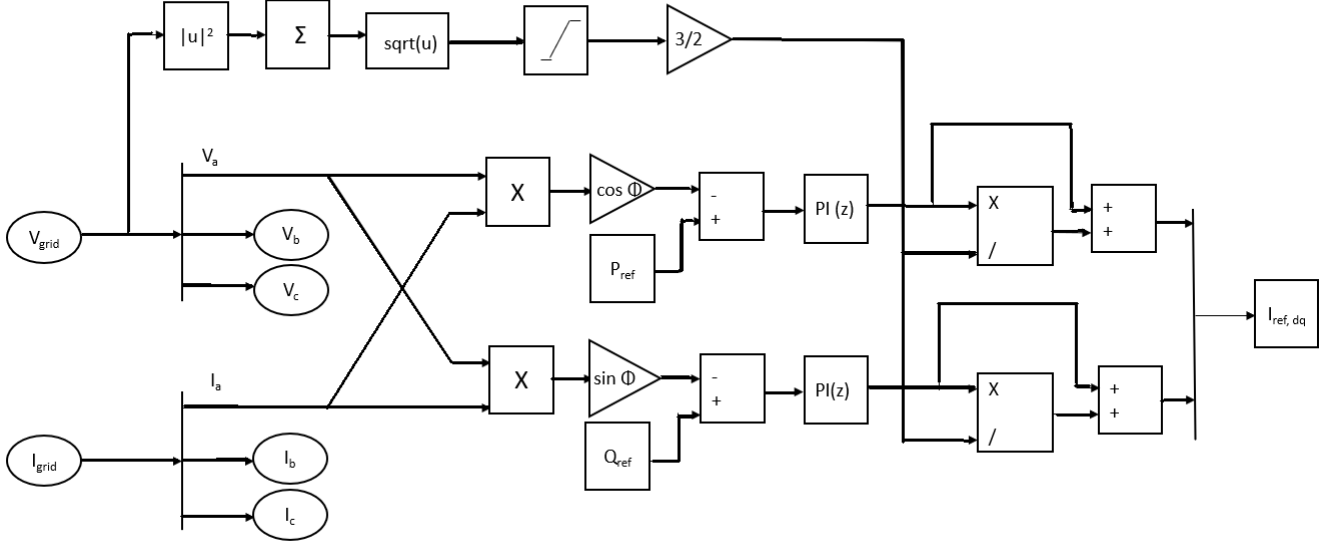

Figure 15: Reference Current generator scheme

According to the scheme shown in figure (15), the grid voltage and current are used to generate the reference current for the current controller. The phase voltages and currents are used to calculate the active and reactive power. This calculated power is compared with the reference power, which was set according to the requirements. The output is passed to a discrete PI controller. The discrete PI controller was tuned using the sisotool. The P and I values were set according to the tuned response. This generated the reference active and reactive power for the current controller.

In order to convert this reference power into reference current in DQ0 format, the active and reactive power are divided by the voltage at the point of common coupling (PCC). The referenec power is added to the result in order to generate the D & Q components of the reference current. The mathematical formulation of the reference currents is shown below:

$$I_{d,ref} = (K_{p1} + \frac{K_{i1}}{s}) \cdot (P_{set,ref} - P_{ref}) + 2 \cdot \frac{P_{ref}}{3V_{PCC}} \tag{11}$$

where, K_{p1} and K_{i1} are the coefficients of the first PI controller, V_{PCC} is the voltage at the point of common coupling, the set reference active power $P_{set,ref} = 1$ and,

$$P_{ref} = V_a \cdot I_a \cdot cos(\phi) \tag{12}$$

And,

$$I_{q,ref} = (K_{p2} + \frac{K_{i2}}{s}) \cdot (Q_{set,ref} - Q_{ref}) + 2 \cdot \frac{Q_{ref}}{3V_{PCC}} \tag{13}$$

where, K_{p2} and K_{i2} are the coefficients of the second PI controller, V_{PCC} is the voltage at the point of common coupling, the set reference active power $Q_{set,ref} = 0$ and,

$$Q_{ref} = V_a \cdot I_a \cdot sin(\phi) \tag{14}$$

3.4.2 Current Controller

The current controller is designed within the DQ0 reference frame. The converter current along with the reference current, generated in section 3.4.1, are the input to the current controller. The following figure (16) gives a working scheme of the current controller.
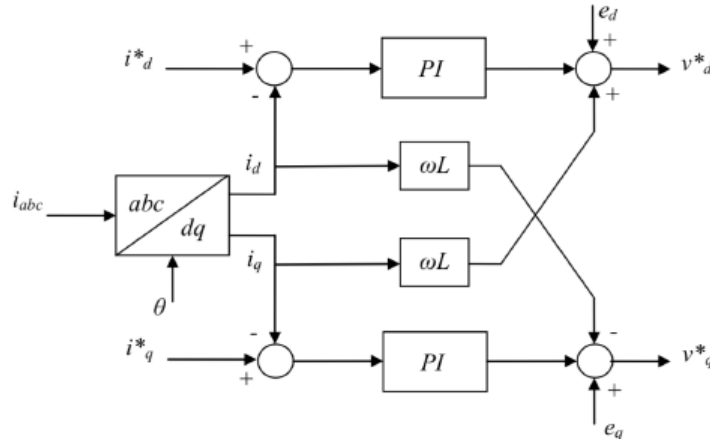
Figure 16: Current controller scheme

The DQ0 components of converter current are compared with the reference current DQ0 values and provided to a PI controller. The PI controller is tuned using the PWM and the LCL filter transfer functions. The result is compared with the converter voltage components in DQ0. The output of the current controller are the controlled DQ0 voltage waveforms towards the PWM.

Following mathematical calculations are significant for the formulation of the current controller:

1. **Conversion of ABC components to DQ0**:

   The DQ reference frame is rotating with the same frequency as the fundamental component of the voltage, meaning the fundamental component of the voltage and current will be DC-components [34].In the control system of the VSC, the reference is set so that the reference frame is in phase with the voltage. This means that the current contributing to the active

power will be set as I_d , while the current contributing to the reactive power will be set as I_q.

The relation between the ABC components and DQ0 components is given by the equation (15):

$$
\begin{bmatrix} v_d \\ v_q \\ v_0 \end{bmatrix} = \frac{2}{3} \begin{bmatrix} cos(\omega t) & cos(\omega t - 2\pi/3) & cos(\omega t + 2\pi/3) \\ -sin(\omega t) & -sin(\omega t - 2\pi/3) & -sin(\omega t + 2\pi/3) \\ 1/2 & 1/2 & 1/2 \end{bmatrix} \cdot \begin{bmatrix} v_a \\ v_b \\ v_c \end{bmatrix} \tag{15}
$$

2. **Calculation of desired DQ0 components** In section 3.3.2 it has been discussed that the LCL filter is mainly used for dealing with the switching ripples. For frequencies lower than half the resonance frequency, the converters with LCL-filters will behave the same way as converters with an RL-filter [38]. Thus the influence of LCL filter will be neglected in the modeling of the current controller.

In order to find the influence of RL filter, following equation (16) can be used:

$$
V_{conv,abc} = R_{filter} i_{abc} + L_{filter} \frac{di_{abc}}{dt} + V_{abc} \tag{16}
$$

Transforming the above equation (16) into DQ0 format using the matrix equation (15) we get,

$$
\begin{bmatrix} v_{conv,d} \\ v_{conv,q} \end{bmatrix} = R \begin{bmatrix} i_d \\ i_q \end{bmatrix} + L \frac{d}{dt} \begin{bmatrix} i_d \\ i_q \end{bmatrix} + \omega L \begin{bmatrix} 0 & -1 \\ 1 & 0 \end{bmatrix} \begin{bmatrix} i_d \\ i_q \end{bmatrix} + \begin{bmatrix} v_d \\ v_q \end{bmatrix} \tag{17}
$$

The above equation (17) shows a cross coupling between the D and Q axis with parameter ωL. This means that the active power and reactive power would also have an influence of i_q and i_d respectively. The control system has been designed in order to decouple this situation. The PI controllers are used for this purpose.

After this decoupling the output voltage in DQ reference frame can be expressed by the equations (18) and (19):

$$
v_d^* = -(K_{p,d} + \frac{K_{i,d}}{s})(i_d^* - i_d) + \omega L i_q + v_{conv,d} \tag{18}
$$

$$
v_q^* = -(K_{p,q} + \frac{K_{i,q}}{s})(i_q^* - i_q) + \omega L i_d + v_{conv,q} \tag{19}
$$

The transfer function of the current controller can be expressed by the equation (20):

$$
H_{PI} = K_P + \frac{K_I}{s} \tag{20}
$$

3.4.3 Pulse Width Modulator

A pulse width modulator (PWM) has been used to tune the PI controller in the current controller circuit. During the MATLAB modeling, a 3-level PWM has been used to generate the gate signals. These gate signals represent the switching scheme for the IGBT converter. The input to the PWM is the reference voltage (v_{abc}^*) as an input and returns the control signal to the switches as the output. The reference voltage given as input is the same voltage that is needed to generate the desired output current from the VSC and is calculated in the current controller.

Following figure (17) shows the gate signals obtained during the simulation of a wind turbine:
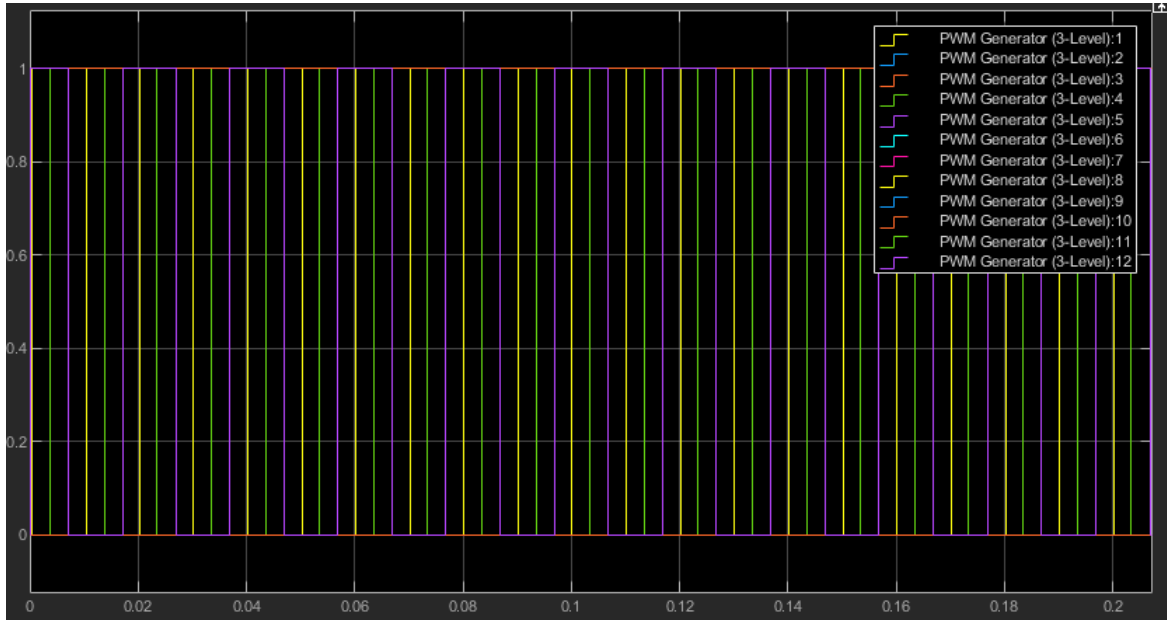

Figure 17: PWM gate signals

According to the literature survey, a PWM based control system for generating switching signals has been found the most common and effective way to control IGBT switching. From the figure (17) it is clear that the gate signals produced by the PWM are square pulses. Since, the PWM generates a switching scheme as its output in order to create closest possible resemblance to the reference signal. The square pulse is compared with a signal similar in magnitude to the DC voltage and a frequency equal to the switching frequency (1.75 kHz). When the generated pulse is greater than the reference signal, it refers to the the upper switches of the IGBT being in "ON" state and lower switches being in "OFF" state. The output voltage waveform in that condition will be equal to the DC voltage. On the other hand, when the generated pulse is smaller than the reference signal, it refers to the the upper switches of the IGBT being in "OFF" state and lower switches being in "ON" state. The output voltage waveform in that condition will be equal to the 0.

The converter switching frequency is defined in the parameters of the PWM. For this thesis the switching frequency is considered as 1.75 kHz. Using the switching frequency of the IGBT converter, the transfer function of the PWM can be defined by the equation (21) as:

$$H_{PWM}(s) = \frac{1}{1 + T_a s} \tag{21}$$

where, T_a is defined as the delay caused due to the PWM. This delay (T_a) can be approxi-

mated as:

$$T_a = \frac{1}{2 \cdot f_s} \tag{22}$$

3.4.4 Step and Bode plot

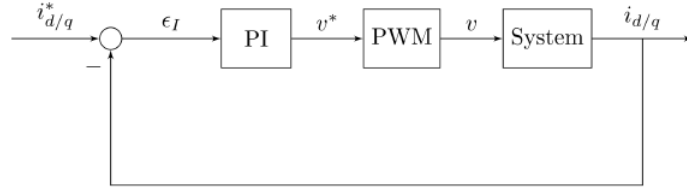The complete system can be represented by the following figure (18):

Figure 18: Complete system representation

The above figure (18) represents a closed loop system of the entire control system. The system transfer function can be calculated as:

$$H_{system} = \frac{R \cdot C_f s + 1}{L_1 L_2 C_f s^3 + (L_1 + L_2) R C_f s^2 + (L_1 + L_2) s} \tag{23}$$

The following observations were made regarding the step and bode plot analysis of the system under normal operating conditions:
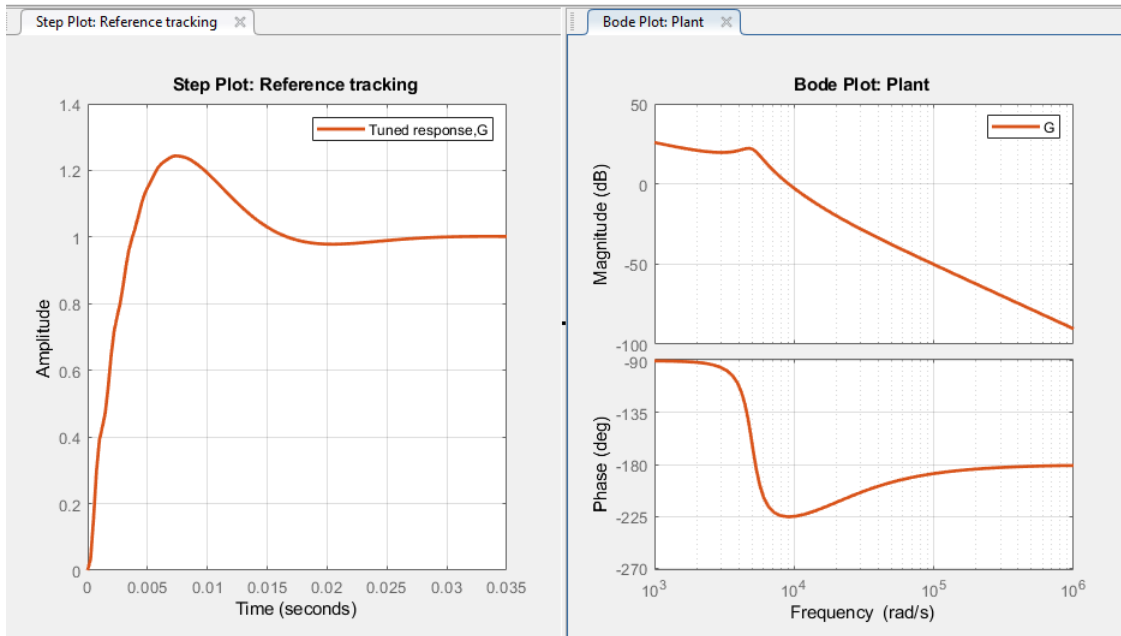

Figure 19: System Bode response

The phase margin Pm = 43.9 degrees at 8.49e3 rad/s and the gain margin Gm = 17.11 dB at 4.27e3 rad/s.

34

4 Grid Design

Harmonics generated by a VSC do not remain constant but vary according to the converter control and the switching scheme [24]. A network grid has been modelled in order to study the harmonic propagation. The wind turbines are connected in a standard network in order to use the known constraints of the network. This simplifies the study, limiting the unknown variables and speeds up the analysis in an organised manner. Modelling has been done as a part of a suggestive measure to develop and connect a wind farm.

4.1 IEEE test grids

The most commonly used Distribution Test Grids are the IEEE test grids [39]. There are several test grids designed by IEEE including test grids with 4, 13, 34, 37, 123, 324, 8500 buses [40]. The test grids with 13, 34, 37 and 123 buses are the classical test grids. The recent test grids include the 8500 bus and the European low voltage test grid [39].

4.2 IEEE-13 bus network

For this thesis, a modified IEEE-13 bus network has been modelled as a primary grid with wind turbines connected at different buses. The following figure shows a prototype IEEE-13 bus network with two onshore wind farms connected to it:
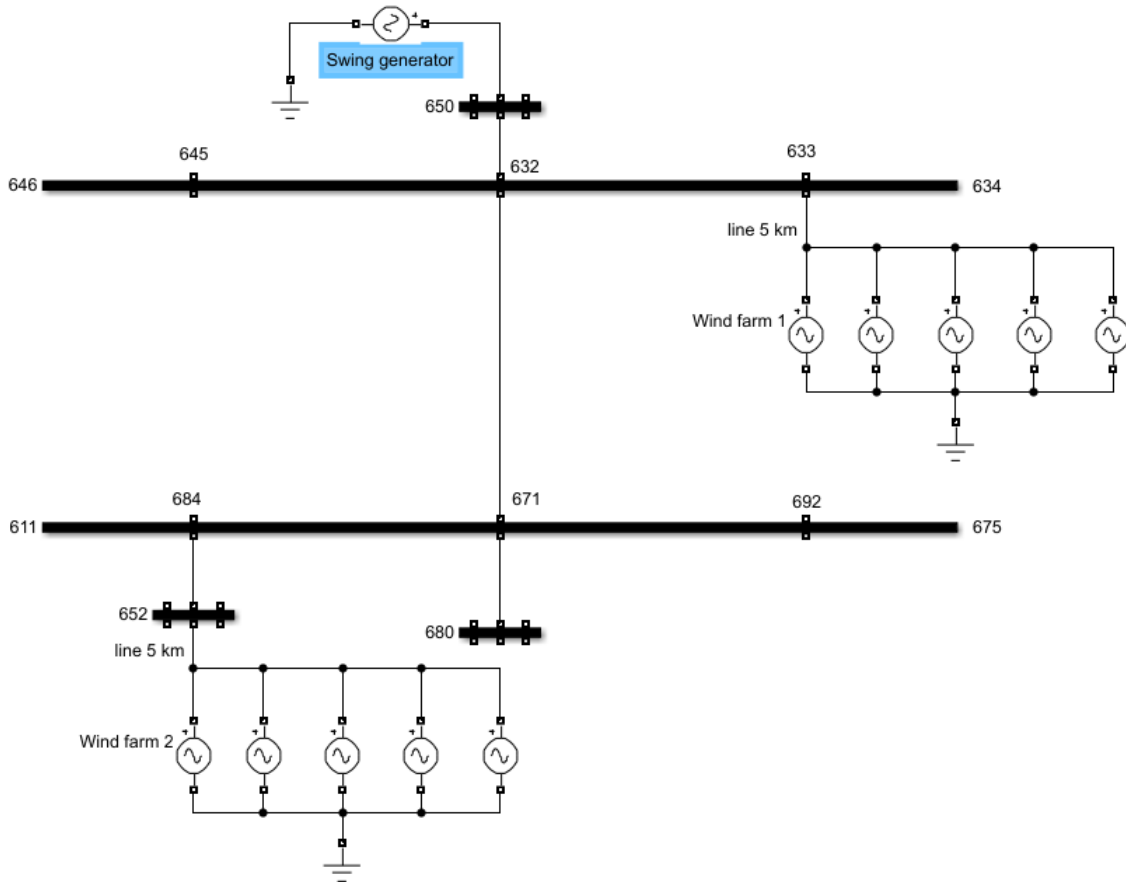

Figure 20: modified-13 bus network

The figure (20) shows a standard IEEE-13 bus network. The two onshore wind farms are connected at buses 633 and 652 of the network. The figure (20) is a depiction of IEEE-13 bus systems being used to represent grid connected onshore wind farms. The network is used by

Stanisavljević et. al. in their paper [41] to discuss the integration of distributed generation in a distribution grid.

In this thesis, a IEEE-13 bus network has been developed in MATLAB/Simulink by modifying the Simulink-inbuilt standard IEEE-13 node feeder. Since, the network contains wind-power generation sources, which inject high amount of power into the network, the capacity of the standard IEEE-13 node feeder was found to be insufficient. Hence, the capacity of the network was increased by increasing the available voltage range of the grid. This was done by assuming a Line Voltage Regulator (LVR) action [42] between the grid and the bus 652. The standard Simulink model neglects the connection of the grid to the bus 652 to simplify the network. The modelling of grid side transformer is skipped in the process and hence the effect of the LVR can be directly modelled by increasing the grid voltage.

For the verification of load flow data, the modified network was first modelled to accommodate two onshore wind farms as done in [41]. Due to the constraints of personal computer, each wind farm has been limited to 5 wind turbines. The wind farms are referred as DG1 (Distributed Generation) and DG2 respectively. The DG1 is rated at 5 MW that is 1 MW/turbine whereas, DG2 is rated at 12.5 MW that is 2.5 MW/turbine. Once the base case results were verified, the network was modified in order to suggest a possible generation side grid for an offshore wind farm. Each turbine is rated 5 MW during the offshore wind farm modeling. The wind turbines were redistributed along the various buses of the network, as compared to the onshore case where they were concentrated at two particular buses (633 and 652). This redistributed network represents each bus as a node or a wind turbine. Thus, the load distribution was allowed to remain unchanged. This would account for the load flow analysis which would also then remain constant. The load flow analysis is further discussed in the next section 4.3.

4.3 Load flow

The following load flow data was obtained for the network connecting two onshore wind farms:

The load flow analysis for the modified IEEE-13 bus sytem has been shown in the above table (4). For the full load flow analysis results, refer to the appendix A.

Bus ID	Bus type	$V_{LF}(pu)$	$Vangle_{LF}(pu)$	$P_{LF}(MW)$	$Q_{LF}(MW)$
632	PQ	1.0210	-2.49	0.02	0.01
632	Swing	1.0210	-2.49	7.92	1.57
652	-	1.0211	-2.54	0	0
692	I	1.0209	-2.53	0	0
675	PQ	1.0208	-2.64	4.6	4
675	Z	1.0208	-2.54	0	-1.04
671	PQ	1.0209	-2.53	0.38	0.22
671	PQ	1.0209	-2.53	1.04	0.69
633	-	1.0210	-2.49	0	0
634	PQ	1.0209	-2.49	0.5	0.36
645	-	1.0210	-2.49	0	0
646	-	1.0210	-2.49	0	0
680	-	1.0209	-2.53	0	0
684	-	1.0210	-2.53	0	0
611	-	1.0210	-2.53	0	0

Table 4: Load flow analysis of the modified IEEE-13 bus model

4.4 Frequency Sweep

The harmonics generated by a PWM controlled converter are generally the integral multiple of the grid frequency (50 Hz, which is also the modulated frequency), the carrier frequency (which is the modulating signal), and a combination of the grid and carrier frequency [43]. These harmonics are often referred as characteristic harmonics, as mentioned in case study 2.5.4 by [24]. The objective of a frequency sweep is to find the equivalent impedance of the entire simulated Wind farm network. In this manner, the harmonic gain for each individual frequency could be calculated [44].

The theoretical idea behind the frequency sweep is to send a current of certain frequency and peak value of 1A and measure the induced voltage over the components. When this simulation is performed over a wide range of frequencies, a frequency-dependant impedance plot can be created. In this thesis the MATLAB/Simulink tool : *power_zmeter* was utilised for the impedance measurement within a wide range of frequencies. The frequency sweep plots for two paths:

1. Path 1: PCC to bus 675

2. Path 2: PCC to bus 652

The following figure (21) shows the result of a frequency scan from the PCC to the wind turbine at bus 671.
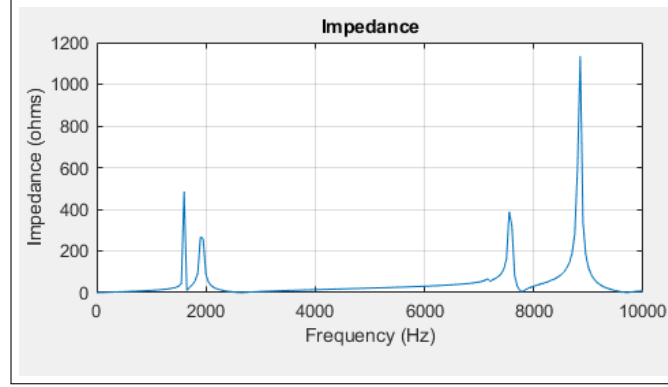
Figure 21: Frequency sweep from PCC to bus 671

The following figure (22) shows the result of a frequency scan from the PCC to the wind turbine at bus 652.
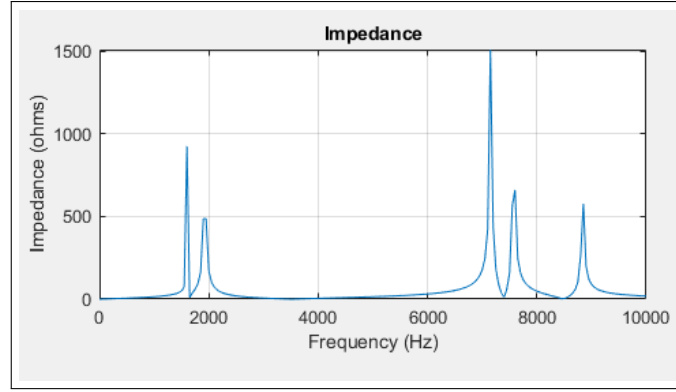

Figure 22: Frequency sweep from PCC to bus 652

According to the above figures (21) and (22), at the fundamental frequency (50 Hz) the impedance is about 0.5674 Ω between the PCC and the bus 671, whereas it is about 0.6930 Ω between the PCC and the bus 652. There are some frequencies with a higher impedance than others ie. 1250 Hz ,1750Hz, 7050 Hz and 9050 Hz. The following table (5) gives a description of the impedance at interested frequencies:

Path	Harmonic order	Impedance (Ω)
PCC-bus 671	25	512
	35	276
	141	394
	181	1136
PCC-bus 652	25	936
	35	398
	141	1500
	181	622

Table 5: Impedance vs Harmonic order

Following these results, a frequency scan of the converter section of a turbine was carried out. The following figure (23) represents the output:
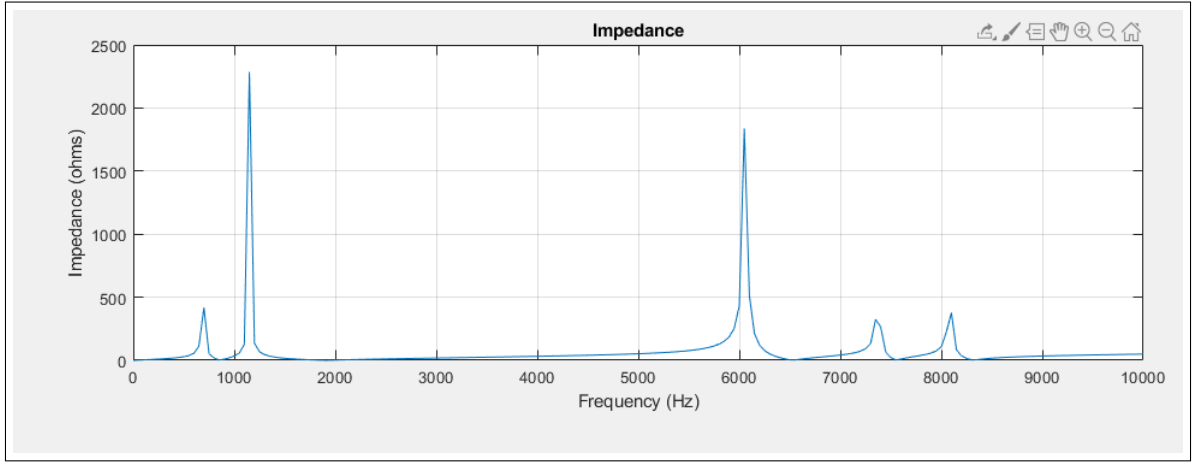

Figure 23: Frequency sweep of the converter side

The inference that can be drawn from the above figure is that the converter side impedance, which mainly consist of the LCL filter impedance is mainly dominated by the inductance of the transformer. There are some local frequency peaks but except the frequency of 7750 Hz or 157th harmonic order, none are similar to the ones found between PCC and the buses. The resonant harmonic orders can be at 5th or 23rd order harmonics.

5 Simulation Results

In the following section, the results obtained from the simulation of the developed network has been discussed. Strating from the output voltage and current waveforms from the turbines, we look at 5 cases including - base case, De-tuned control system , disconnection of a part of the grid, wind speed dynamics and lastly a combination of the above cases - termed as the worst case scenario.

5.1 Converter Waveforms

The following section shows the converter voltage and current at the turbine during the normal turbine operation:
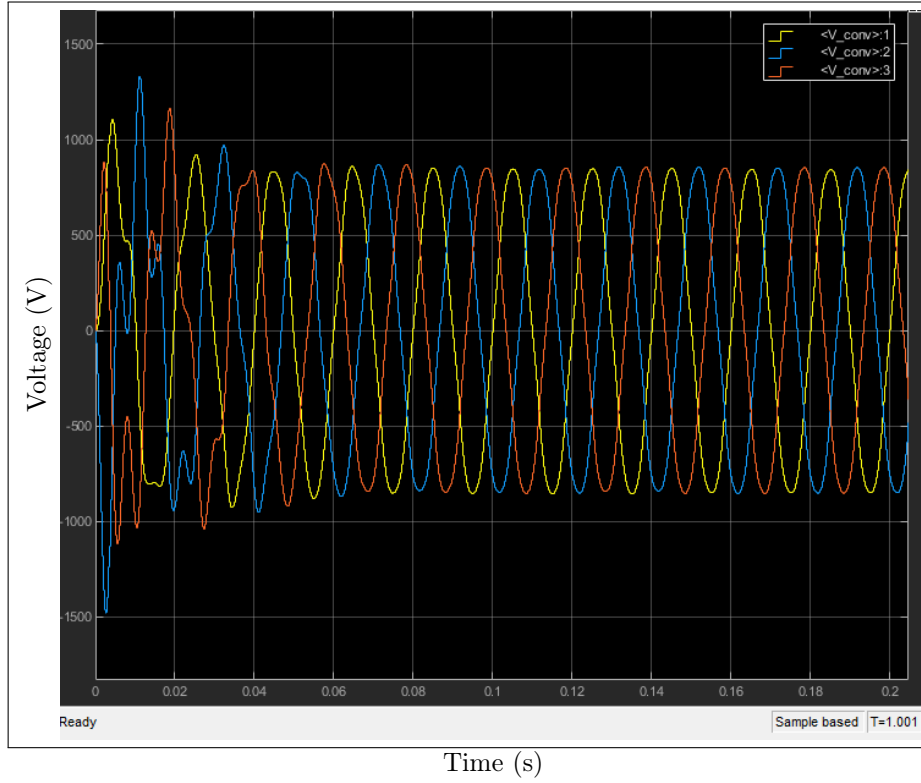

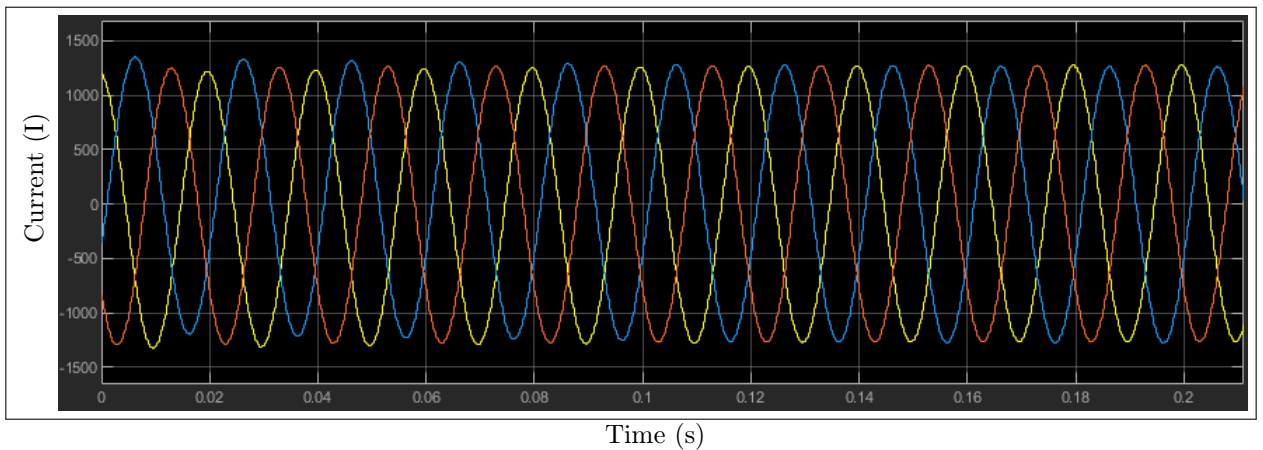
Figure 24: Converter Voltage waveform (3 phase)

Figure 25: Converter Current waveform (3 phase)

5.2 Base Case

The first scenario represents the base case. All the turbines are providing their rated output (5 MW). The converters and filters are tuned. There is no dynamics involved. The simulation is run under steady state conditions for 2 s. The fft analysis is run after the completion of the simulation and harmonics are analysed at the converter and individual buses.

5.2.1 Bus Voltage Waveforms

The following section shows the voltages at individual buses during the base case:
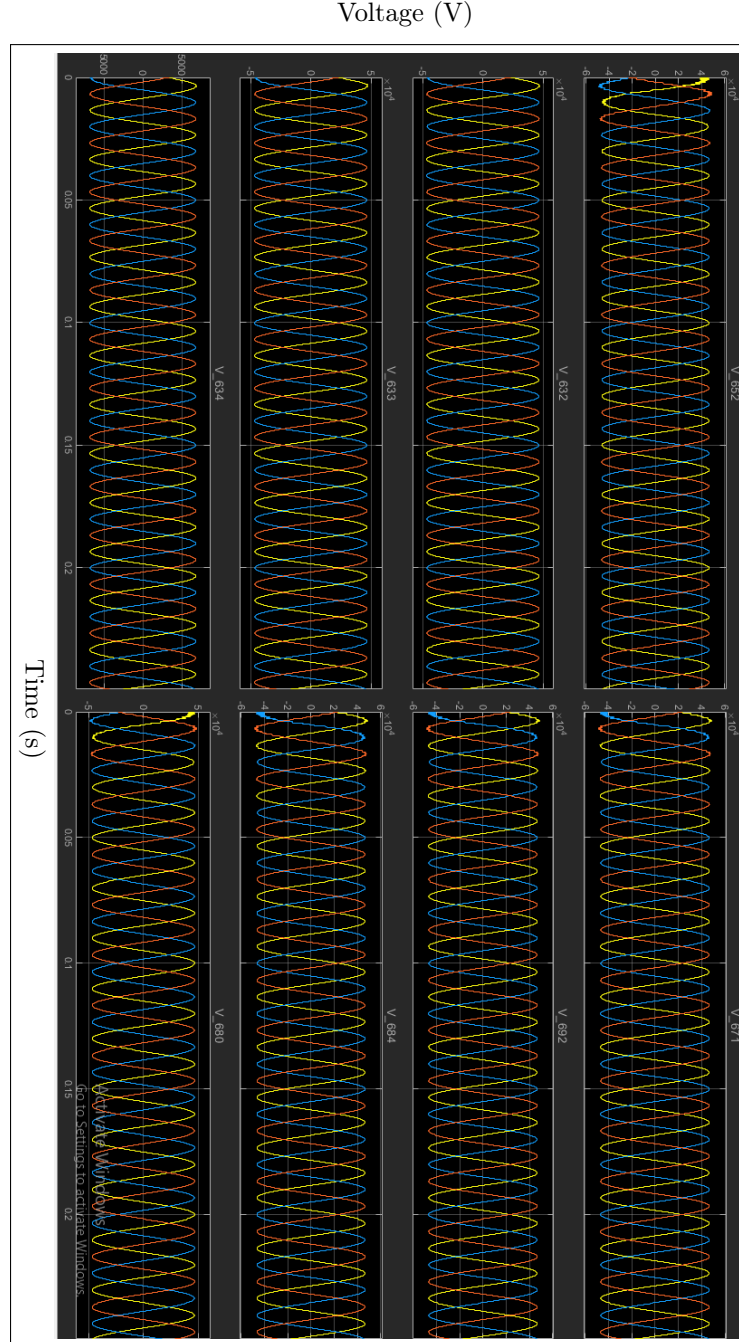

Figure 26: Voltages at different buses

5.2.2 Wind turbines Output Power

The following section shows the output power of individual wind turbines during the base case:
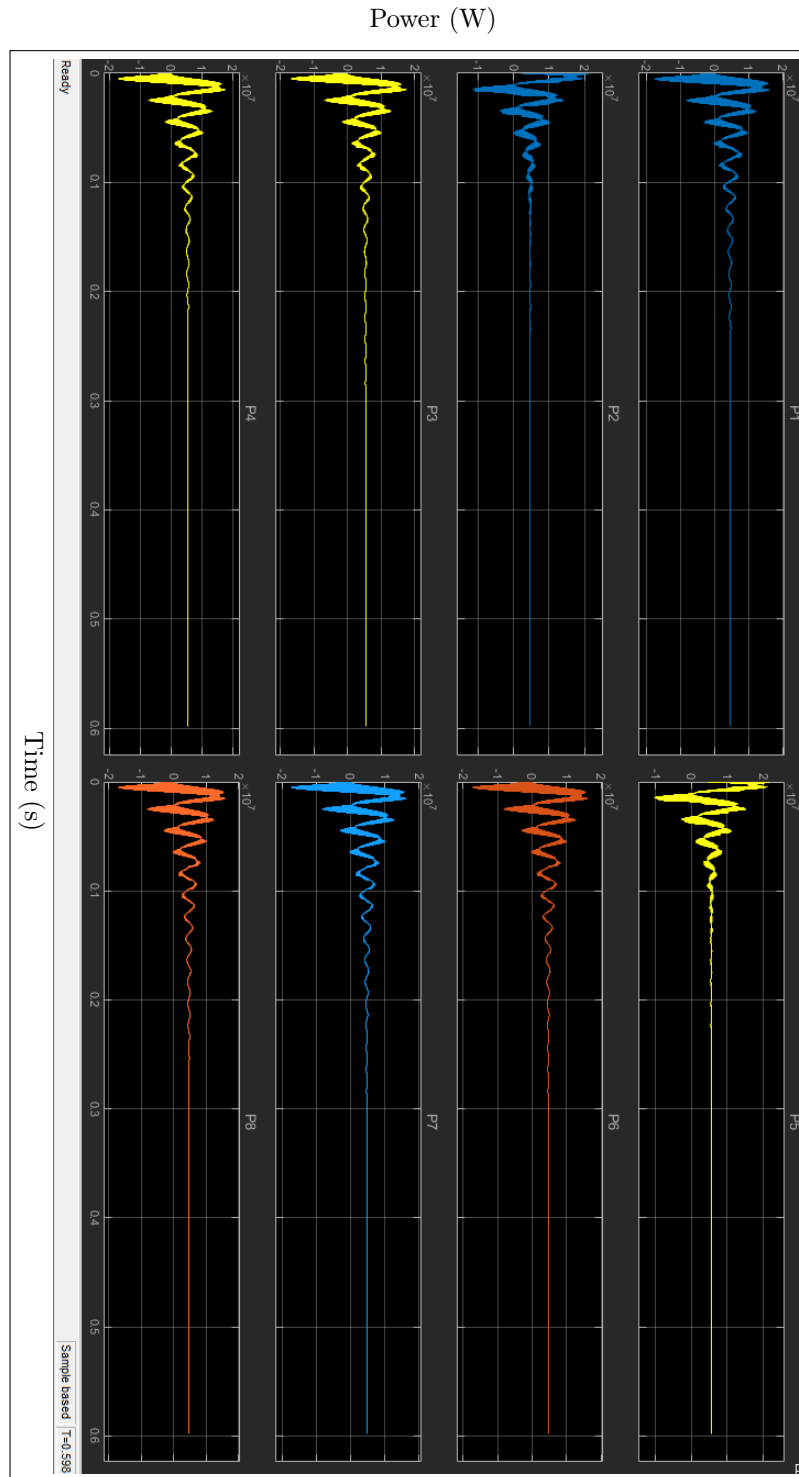
Power (W)

Figure 27: Wind turbines Output power

5.2.3 Harmonics at the turbine

The following section shows the current and voltage harmonics at the wind turbine during the base case:
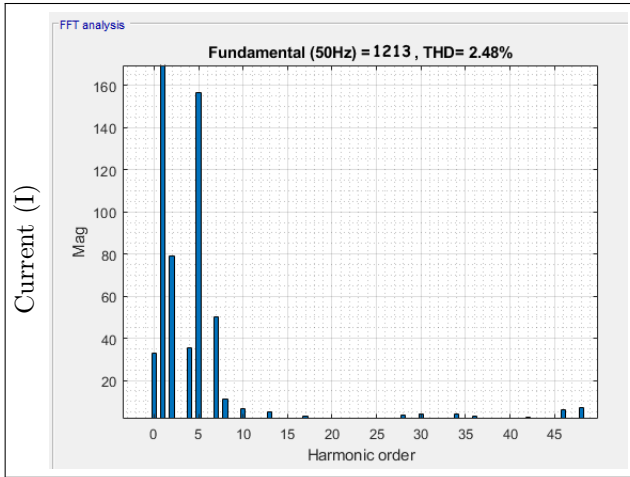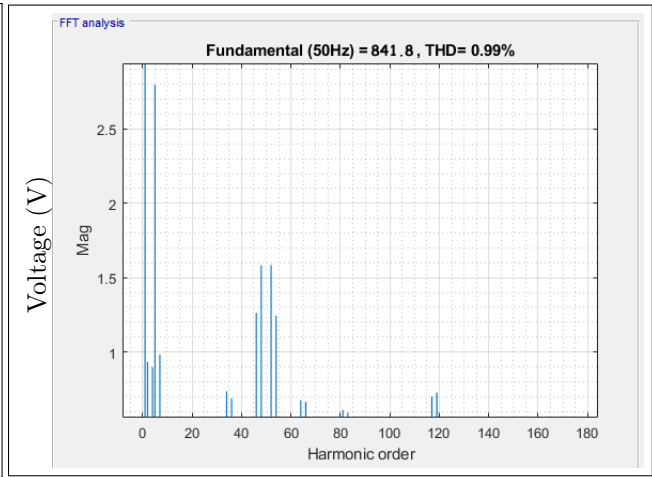

Figure 28: Current harmonics

Figure 29: Voltage harmonics

5.2.4 Voltage harmonics at different buses

The following section shows the voltage harmonics at individual buses during the base case:
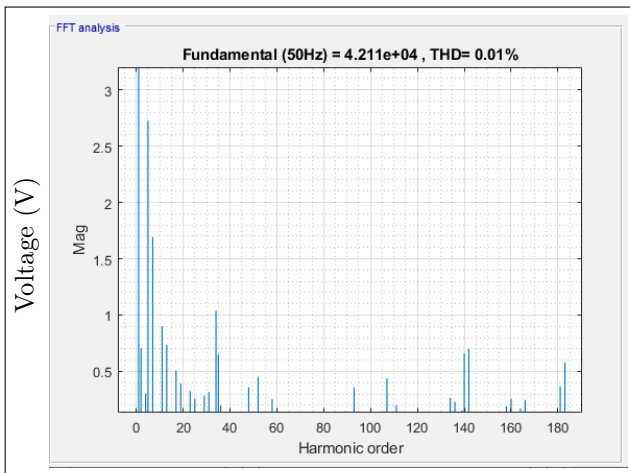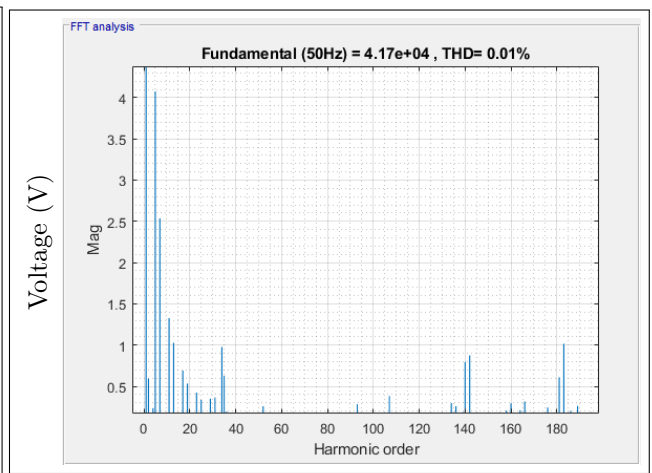

Figure 30: Voltage THD bus 633

Figure 31: Voltage THD bus 645

Figure 32: Voltage THD bus 646

Figure 33: Voltage THD bus 611

Figure 34: Voltage THD bus 652

Figure 35: Voltage THD bus 680
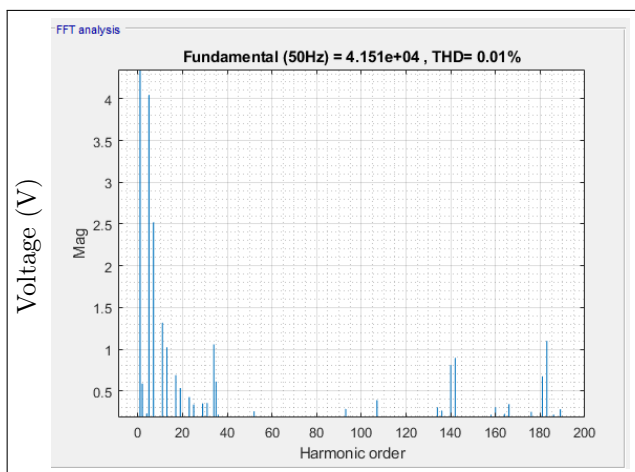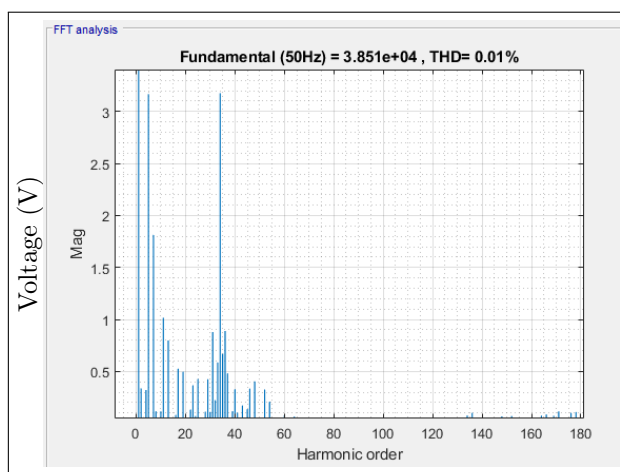
Figure 36: Voltage THD bus 684

Figure 37: Voltage THD bus 692

Figure 38: Voltage THD bus 675
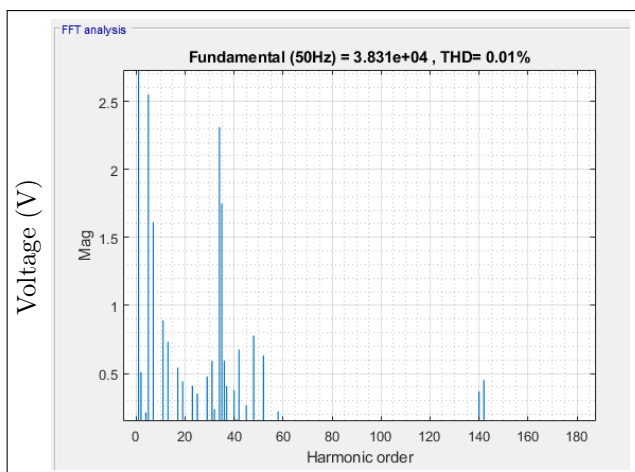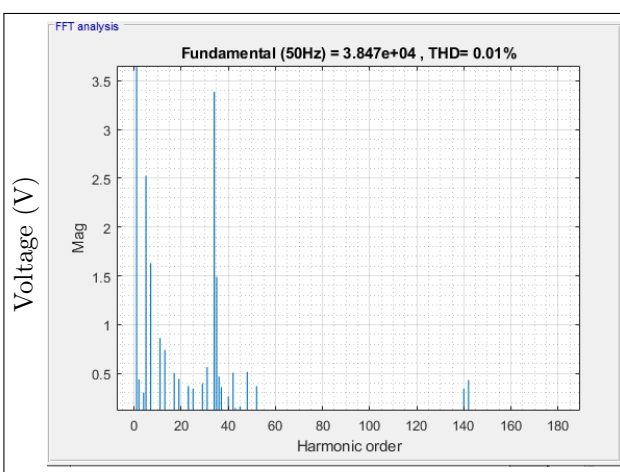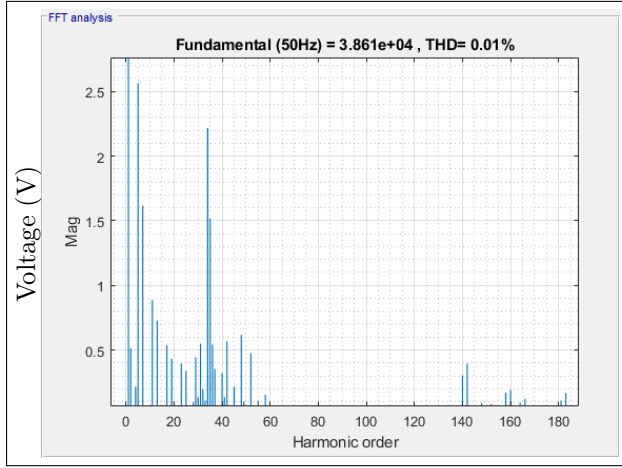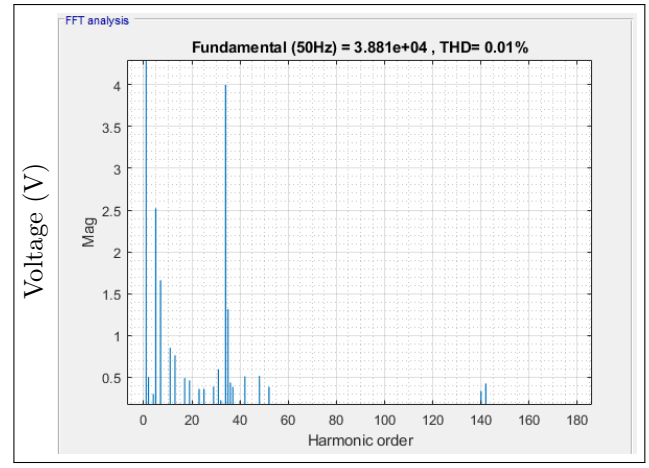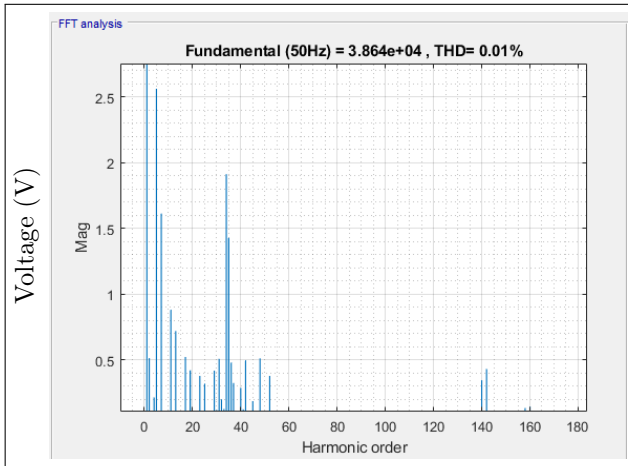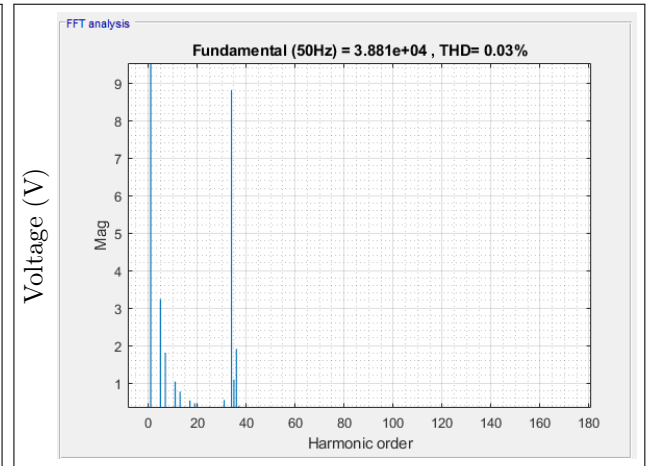

Figure 39: Voltage THD bus 671

The above figures represent the voltage harmonics at various buses of the grid. The most recurring disturbing harmonic as can be seen from the figures is 5th, 35th and 141st harmonic order. These figures are discussed further in the section 6.

5.3   De-tuned control system

During the base case discussed in the previous section 5.2, a tuned control system was used in simulation. This included an ideal PLL, tuned PI controllers and tuned LCL filter. A tuned filter functions better in eliminating the harmonics [45].

In this section we look at the performance of the converter without tuning. For the de-tuned control system, the system is simulated with random PI controller values. Thus, we are relying only on a random LCL filter to curb the harmonic injection into the grid. The following figures show the current and voltage harmonics at the converter side:
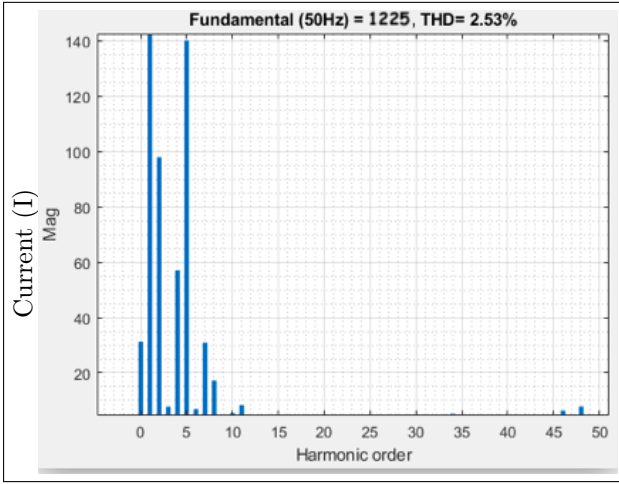
Figure 40: Current harmonics
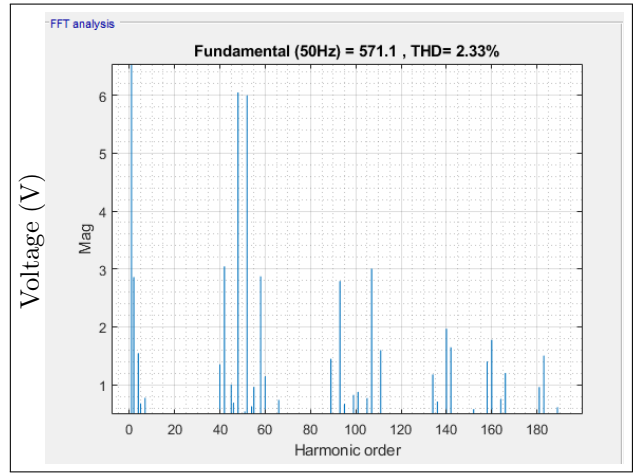
Figure 41: Voltage harmonics

From the figure (40), we can see that the magnitude of the fundamental current waveform is 1225 A, which is only slightly more than in the base case (1213 A). The current harmonics distortion is 2.53 %, which are again with a slight increase from the 2.48 % in the base case. Now, observing the figure (41), we see the magnitude of fundamental voltage waveform as 871.1 V, which is more slightly more than the 841.8 V in the base case. However, when we observe the voltage harmonics, we can see that the voltage harmonics distortion is 2.33 %, up from the 0.99 % in the base case. Therefore, we can say that the de-tuning of control system have a substantial effect on voltage harmonics but not as much on the current harmonics. The results from this section are discussed further in the section 6.

5.4 Disconnection of a part of the grid

The following figure (42) shows the grid network with the circuit breaker (inboxed in red) used to disconnect a part of the grid. The disconnected part of grid consist of the the two buses namely: bus 692 and bus 675. This would disconnect two wind turbines from the network.
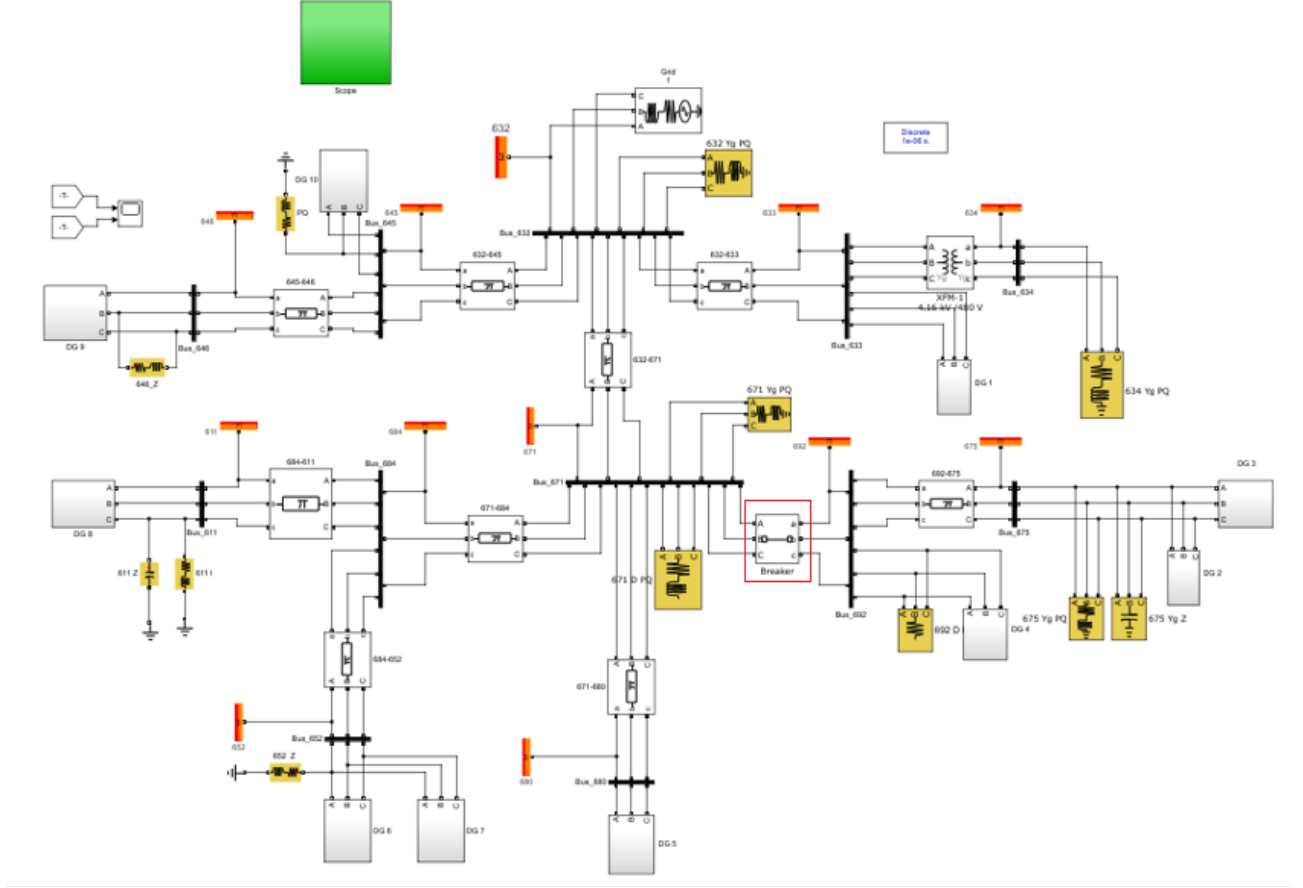
Figure 42: The circuit breaker disconnecting a part of the grid

The circuit breaker is activated after a certain operation period. This would be helpful in displaying the dynamics due to the sudden change in power flow throughout the grid. For the simulation, a time of 0.5 s was chosen to activate the circuit breaker. After this simulation time, the system has settled down.

A 3-phase circuit breaker was used for the disconnection. It controls the switching of the all the three phases simultaneously. Initially the breaker is switched on to allow all the three phases to stay connected with the grid. After 0.5 s, the breaker is activated, switching off the buses 692 and 675 from the grid. The consequences for the lost turbines are compensated by the rest of the network. The voltage drop on the rest of the buses increase. The grid power requirements are satisfied by an increase in the power output of the active remaining turbines.

5.4.1 Bus Voltage Waveforms

The following section shows the voltage waveforms at individual buses during the disconnected case:

Figure 43: Voltages at different buses

48

5.4.2 Wind turbines Output Power

The following section shows the output power of individual wind turbine during the disconnected case:

Figure 44: Wind turbines Output power

5.4.3 Voltage harmonics at different buses

The following section shows the voltage harmonics at individual buses during the disconnected case:
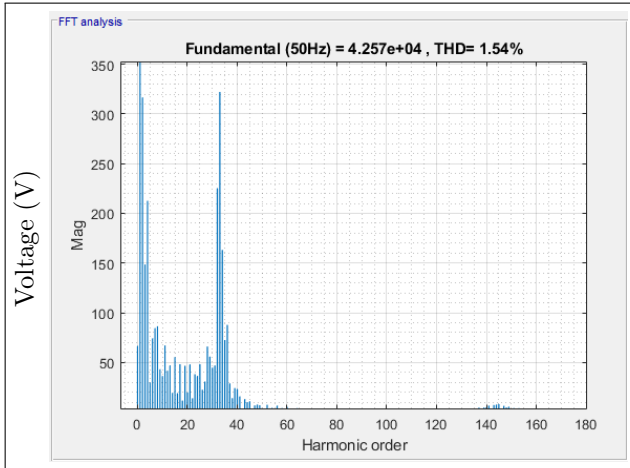
Figure 45: Disconnected case voltage THD bus 633
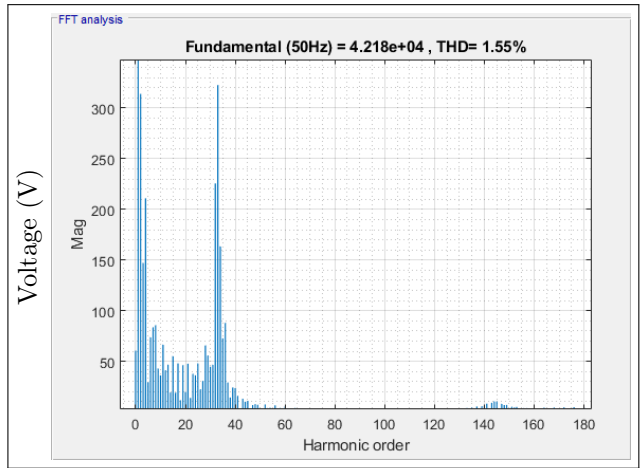
Figure 46: Disconnected case voltage THD bus 645
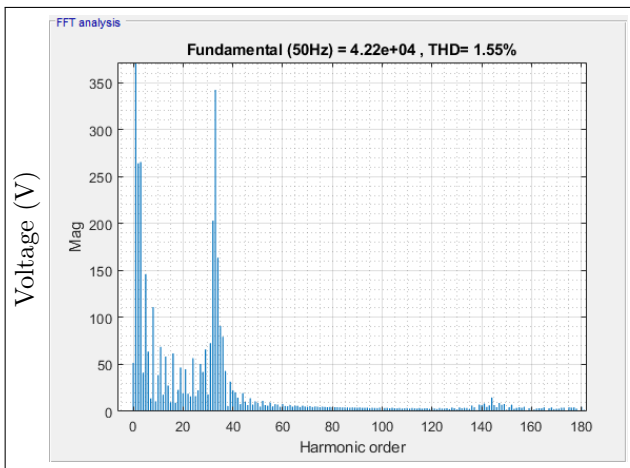
Figure 47: Disconnected case voltage THD bus 646
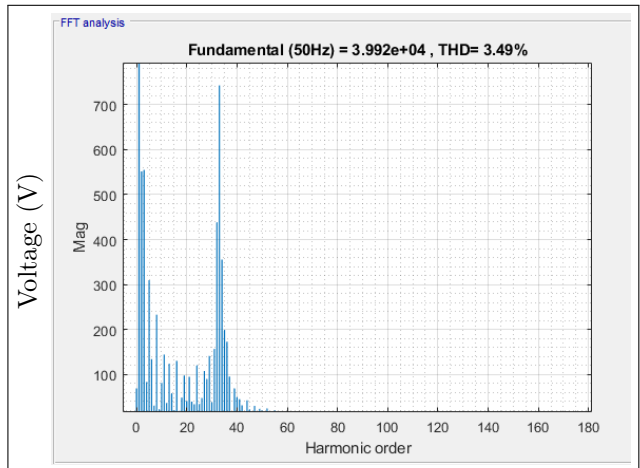
Figure 48: Disconnected case voltage THD bus 611
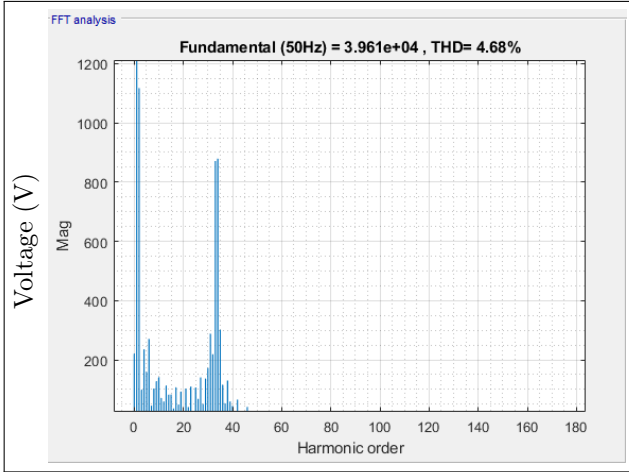
Figure 49: Disconnected case voltage THD bus 652
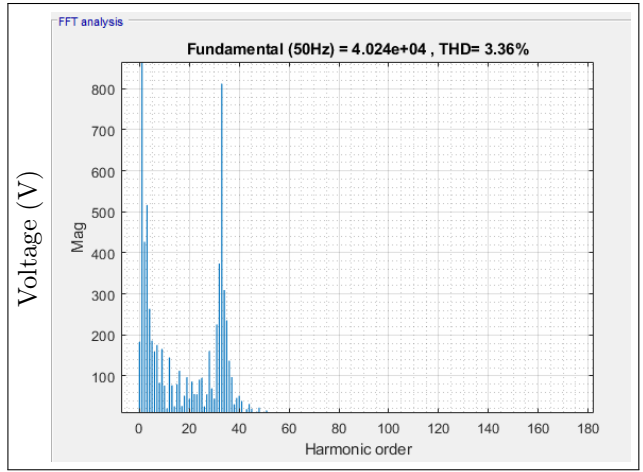
Figure 50: Disconnected case voltage THD bus 684
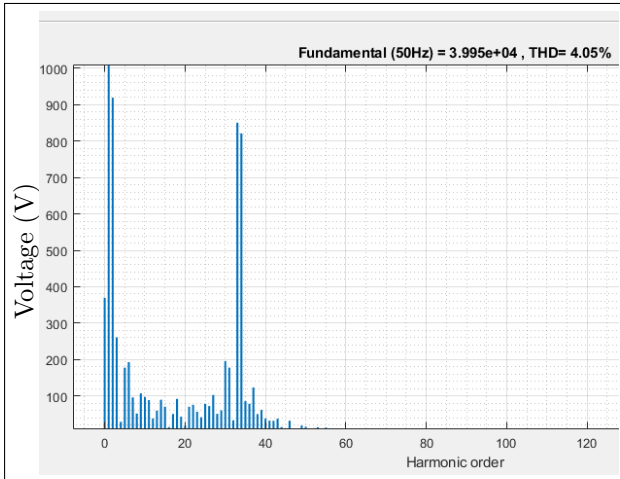
Figure 51: Disconnected case voltage THD bus 680
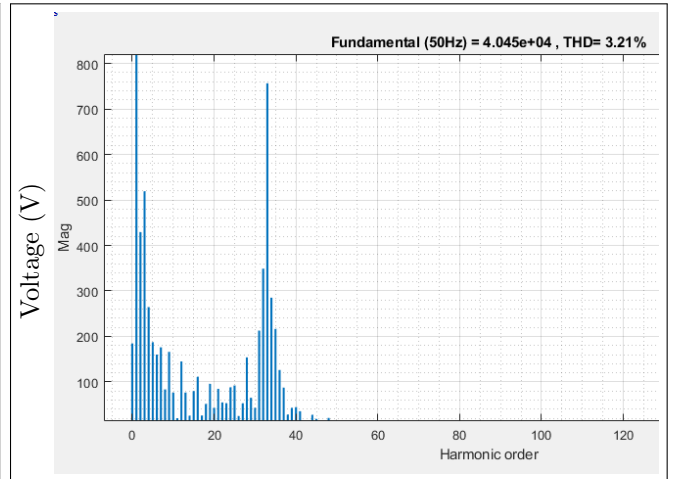
Figure 52: Disconnected case voltage THD bus 671

The above figures represent the voltage harmonics at various buses of the grid. The most recurring disturbing harmonic as can be seen from the figures is the 35th harmonic order. These figures are discussed further in the section 6.

5.5   Change in wind speed

The following figure (53) shows the current control scheme of the converter. The dynamics of the wind speed is represented by ramp functions (encircled in red). The wind speed dynamics are assumed to be uniform for all wind turbines, that is, a change in wind speed will be assumed to affect each wind turbine equally regardless of their location.
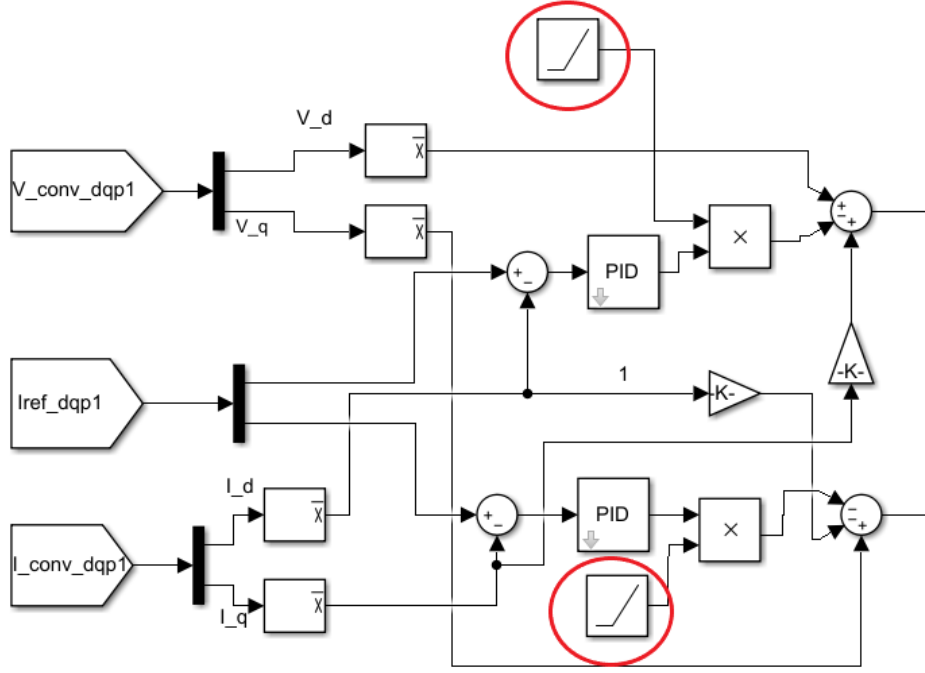
Figure 53: Ramp functions representing the wind speed dynamics

A ramp function is used to represent the dynamics of the wind speed. The idea is to choose the ramp parameters which produce an output closely resembling the Wind Energy Ramp tool as used in [46]. This tool as discussed by Bianco et al, creates a ramp event with wind power changing approximately as a cube of wind speed. If a large and sudden change in wind speed occur, it can produce a huge dynamic in wind power generation. Therefore, a balance is needed in order to keep the dynamics compensated. A large sudden change in wind power generation can be economically and physically damaging to the grid, especially if it is neither forecast nor be controlled in real time. [47].

In this thesis, the two ramp functions are connected to the respective PI controllers in the DQ current controller. Intially, the wind speed is considered to be driving the wind turbines to the rated output as in the base case. The ramp functions are activated after 0.25 s. They are defined with a negative slope to decrease the wind speed during the simulation. Hence, the output of the turbines will keep on decreasing continuously as can be seen from the figure (54).

5.5.1 Bus Voltage Waveforms

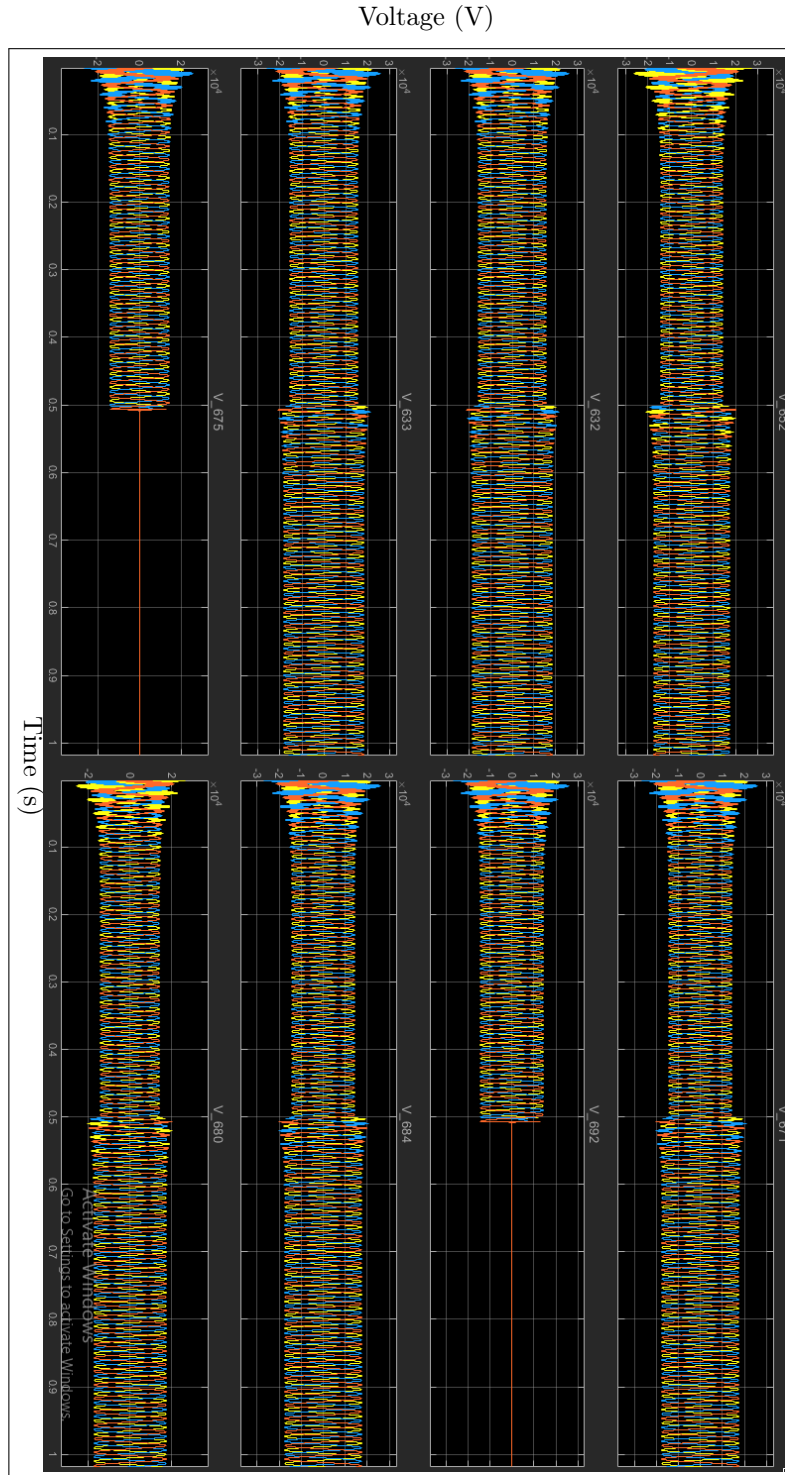The following section shows the voltage waveforms at individual buses during the wind dynamics case:
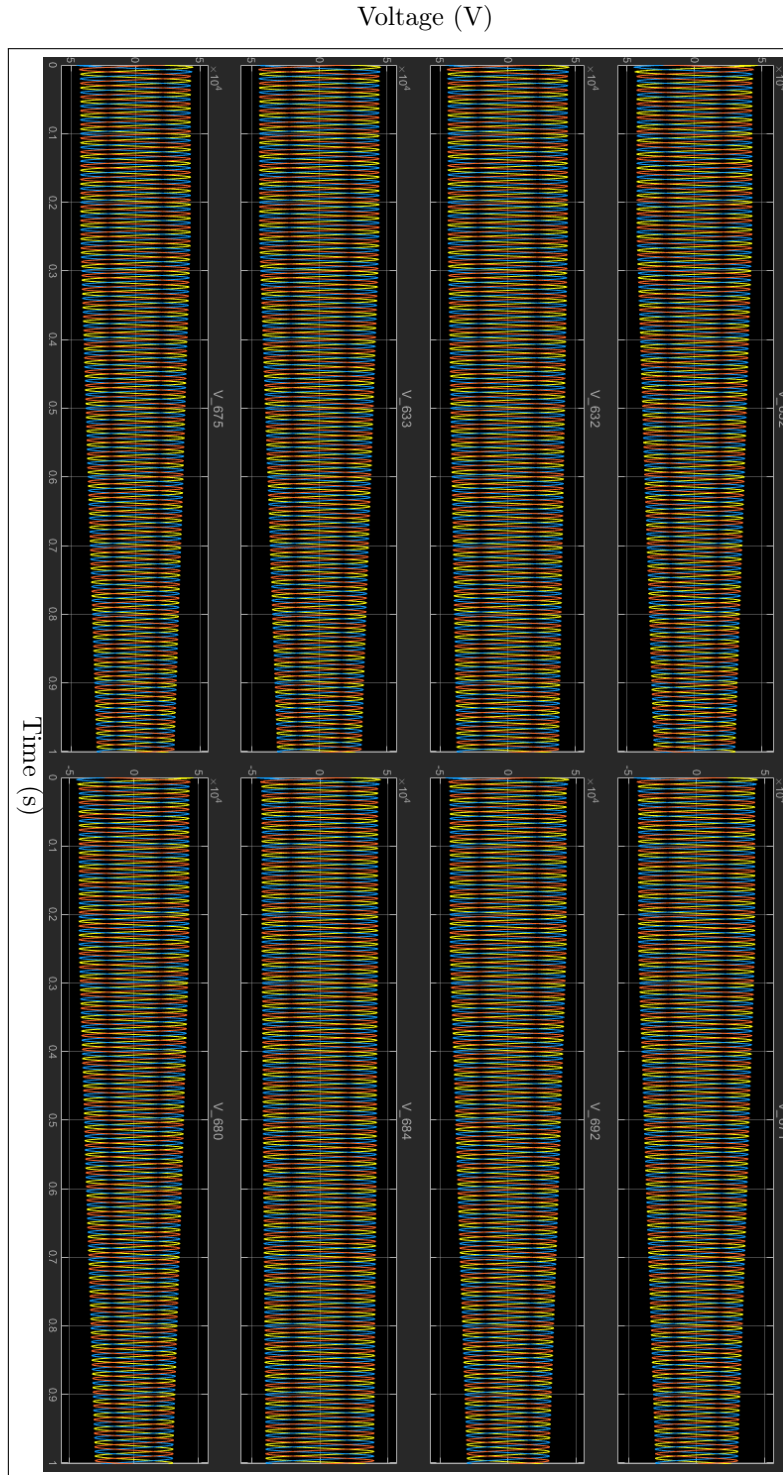
Figure 54: Voltage waveforms with constant wind speed dynamics

5.5.2 Wind turbines Output Power

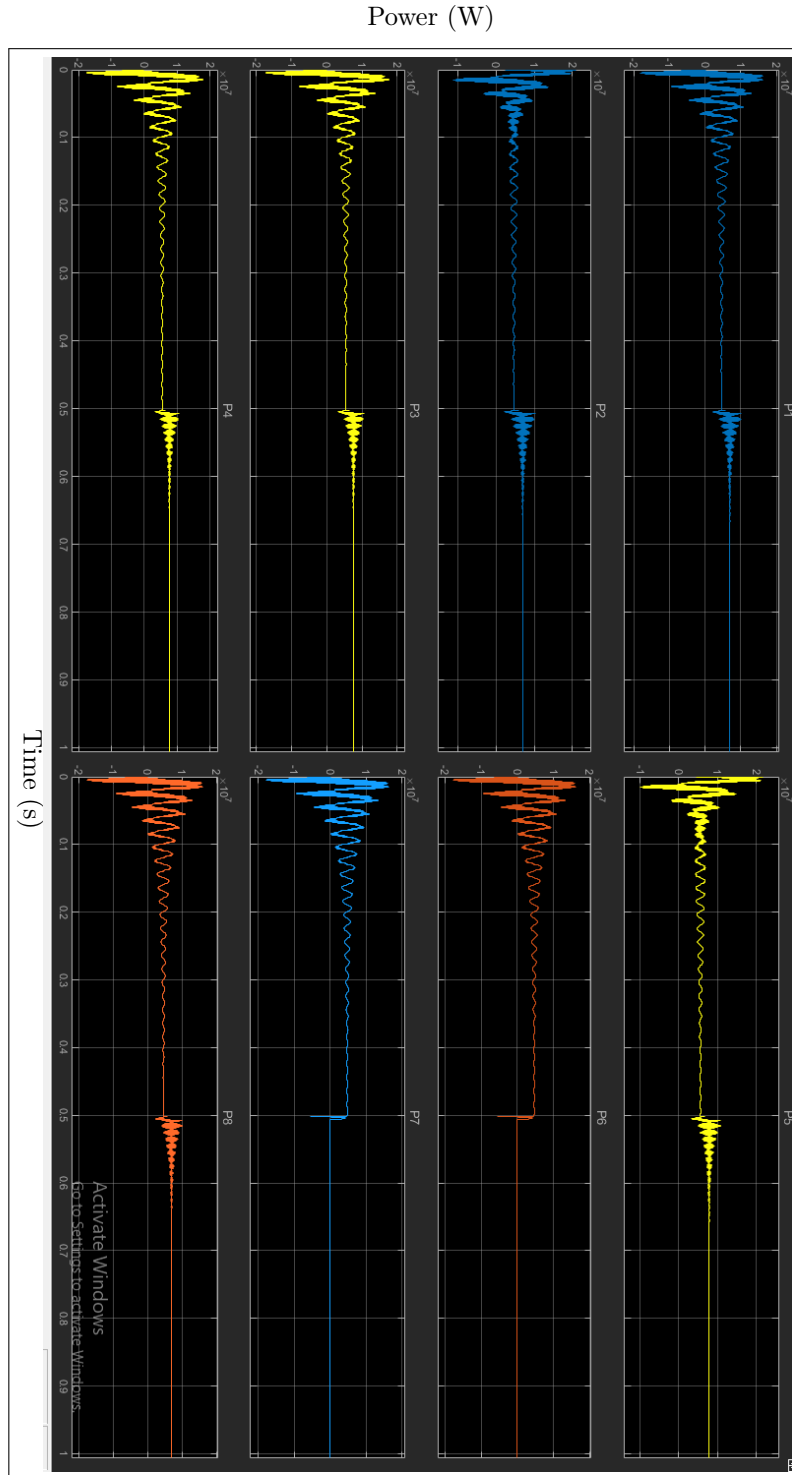The following section shows the output power of individual wind turbines during the wind dynamics case:
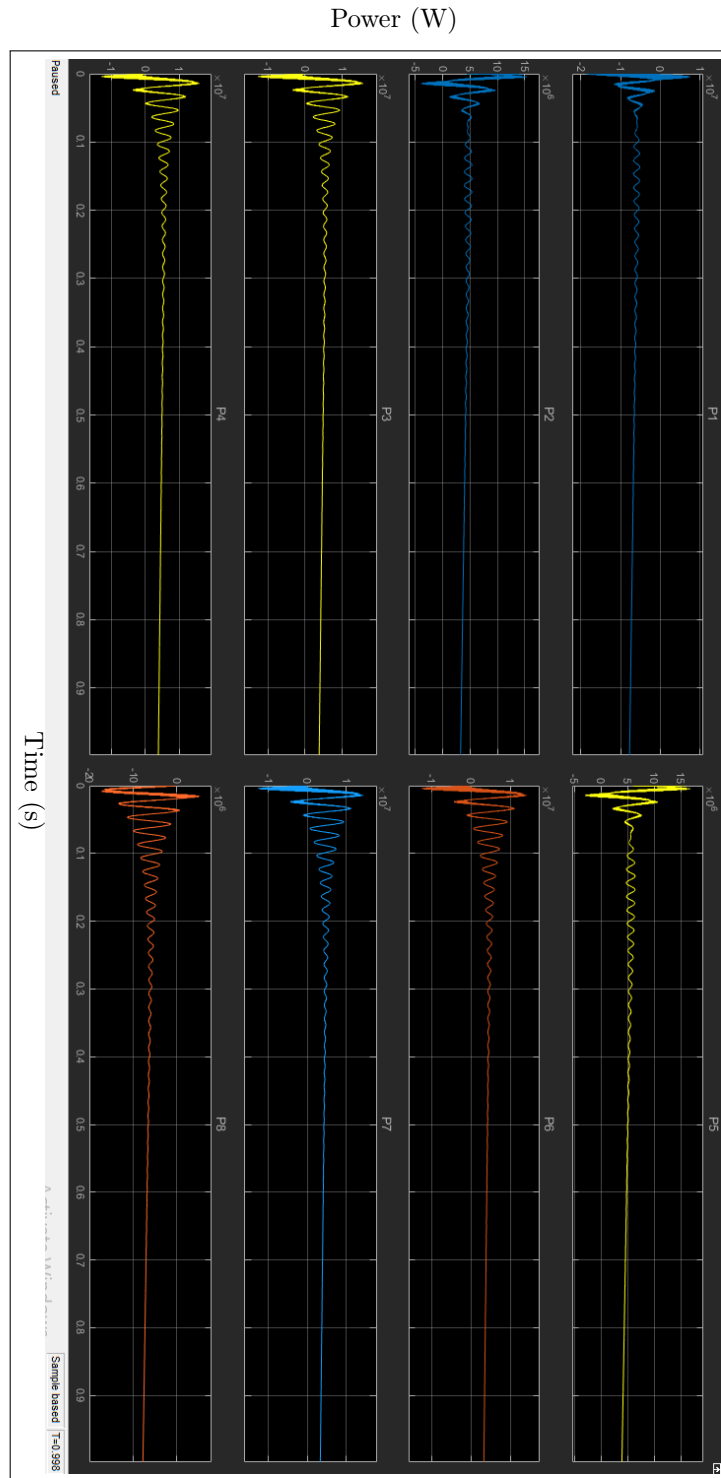
Figure 55: Power waveforms with constant wind speed dynamics

5.5.3 Voltage harmonics at different buses

The following section shows the voltage harmonics at individual buses during the wind dynamics case:
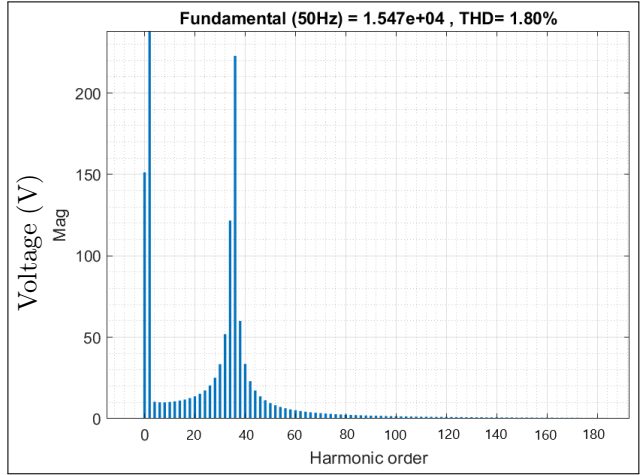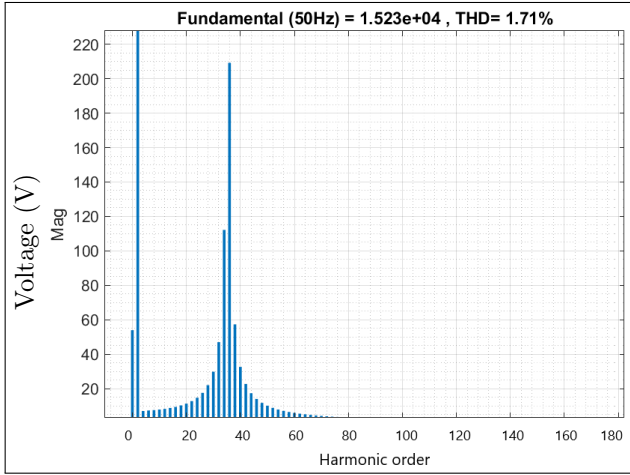
Figure 56: Wind dynamics case voltage THD bus 646

Figure 57: Wind dynamics case voltage THD bus 633
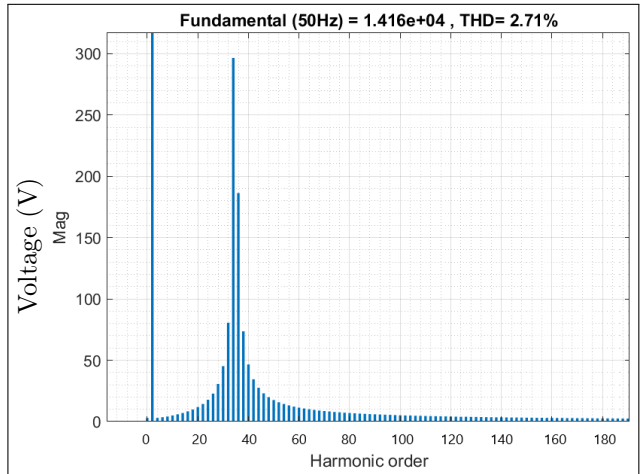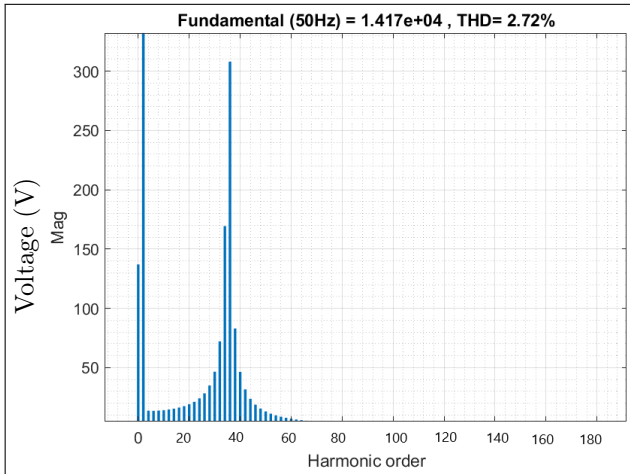
Figure 58: Wind dynamics case voltage THD bus 652

Figure 59: Wind dynamics case voltage THD bus 680
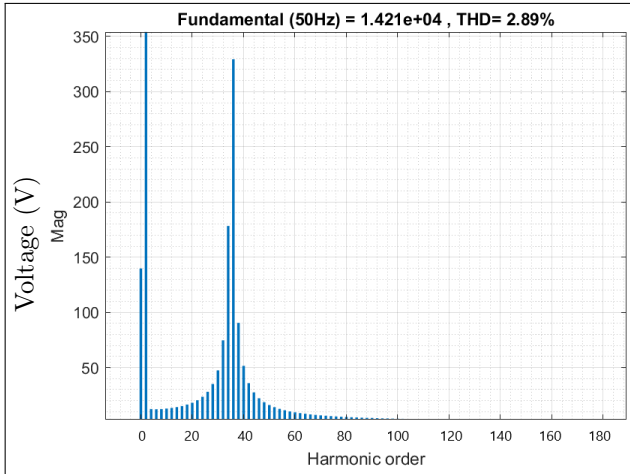
Figure 60: Wind dynamics case voltage THD bus 684
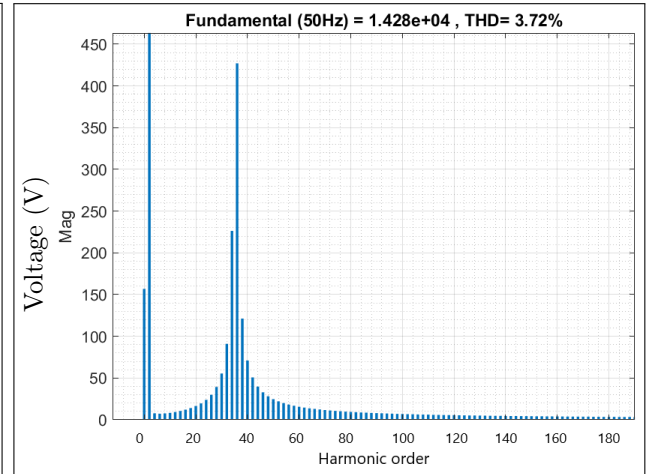
Figure 61: Wind dynamics case voltage THD bus 671
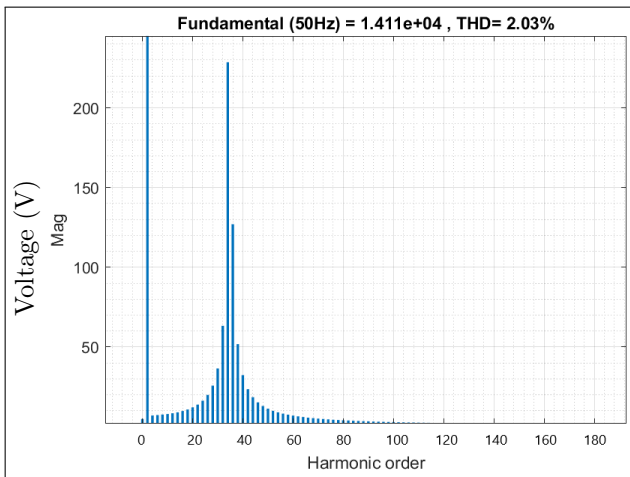
Figure 62: Wind dynamics case voltage THD bus 611
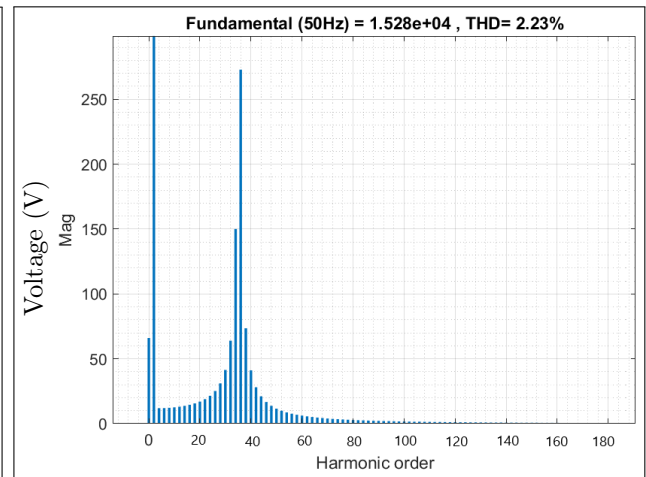
Figure 63: Wind dynamics case voltage THD bus 645
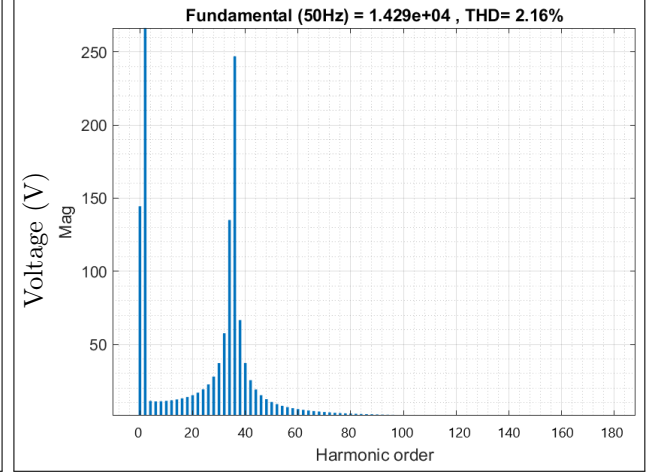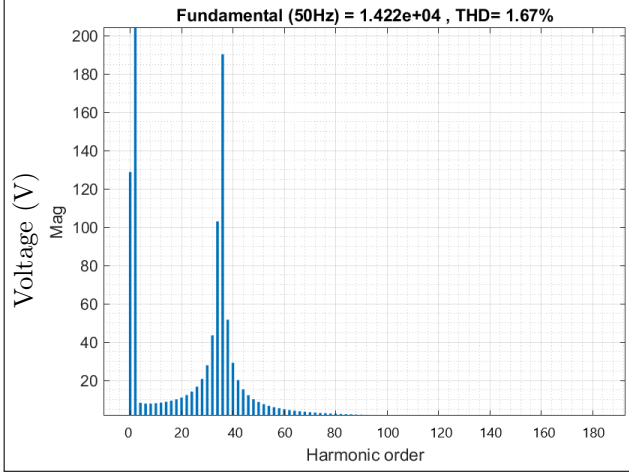
Figure 64: Wind dynamics case voltage THD bus 675 Figure 65: Wind dynamics case voltage THD bus 692

These figures are discussed in detail in the section 6.

5.6 Worst Case Scenario

The following section observes the worst case scenario for the offshore grid network. Previously, we have seen the results of harmonic propagation through the network in case of disconnecting a part of the grid, de-tuned control system and wind speed dynamics. Prior to these cases, a frequency sweep was carried out and we found the resonant frequencies of the network.

The worst case scenario is obtained by a combination of the above cases. The wind turbine has a de-tuned control system coupled with continuously changing wind turbine power output through wind speed dynamics, in addition to disconnecting a part of the grid at a certain moment. Furthermore, the switching frequency is kept close (within 1%) to the resonance frequency. This would enhance the possibility of the harmonic resonance occurring in the network.

5.6.1 Bus Voltage Waveforms

The following section shows the voltage waveforms at individual buses during the worst case:
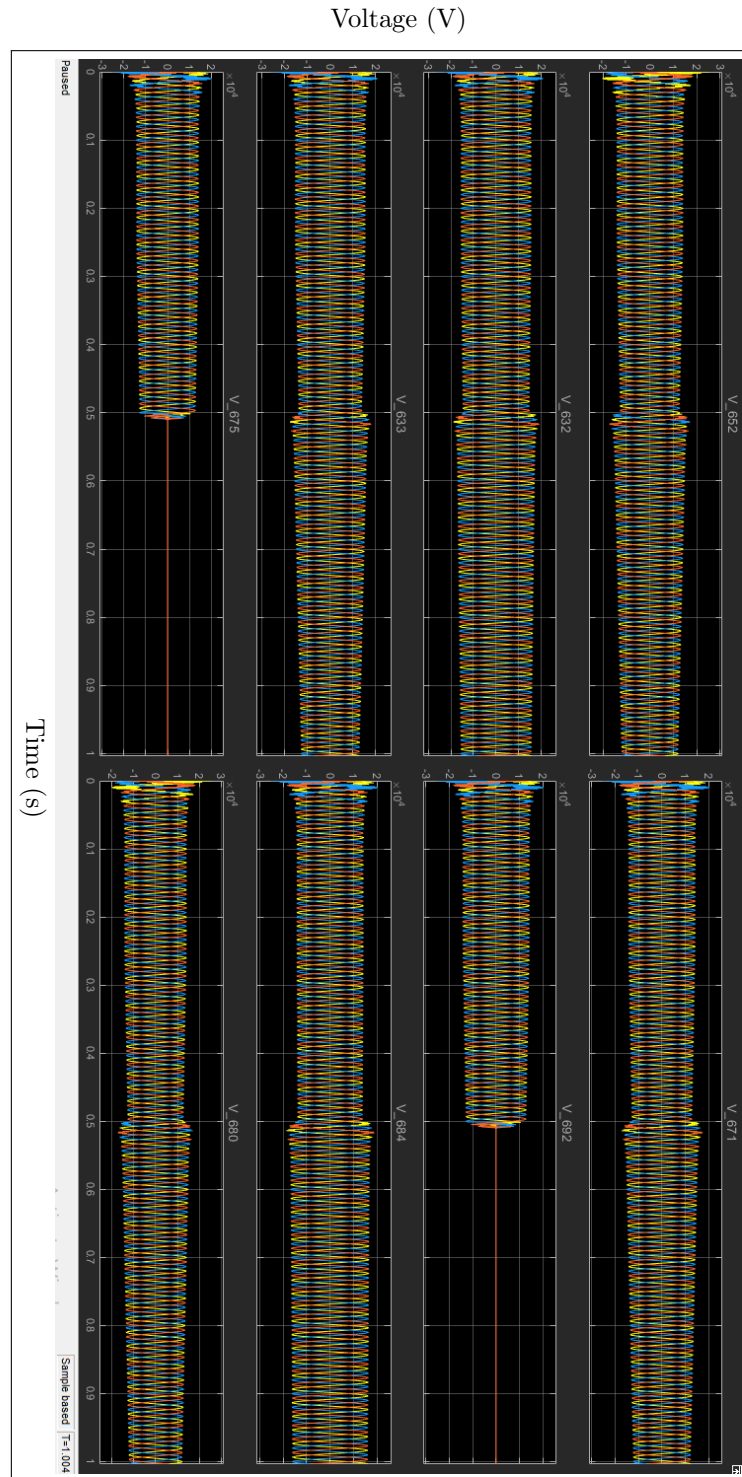
Figure 66: Voltage waveforms under worst case scenario

5.6.2 Wind turbines Output Power

The following section shows the output power of individual wind turbines during the worst case:
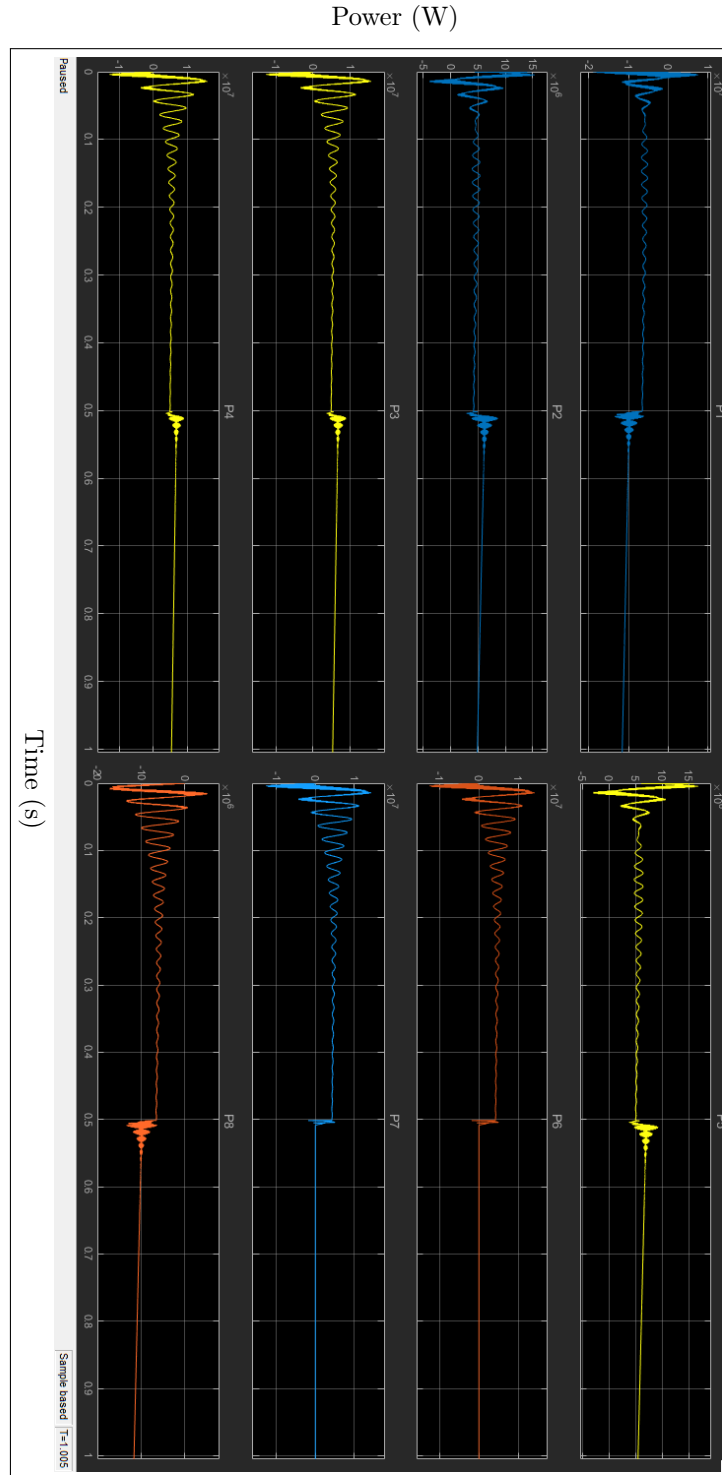
Figure 67: Power waveforms under worst case scenario

5.6.3 Voltage harmonics at different buses

The following section shows the voltage harmonics at individual buses during the worst case:
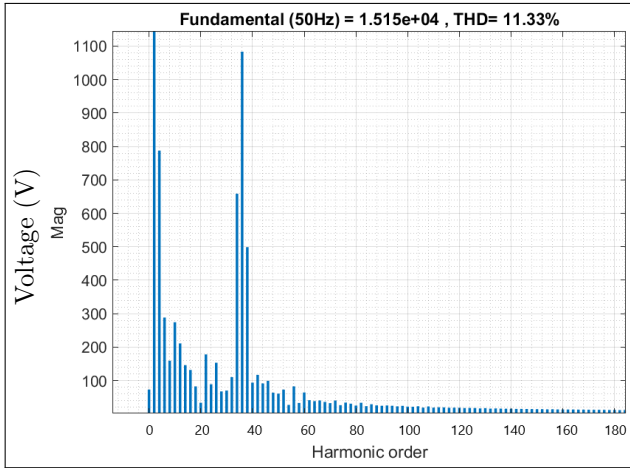
Figure 68: Worst case voltage THD bus 646
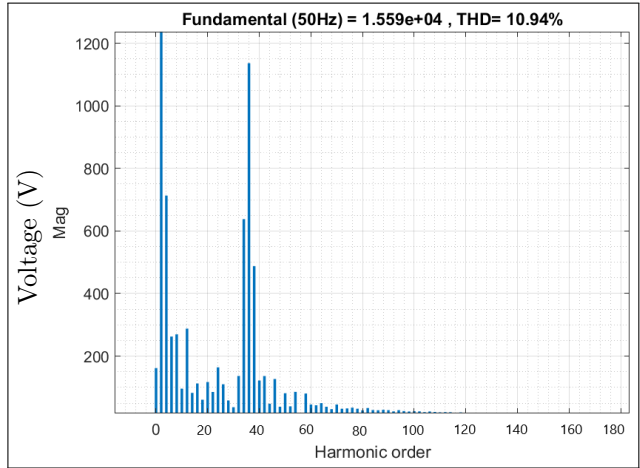
Figure 69: Worst case voltage THD bus 633
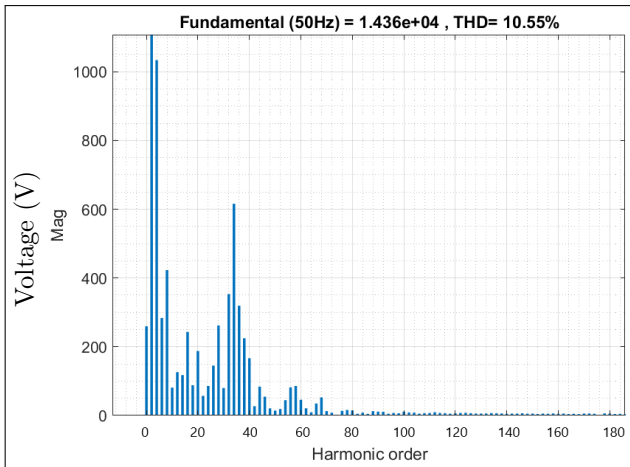
Figure 70: Worst case voltage THD bus 652
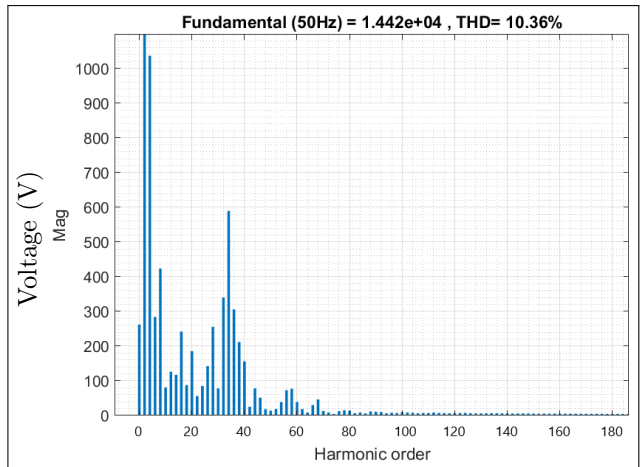
Figure 71: Worst case voltage THD bus 680
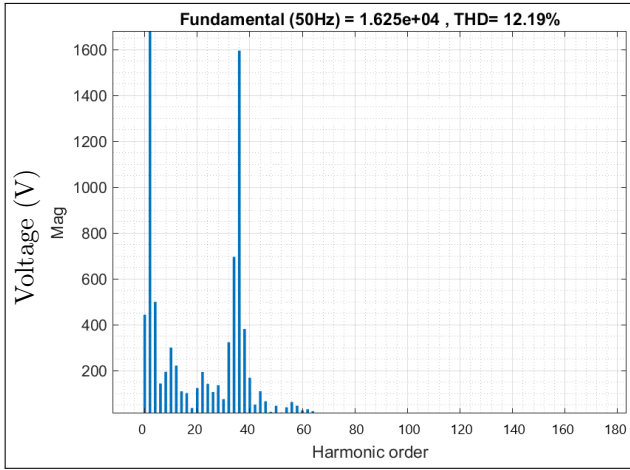
Figure 72: Worst case voltage THD bus 684
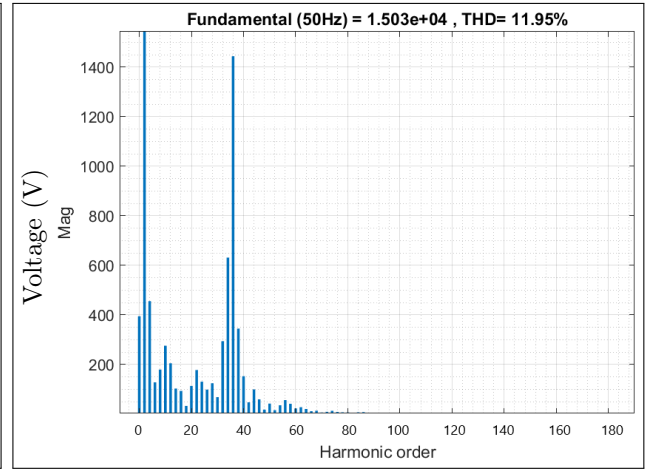
Figure 73: Worst case voltage THD bus 671
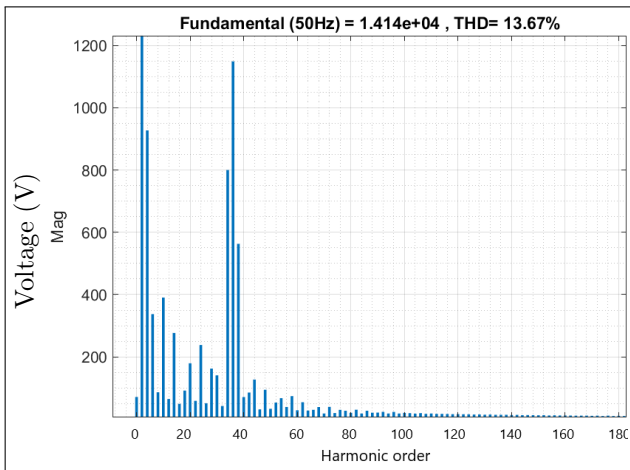
Figure 74: Worst case voltage THD bus 611
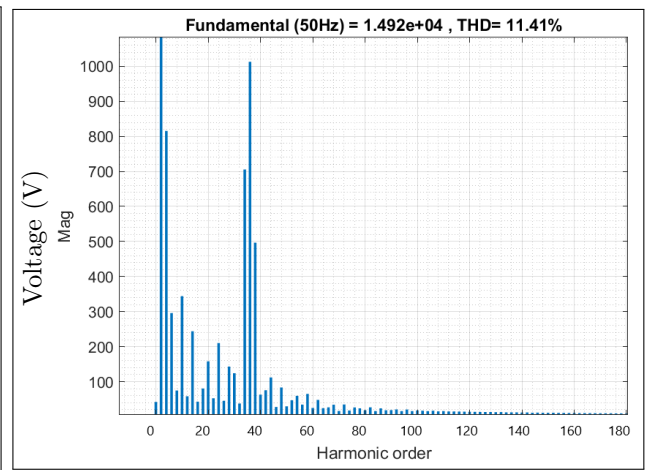
Figure 75: Worst case voltage THD bus 645

These figures are discussed in detail in the section 6.

6 Discussion

This section deals with in-depth analysis of the results obtained in the previous sections. There will also be a discussion of high frequency harmonics from a component based previous study. Finally, the limitations of the thesis will be discussed.

6.1 Result Inference

From table (5), it can be seen that for the modelled network, the resonant frequencies are found to be 1250 Hz, 1750 Hz, 7050 Hz and 9050 Hz. As mentioned before, these frequencies are the result of the frequency scan of the modelled network.

1. Starting the discussion with the peak voltage at each bus, it is approximately $\sqrt{2}$ times the base voltage of the grid. With the base voltage being 33 kV, the peak voltage at each bus should be around 46.6 kV, while at bus 634 it is 6.776 kV (because of the transformer) as can be seen in figure (26). From the same figure (26), it can be seen that there is some disturbance at the start of the voltage waveforms of most buses. This disturbance arises due to the converter switching of the wind turbines. It stabilises within few microseconds. When a certain part of the grid is disconnected amid a continuous operation, 2 turbines at buses 692 and 675 respectively gets disconnected from the grid. This would make the voltage across these buses drop to 0, causing overvoltage in the rest of the network. It is assumed that the rest of the network has enough capacity to compensate for this overvoltage and hence we observe raised voltage drops on the rest of the buses as seen in figure (43. Next scenario was the change in wind speed. A continuously decreasing wind speed was modelled. With the decrease in wind speed, the voltage across each turbine would decrease [48] as shown in figure (54). The final case was the worst case scenario representing a combination of the above two cases coupling with a de-tuned filter. With wind speed continuously decreasing and then a part of the grid is disconnected. The voltage across each turbine decreases continuously with wind, but suddenly have an upward spike to accommodate the overvoltage created by the disconnection of the part of the grid as shown in figure (66).

2. For the output power, the base case delivers the rated output for each wind turbine. The rated active power (P) is chosen to be 5 MW with 0 rated reactive power (Q). Compared with the voltage waveforms, the power waveforms take a little longer time to give stable output as shown in figure (27). For the disconnection case, the turbines at buses 692 and 675 would cease their contribution to the grid after being disconnected. Thus to maintain power balance from the wind farm to the grid, the rest of the turbines would have to compensate by increasing their output as seen in figure (44). However, if the turbines are already working at their maximum limit, then their output would not increase. In the next case, by continuously decreasing the wind speed, the output of each wind turbine would also decrease continuously and hence will decrease the power injected by the wind farm to the grid. This could cause shortage of power in the distribution side of the grid and hence the power grid operator has to constantly keep the power balance in check [6]. The continuous decrease in wind power is shown in figure (55). In the final case, there will be a continuous decrease in each turbine output. Then there is the disconnection of buses 692 and 675 which momentarily increases the output of the rest of the turbines to compensate for the lost power as shown in figure (67).

3. Moving on to the harmonic analysis at the turbine, during the base case the magnitude of voltage harmonics at the converter side of the turbine is 0.99%. The contributing order of harmonics are quite scattered. According to the frequency sweep of the converter side of

the turbine, as shown in figure (23), the resonating frequencies are 850 Hz ,1250 Hz, 6050 Hz and some further high orders. The maximum voltage distortion occurs at 5th harmonic order followed by 63rd and 57th harmonic order as shown in figure (29). There is also some distortion at higher order like 119th and 121st. The magnitude of current harmonics is 2.48 % and the major contributing harmonic order is 5th followed by 3rd and 7th as shown in figure (28). Higher frequency harmonics of the order 47th and 49th are present with little influence over the harmonics magnitude and propagation. Both voltage and current harmonics are within the standard acceptable limit as specified in the tables (2) and (3). In comparison, the case of de-tuned control system has a similar distribution of current harmonics with same harmonic orders (5th, 3rd and 7th) responsible for maximum distortion as shown in figure (40). However, the difference lies in the voltage harmonics as shown in figure (41). There is increase in the magnitude of voltage THD as well as higher order harmonics such as 41st, 49th, 51st, 59th 91st, 93rd, 109th, 111th, 141st, 159th and 181st have a significant impact on the THD. However, the THD levels in this case also lie within the standard acceptable limit as specified in the tables (2) and (3).

4. The inference drawn from above comparison is that even after de-tuning the control system, the passive LCL filter does a remarkable job in maintaining constant current THD value. The rise in voltage THD value can be attributed to the rise in voltage harmonics at the PCC. A scheme utilizing virtual impedance to emulate harmonic voltage shifts can reduce the voltage harmonics at the PCC as performed in their work by Shukla et al. in [49]. The above results are comparable with the results of ITHD and VTHD by Yusran et al. in [50].

5. Finally, let us discuss the analysis of voltage harmonics at individual buses. Since an ideal grid is considered during this thesis, the current harmonics remain static but voltage harmonics change due to the voltage drop over the passive elements of the offshore network. This lead to an investigation based on voltage THD to study the harmonic propagation under different cases inside the modified IEEE-13 bus node feeder. During the base case, the magnitude of voltage harmonics is very small (0.01 % THD). This is expected since the grid is modelled in such a way so as to compensate the harmonic content. This reduction in voltage THD values at the buses (medium/high voltage) has been observed in previously by Costea et al. in [51] and is considered a normal process. The small distortions are mainly due to the harmonic orders 5th, 7th and 9th. However, significant higher order harmonics can also be seen in the figures (30 - 39). These higher order harmonics include 35th, 141st and 181st etc. order harmonics. Despite being negligible compared to the fundamental frequency, the occurrence of a significant 35th order harmonic represents the presence of harmonic resonance. While the wind farm was running at base speed, a certain part of the grid stopped working. Hence it was assumed to be immediately disconnected by the circuit breaker operation. This transition would inject further harmonic content into the network as can be seen from figures (45 - 52). The increased voltage THD values are reflective of the distance of the buses from the grid [52]. Buses 633, 645 and 646 being closer to the grid have an average THD of 1.55 % up from 0.01 % in the base case. The far most buses 611, 652 and 671 have much higher voltage THD with an avergae of 3.3 %, whereas the local PCCs including buses 684, 692 and 671 have much higher THD with an average of 4.5%. The major contributors to the large voltage THD are harmonic orders 3rd, 5th and high frequency harmonic order 35th. In several buses, harmonic orders 9th and 33rd have also contributed significantly to the voltage THD. Furthermore, looking at the base case, the wind speed changes continuously. An assumed continuous decrease in wind speed has been modelled using the ramp function. This would inject more harmonic content into the network. The voltage THD values for respective buses are comparable to those from the disconnection case as can be seen from figures (56 - 65). The effect of higher frequency harmonic order 35th is the most prominent for this increased voltage THD. This indicates the occurrence of har-

monic resonance. Lastly, we discuss the worst case wherein a part of the grid was disconnected coupled with a continuous change in wind speed. The figures (69 - 73) shows the voltage THD of different buses. The major THD contributing harmonic orders are 5th, 7th and 33rd but the most significant contribution came from 35th harmonic order which also represent the harmonic resonant frequency. The results for all the above cases were compared with the standard acceptable limit as specified in the tables 2 and 3. The voltage THD values for the base case are well within the acceptable limits. For the disconnection case and the wind speed dynamics case, THD values also do not violate the acceptable limits. However, for the worst case all the buses exceeded the standard voltage THD limits.

6. The above discussion answers the research question regarding the effects of harmonic resonance on the order and magnitude of harmonics inside the power system network. And by comparing the harmonic magnitude with the standard acceptable limit, the second research question regarding those harmonic orders causing significant damage is discussed as well. For the last question regarding the propagation of harmonics in the network, we observe that while navigating inside the network, as we move closer to the grid, the magnitude of voltage THD decreases continuously. This is noticeable from all the case scenario considered in this thesis. The reason is that the voltage drop over the passive elements (inductive, capacitive elements etc.) is responsible for the harmonic production and propagation. As we move towards the grid, the influence of active elements (the 3-phase AC voltage source in this thesis) grows and that of the passive elements declines. The magnitude of THD at the turbine produced during the base case is comparable with real wind turbine data. The voltage THD being 0.99 % and the current THD being 2.48 %. The most dominant harmonic order is the 5th order during the base case, but when the control system is de-tuned the voltage THD changed drastically in magnitude (2.53 %) and harmonic order (with higher order frequencies more dominating). Meanwhile, the current THD did not change significantly at 2.53 %, with the 5th harmonic order staying the most dominant.

6.2 Impact on cable termination

In this section, the effect of high frequency harmonics are discussed on a cable accessory. The cable termination has a copper core, with an outer XLPE insulation along with a resistive field grading type termination. During the component study done within the extra project, following results were obtained as shown in figures (76) and (77):
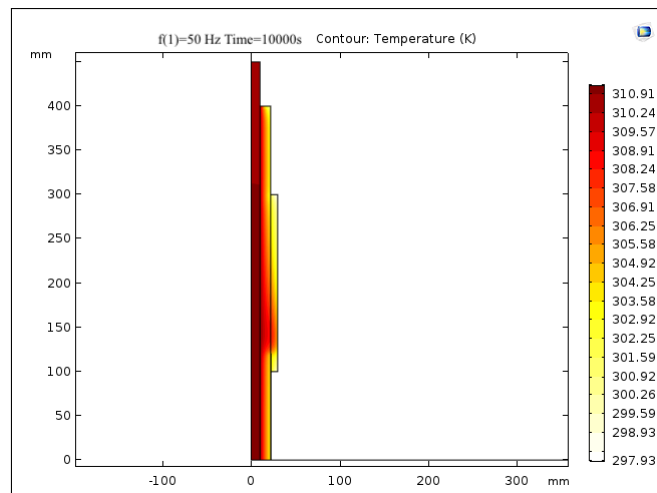
Figure 76: Temperature of Cable termination at fundamental frequency after being in operation for 10,000 s
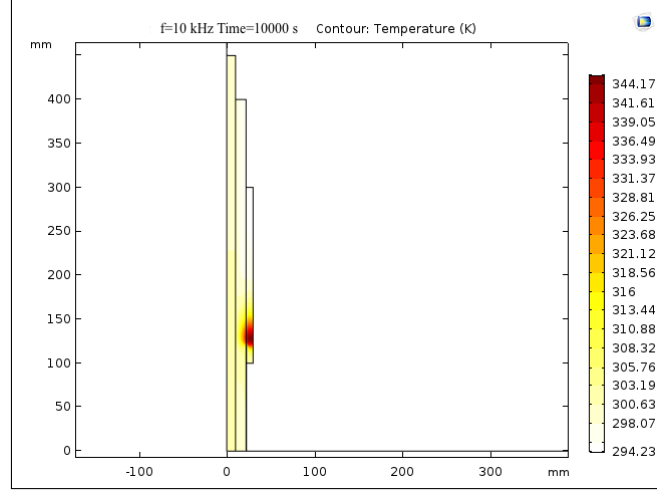
Figure 77: Temperature of Cable termination at higher frequency (10 kHz) after being in operation for 10,000 s

The above figures (76) and (77) represent a cable termination modelled in COMSOL Multiphysics software during the extra project. These graphs are the results of a thermal sweep for a full voltage operation at fundamental and higher frequency. We can observe that at the fundamental frequency, the rise in temperature within the conductor is the highest. However, at higher frequencies (10 kHz), the temperature rise at the junction of resistive stress grading layer and the insulation can be observed to exceed the temperature rise within the conductor. The reason is discussed in brief in the following paragraph.

For the extra project, the Dielectric spectroscopy measurements were conducted and the same experimental data was used in the modelling of the cable including electrical conductivity variation with temperature, and frequency. The results from the above figure depict increased temperature at the cable stress-grading layer (resistive) whilst exposure to higher frequencies. This is due to higher dielectric losses at higher frequencies, resulting in additional heating combined with an increase in AC resistance and copper losses [53]. During the component study, the issue about the rise of temperature at the cable stress-grading junction was solved by replacing the resistive stress-grading with a geometric type stress-grading arrangement. Based on the extra project, even under high frequencies, the phenomenon of overheating seemed to be unlikely in the cable termination. This was since the extra project was carried out under the nominal voltage at high frequency. For complete results regarding the component study and experimental data please contact the author.

From the results of section 5, it is clear that the converter switching in a wind farm leads to the generation of high frequency harmonics. Thus, the component based study is mentioned to provide a comparison between the effects of normal (50 Hz) and higher frequencies (10 kHz) on the individual cable accessory.

6.3   Applicability to a generalized power system

In this thesis we have developed a modified IEEE-13 bus network which accommodates an offshore wind farm. The wind farm constitute of 10 wind turbines connected at various nodes of the network as shown in figure (B.1.1). The results in section 5 are based on the simulation of an offshore wind farm network. However, in the previous section 4, the network is also proposed to work as an onshore grid with 5 wind turbines located at the buses 633 and 652 respectively. Thus, the network can serve as an onshore as well as offshore grid. The modeling

done in [41] depicts another modified IEEE-13 bus network working with a wind farm and a solar PV farm connected at the same buses 633 and 652 respectively. All these studies show that the IEEE-13 bus network can be modified to work not only as an offshore wind farm as shown in this thesis but as an onshore wind farm network as well as a solar PV farm network. Keeping in mind the capacity of the grid, harmonic propagation from various power systems can be studied with this network.

6.4   Limitations

The network modelled in this thesis to represent an offshore wind farm provides an insight into harmonic study into the network within the discussed case scenarios. The scale of the wind farm is too small (10x5 MW) to obtain detailed results for a real offshore wind farm. As discussed during the harmonic propagation, the magnitude of harmonics will be influenced with the number of wind turbines and/or by changing the grid capacity. For example, during the sudden loss of two turbines as shown in section 5.4, the THD at bus 684 changes from 0.01% during the base case to 3.36%.

The control system has been modelled to deal with the grid side harmonics. Hence it neglects the converter side model which actually simplifies the model for the study concerning this thesis. However, this causes variation with the real life processes like changing wind speed speeds etc. In the thesis this case has been simulated with an assumption of unidirectional change of wind speed.

Another deficiency is the recognition of the existing harmonic standards that only the harmonic currents are measured. For wind turbines, harmonic currents measured at the wind turbine terminals are the vector sum of the wind turbine harmonic current distortion, and the background harmonic voltage from the grid [25].

Finally, the grid is assumed to be ideal. It means that the distribution side grid is assumed to inject no harmonics in the modelled generation side of the grid. This might result in slightly reduced grid side harmonics for this thesis. Using a distribution side grid with real parameters may cause certain changes within the harmonic generation and propagation.

7 Conclusion

The general outcome of this thesis is considered as positive due to the fulfillment of the stated research questions. The observed phenomena has been explained from the power system point of view and simulations have been carried out to verify the same. The successful results of the thesis can be evaluated by the achievement of the objectives. Following conclusions can be drawn:

- Grid integration of wind turbines via a VSC lead to the injection of certain harmonics into the grid. The system operates well with a perfectly tuned filter in several contingencies. However, with a detuned-filter and combined contingencies the harmonic generation violates the acceptable limit.

- For a general wind farm, the most dominating harmonic order is usually 5th order. That is the case in this thesis as well until the contingency cases highlight the occurrence of harmonic resonance. This phenomenon is responsible for the generation of higher order harmonics.

- A tuned passive LCL filter is used to suppress the occurrence of higher order harmonics. The combined model had 5th, 7th and 35th order harmonics as the most dominant ones. The 35th harmonic order also represents the resonance frequency from the frequency scan of the network and hence signifies the occurrence of harmonic resonance into the network.

- The harmonic propagation occurs from the passive elements towards the active elements of a network. The magnitude of harmonics decreases continuously as they move towards the grid. While active filtering might be used to minimise the production of these harmonics, it is beyond the scope of this thesis.

The results of this thesis should be used to compare the harmonic propagation in the most common disruptive scenarios of a grid-connected wind farm.

8 Recommendations and Future Work

This thesis dissertation focused on broadening the scope of study for the harmonic propagation in the offshore wind farms. A suggestive model utilizing a modified IEEE-13 node feeder to represent an offshore wind farm has been proposed. Based on the Simulink modelling and result analysis, following areas could be worked on in further expanding the harmonic study of offshore wind farms:

- Expanding the number of wind turbines connected to the network to resemble a real offshore wind farm. A more complex standard network might be needed to accommodate more number of wind turbines. This could yield insightful results in harmonic propagation. Further, the harmonic resonance could be studied at a larger scale. The results of higher node feeders could be compared with the results of this thesis.

- Modelling converter side of wind turbine. This includes a a/synchronous generator which utilize the energy from the wind to produce torque and require a modification in the converter side control system for controlling the AC-AC converter.

- A more realistic model for studying bidirectional change of wind speed could be developed. This could be done by designing the mechanical side of the turbine, along with all the data from real wind turbines. The wind energy would rotate the turbine generator depending upon the wind speed (and direction) data from the references.

- Expanding the filtering technique used in the offshore wind farms. This thesis used the conventional passive filtering from the LCL filter to tune the turbine output. However, further studies into active filtering techniques might yield some new results.

- For practical purposes, a harmonic measurement scheme at the point of common coupling (PCC) between the transmission/distribution side grid and the generation side grid should be present. These measurements provide data for modeling pre-existing harmonic distortion

- This study was done within the university without any external collaborations. This means that any use of parameter or data was subject to their availability and accessibility to master students. Mostly the data used in real wind farms are kept confidential by the responsible TSO/production company. Thus for obtaining the real parameters used in wind farms, a collaboration with one of the TSOs handling the grid - wind farm connection could be extremely helpful.

Appendices

A   Model Parameters

A.1   Load Flow data

Bus A	Bus B	Length of line (m)	Configuration
632	645	152.4	601
632	633	152.4	601
633	634	0	XFM-1
645	646	91.4	601
650	632	609.6	601
684	652	243.8	606
632	671	609.6	601
671	684	91.4	601
671	680	304.8	601
671	692	0	Switch
684	611	91.4	601
692	675	152.4	606

Table 6: Feeder Data

Bus	Active Power (kW)	Reactive Power (kVAR)
632	100	58
633	400	290
645	170	125
646	230	132
671	1255	718
692	170	151
675	843	462
611	170	80
652	128	86

Table 7: Power flow data

	Block type	Bus type	Bus ID	Vbase (kV)	Vref (pu)	Vangle (deg)	P (MW)	Q (Mv...	Qmin (Mvar)	Qmax (Mvar)	V_LF (pu)	Vangle_LF (deg)	P_LF (MW)	Q_LF (Mvar)	Block Name
1	RLC load PQ		632	33.00	1.0210	-2.49	0.02	0.01	-Inf	Inf	1.0210	-2.49	0.02	0.01	632 Yg PQ
2	Vsrc	swing	632	33.00	1.0210	-2.49	0.05	0.00	-Inf	Inf	1.0210	-2.49	7.92	1.57	Grid 1
3	Bus	-	652	33.00	1	0.00	0.00	0.00	0.00	0.00	1.0211	-2.54	0.00	0.00	Load Flow Bus10
4	RLC load I		692	33.00	1	0.00	0.00	0.00	-Inf	Inf	1.0209	-2.53	0.00	0.00	692 D I
5	RLC load PQ		675	33.00	1	0.00	4.60	4.00	-Inf	Inf	1.0208	-2.54	4.60	4.00	675 Yg PQ
6	RLC load 2		675	33.00	1	0.00	0.00	-1.00	-Inf	Inf	1.0208	-2.54	0.00	-1.04	675 Yg Z
7	RLC load PQ		671	33.00	1	0.00	0.39	0.22	-Inf	Inf	1.0209	-2.53	0.38	0.22	671 D PQ
8	RLC load PQ		671	33.00	1	0.00	1.04	0.69	-Inf	Inf	1.0209	-2.53	1.04	0.69	671 Yg PQ
9	Bus	-	633	33.00	1	0.00	0.00	0.00	0.00	0.00	1.0210	-2.49	0.00	0.00	Load Flow Bus3
10	RLC load PQ		634	4.80	1	0.00	0.50	0.36	-Inf	Inf	1.0209	-2.49	0.50	0.36	634 Yg PQ
11	Bus	-	645	33.00	0	0.00	0.00	0.00	0.00	0.00	1.0210	-2.49	0.00	0.00	Load Flow Bus5
12	Bus	-	646	33.00	0	0.00	0.00	0.00	0.00	0.00	1.0210	-2.49	0.00	0.00	Load Flow Bus6
13	Bus	-	680	33.00	1	0.00	0.00	0.00	0.00	0.00	1.0209	-2.53	0.00	0.00	Load Flow Bus7
14	Bus	-	684	33.00	1	0.00	0.00	0.00	0.00	0.00	1.0210	-2.53	0.00	0.00	Load Flow Bus8
15	Bus	-	611	33.00	0	0.00	0.00	0.00	0.00	0.00	1.0210	-2.53	0.00	0.00	Load Flow Bus9

Figure 78: Fully converged load flow analysis

A.3 Transformer data

The transformer data used in the modeling of the wind turbine transformer and in the modeling of the IEEE-13 bus network transformer at bus 634 is shown in table (8) and (9) respectively [39] [54].:

Data	Value
Nominal Power	5 MW
Nominal Frequency	50 Hz
Primary side voltage	33 kV
secondary side voltage	600 V
Winding 1	D1
Winding 2	Yg
R1 (pu) = R2 (pu)	0.002675
L1 (pu) = L2 (pu)	0.0375
Magnetization Rm (pu)	0.2
Magnetization Lm (pu)	0.0667

Table 8: Turbine Transformer data

Data	Value
Nominal Power	0.5 MW
Nominal Frequency	50 Hz
Primary side voltage	33 kV
secondary side voltage	480 V
Winding 1	Yg
R1 (pu)	0.011
L1 (pu)	0.02
Winding 2	Yg
R2 (pu)	0
L2 (pu)	0
Magnetization Rm (pu)	1.1
Magnetization Lm (pu)	2

Table 9: Turbine Transformer data

A.4 Wind turbine data

The following table (10) represents the base values and the parameters used in the wind turbine modeling

Data	Value
Base Power	5 MVA
Base Voltage	600 V
Base Impedance	0.2880 Ω
Base Inductance	0.91 mH
Base Capacitance	0.0111 F
Base Current	2.4 KA
Grid Frequency	50 Hz
Converter side Inductance (L1)	0.4 mH
Filter Capacitance	0.033 F
Grid side Inductance	34.1 μH
Damping Resistance	20.09 Ω

Table 10: Wind Turbine data

B MATLAB/Simulink

The section B of appendix shows the screenshots of MATLAB/Simulink models that were developed and used during the simulations. Feel free to contact the author for the full model or similar discussions.

B.1 Wind Parks

B.1.1 Offshore wind park
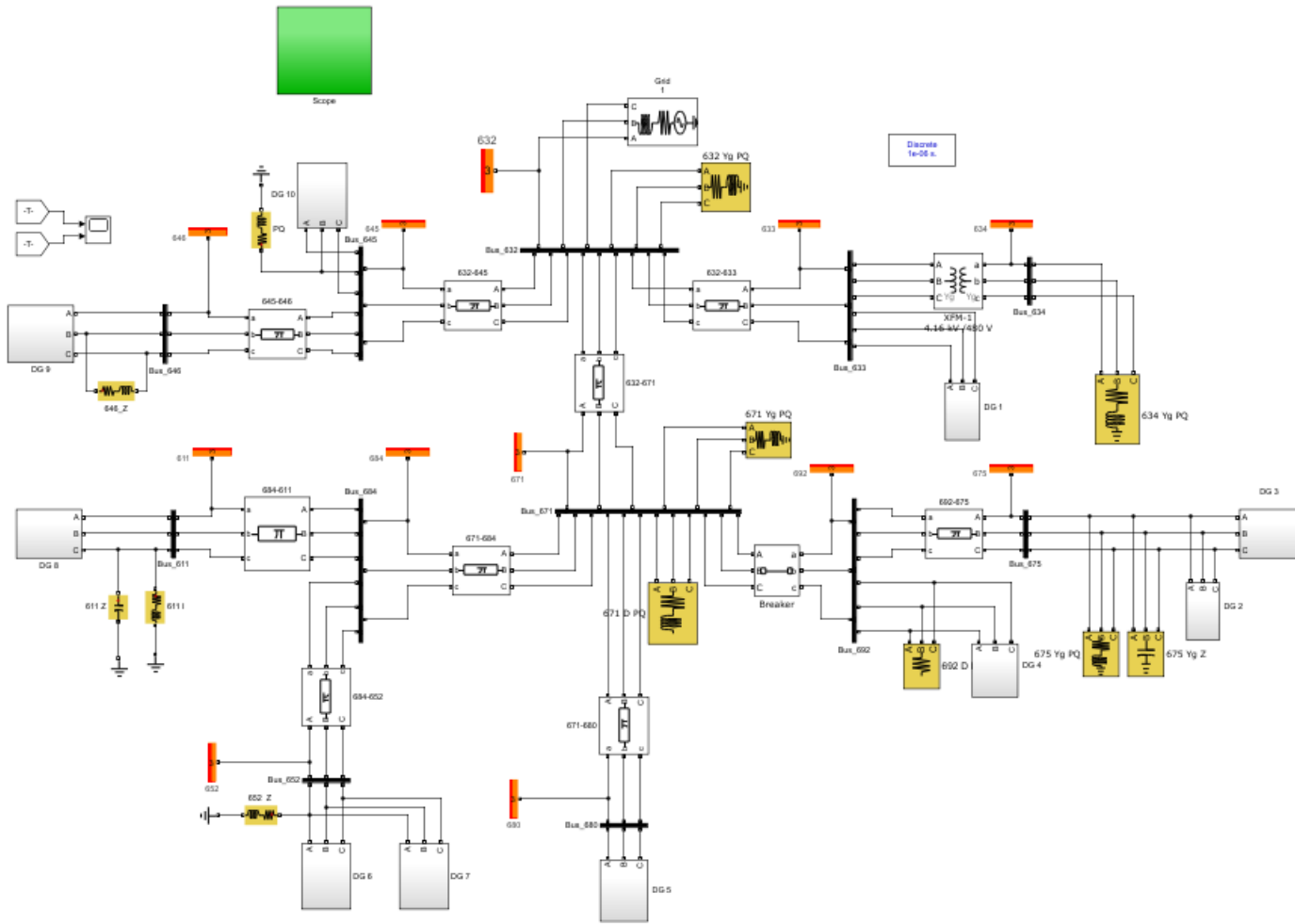

Figure 79: Offshore wind park
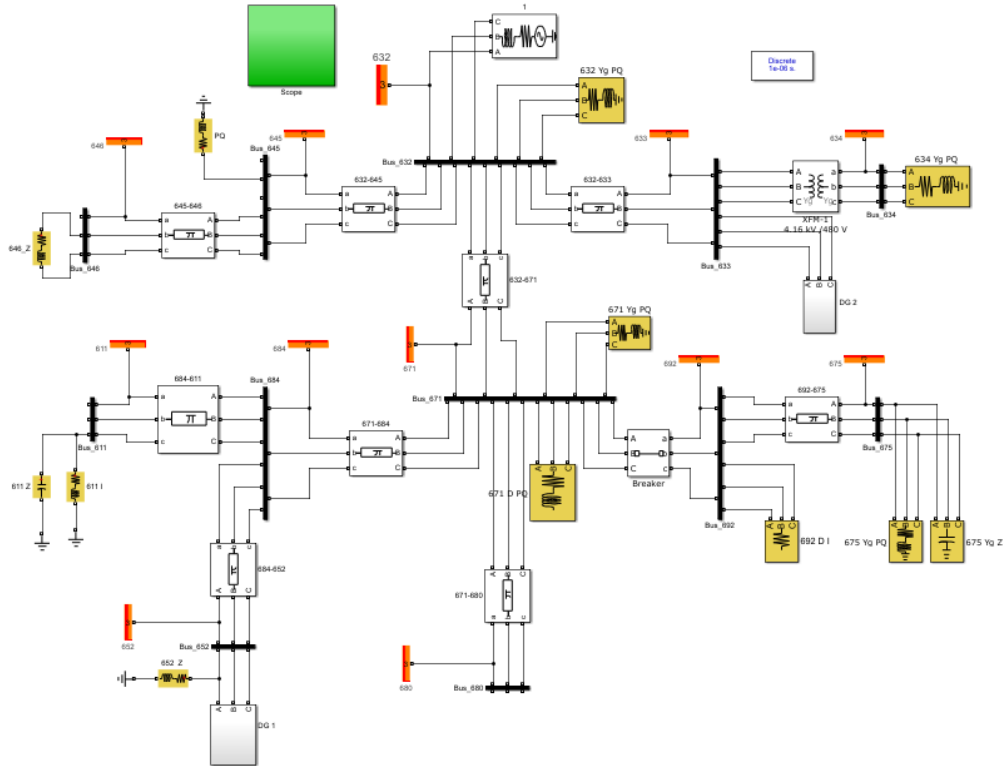
B.1.2 Onshore wind park

Figure 80: Onshore wind park

B.2 Wind Turbine
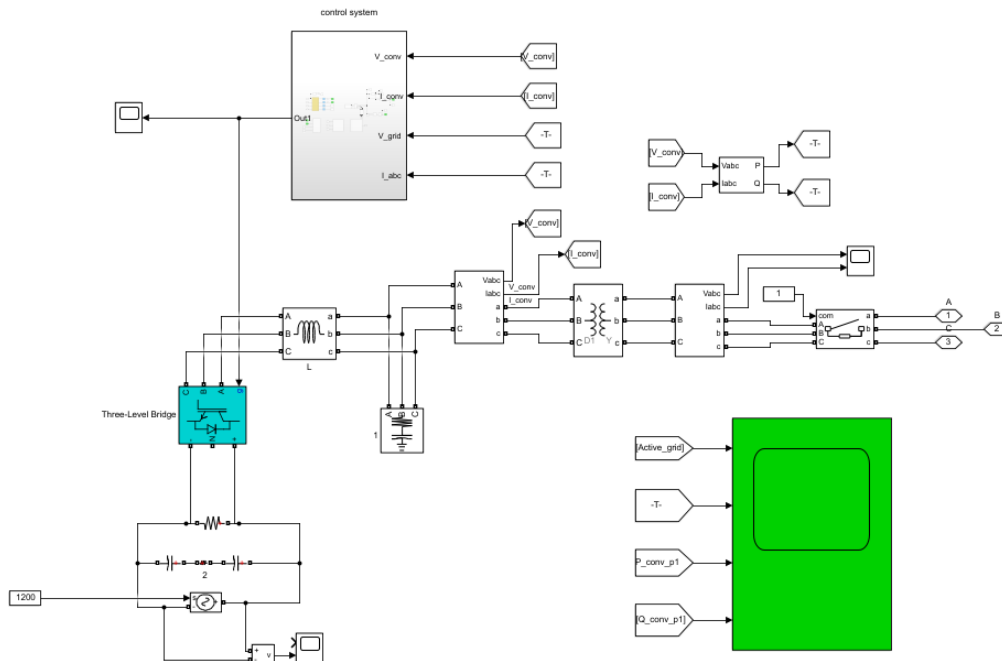
Figure 81: Screen shot of Wind turbine

B.3 Control System

B.3.1 Control system overview
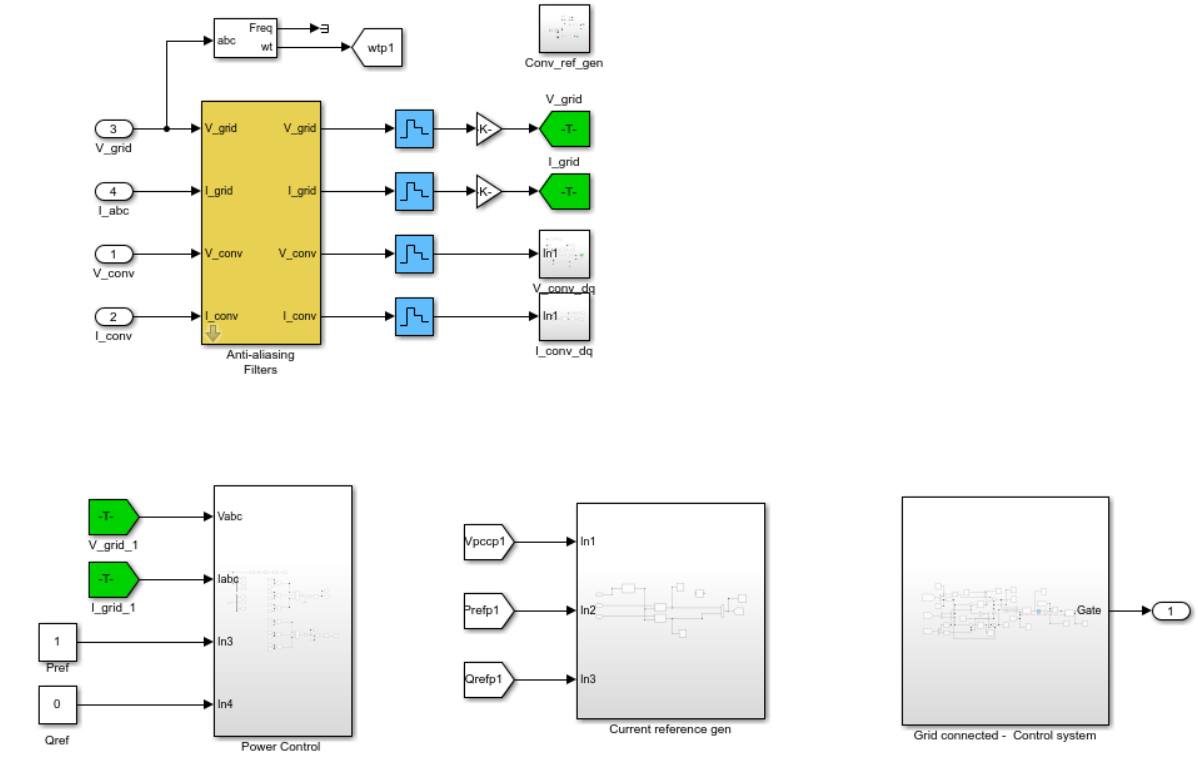
Figure 82: Control System

B.3.2 Reference current generator
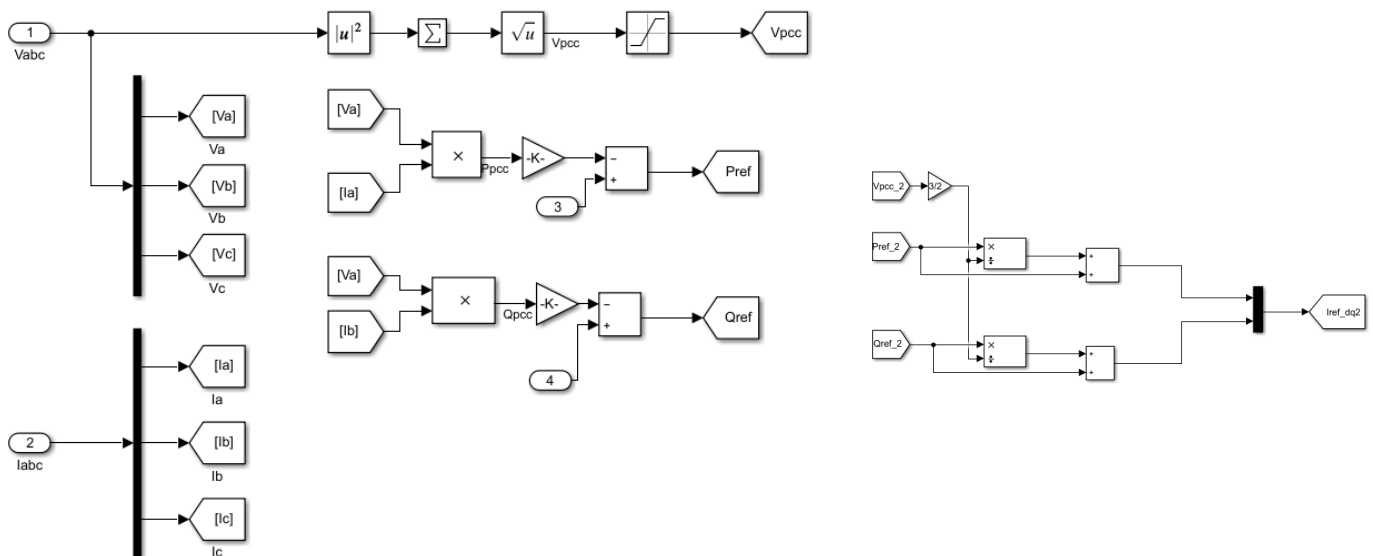
Figure 83: Reference current generator

B.3.3 Current Controller
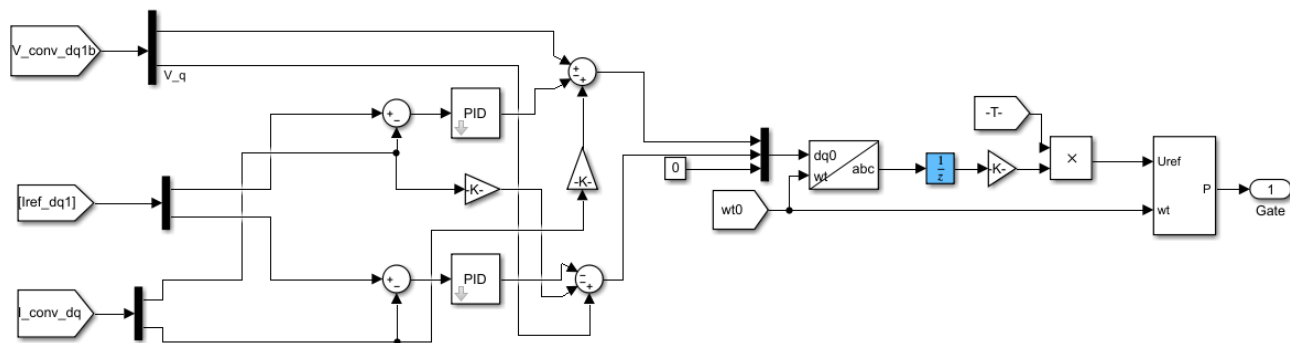
Figure 84: Current Controller

B.4   MATLAB Code

```
%frequency constants
fn = 50; %grid frequency
fs = 1.75e3; %switching frequency
wn = 2*pi*fn;

    % PU variables
Sbase = 5e6; %Sn
Vbase = 1200; %V_LL_rms
```
$$Zbase = Vbase^2/Sbase; \%Zn$$
$$Lbase = Zbase/wn; \%Ln$$
$$Cbase = 1/(wn * Zbase); \%Cn$$
$$Ibase = Sbase/(sqrt(3) * Vbase); \%In$$

```
    % Variables in the rest of the system
Vgrid = 4.16e3; %Offshore grid voltage at PCC
Igrid = Sbase/(1.732*Vgrid);
Vdc=1.2e3; %DC voltage at converter side

    %LCL Filter :
L1=4e-4;
Rc=20.93025;
Cf=3.293e-3;
L2=0.075*Lbase;
L=L1; %For controlsystem

    % Variables in Control System:
Pref = 1;
Qref = 0;
Tsum=1/(2*fs ) ;

    %PI values found using sisotool and LCLBodeplot.m Ziegler Nichols
Ki=57.685; Kp=0.04684;
%PI values for the PLL, taken from Converters.m
wpll=10; %frequency pll crossover
KpPLL=2*wpll;
KiPLL=wpll^2;
```
$$fres = 1/(2 * pi) * sqrt((L1 + L2)/(L1 * L2 * Cf));$$

```
    %Time constants for power and current control
```
$$\text{Ts}_{Power} = 5e - 6;$$
$$Ts_{Control} = 1e - 4;$$

References

1. "Iea, "electricity generation mix, 2018", iea, paris," 2019. [Online]. Available: https://www.iea.org/data-and-statistics/charts/electricity-generation-mix-2018(lastvisitedon05/01/2020)

2. N. G. M. Thao, K. Uchida, K. Kofuji, T. Jintsugawa, and C. Nakazawa, "A comprehensive analysis study about harmonic resonances in megawatt grid-connected wind farms," in *2014 International Conference on Renewable Energy Research and Application (ICRERA)*. IEEE, 2014, pp. 387–394.

3. K. Radhakrishnan, "Passive filter design and optimisation for harmonic mitigation in wind power plants," Master's thesis, NTNU, 2016.

4. K. Temma, F. Ishiguro, N. Toki, I. Iyoda, and J. J. Paserba, "Clarification and measurements of high frequency harmonic resonance by a voltage sourced converter," *IEEE transactions on power delivery*, vol. 20, no. 1, pp. 450–457, 2005.

5. R. Zheng, M. H. Bollen, and J. Zhong, "Harmonic resonances due to a grid-connected wind farm," in *Proceedings of 14th International Conference on Harmonics and Quality of Power-ICHQP 2010*. IEEE, 2010, pp. 1–7.

6. ""the european wind energy association: Ewea"," 2020. [Online]. Available: https://www.ewea.org/fileadmin/files/library/publications/scenarios/EWEA-Wind-energy-scenarios-2020.pdf(lastvisitedon04/01/2020)

7. N. Eghtedarpour, M. Karimi, and M. Tavakoli, "Harmonic resonance in power systems-a documented case," in *2014 16th International Conference on Harmonics and Quality of Power (ICHQP)*. IEEE, 2014, pp. 857–861.

8. W. Xu, Z. Huang, Y. Cui, and H. Wang, "Harmonic resonance mode analysis," *IEEE Transactions on Power Delivery*, vol. 20, no. 2, pp. 1182–1190, 2005.

9. C. Yang, K. Liu, and D. Wang, "Harmonic resonance circuit's modeling and simulation," in *2009 Asia-Pacific Power and Energy Engineering Conference*, 2009, pp. 1–5.

10. C. Yang, K. Liu, and D. Wang, "Harmonic resonance circuit's modeling and simulation," in *2009 Asia-Pacific Power and Energy Engineering Conference*. IEEE, 2009, pp. 1–5.

11. M. V. Chavez-Baez, O. Anaya-Lara, and J. McDonald, "Review of harmonics in offshore wind farms," *UPEC*, 2013. [Online]. Available: https://ieeexplore.ieee.org/document/6715010

12. G. Lemieux, "Power system harmonic resonance-a documented case," *IEEE Transactions on Industry Applications*, vol. 26, no. 3, pp. 483–488, 1990.

13. N. Kularatna, A. S. Ross, J. Fernando, and S. James, *Design of Transient Protection Systems: Including Supercapacitor Based Design Approaches for Surge Protectors*. Elsevier, 2018.

14. H. J. Nussbaumer, "The fast fourier transform," in *Fast Fourier Transform and Convolution Algorithms*. Springer, 1981, pp. 80–111.

15. Z. Li, H. Hu, L. Tang, Y. Wang, T. Zang, and Z. He, "Quantitative severity assessment and sensitivity analysis under uncertainty for harmonic resonance amplification in power systems," *IEEE Transactions on Power Delivery*, 2019.

16. J. Das, *Power system harmonics and passive filter designs*. John Wiley & Sons, 2015.

17. H. Hu, Y. Shao, L. Tang, J. Ma, Z. He, and S. Gao, "Overview of harmonic and resonance in railway electrification systems," *IEEE Transactions on Industry Applications*, vol. 54, no. 5, pp. 5227–5245, 2018.

18. J. Balcells and D. Gonzalez, "Harmonics due to resonance in a wind power plant," in *8th International Conference on Harmonics and Quality of Power. Proceedings (Cat. No. 98EX227)*, vol. 2. IEEE, 1998, pp. 896–899.

19. G. L. Calzo, A. Lidozzi, L. Solero, and F. Crescimbini, "Lc filter design for on-grid and off-grid distributed generating units," *IEEE transactions on industry applications*, vol. 51, no. 2, pp. 1639–1650, 2014.

20. L. SARIBULUT, A. TEKE, M. E. Meral, and M. Tumay, "Active power filter: review of converter topologies and control strategies," *Gazi university journal of science*, vol. 24, no. 2, pp. 283–289, 2011.

21. H. Brantsæter, Ł. Kocewiak, A. R. Årdal, and E. Tedeschi, "Passive filter design and offshore wind turbine modelling for system level harmonic studies," *Energy Procedia*, vol. 80, pp. 401–410, 2015.

22. M. B. Said-Romdhane, M. W. Naouar, I. S. Belkhodja, and E. Monmasson, "Simple and systematic lcl filter design for three-phase grid-connected power converters," *Mathematics and Computers in Simulation*, vol. 130, pp. 181–193, 2016.

23. H. Yin, M. Sahni, N. Karnik, and H. K. Nia, "Root cause analysis for harmonic resonance tripping in wind power plants: An ercot case study," in *2017 IEEE Power & Energy Society General Meeting.* IEEE, 2017, pp. 1–5.

24. B. Badrzadeh and M. Gupta, "Power system harmonic analysis in wind power plants—part ii: Practical experiences and mitigation methods," in *2012 IEEE Industry Applications Society Annual Meeting.* IEEE, 2012, pp. 1–8.

25. B. Badrzadeh, M. Gupta, N. Singh, A. Petersson, L. Max, and M. Høgdahl, "Power system harmonic analysis in wind power plants—part i: Study methodology and techniques," in *2012 IEEE Industry Applications Society Annual Meeting.* IEEE, 2012, pp. 1–11.

26. L. H. Kocewiak, J. Hjerrild, and C. L. Bak, "Harmonic analysis of offshore wind farms with full converter wind turbines," in *Proc. 7th International Workshop on Large Scale Integration of Wind Power and on Transmission Networks for Offshore Wind Farms*, 2009, pp. 539–544.

27. R. LANGELLA, A. TESTA, and E. Alii, *IEEE recommended practice and requirements for harmonic control in electric power systems.* IEEE, 2014.

28. M. Khater, "Electric power generators for wind turbines," 09 2005.

29. N. Goudarzi and W. D. Zhu, "A review on the development of wind turbine generators across the world," jun 2013. [Online]. Available: https://doi.org/10.1007/s40435-103-0016-y

30. H. Polinder, D.-J. Bang, H. Li, Z. Chen, M. Mueller, and A. McDonald, "Concept report on generator topologies, mechanical and electromagnetic optimization," *Project UpWind*, 2007.

31. J. Soens, "Impact of wind energy in a future power grid," *Leuven, Belgica, Katholieke Universiteit Leuven*, vol. 63, 2005.

32. V. Yaramasu, B. Wu, P. Sen, S. Kouro, and M. Narimani, "High-power wind energy conversion systems: State-of-the-art and emerging technologies," *Proceedings of the IEEE*, vol. 103, pp. 740 – 788, 05 2015.

33. "Wind farm transformer design considerations," Aug 2019. [Online]. Available: https://www.power-eng.com/2011/11/01/wind-farm-transformer-design-considerations/#gref

34. G. Jose and R. Chacko, "A review on wind turbine transformers," in *2014 Annual International Conference on Emerging Research Areas: Magnetics, Machines and Drives (AICERA/iCMMD).* IEEE, 2014, pp. 1–7.

35. D. Schwanz, A. Bagheri, M. Bollen, and A. Larsson, "Active harmonic filters: Control techniques review," in *2016 17th International Conference on Harmonics and Quality of power (ICHQP).* IEEE, 2016, pp. 36–41.

36. Ł. H. Kocewiak, B. L. Ø. Kramer, O. Holmstrøm, K. H. Jensen, and L. Shuai, "Resonance damping in array cable systems by wind turbine active filtering in large offshore wind power plants," *IET Renewable Power Generation*, vol. 11, no. 7, pp. 1069–1077, 2017.

37. "'ideal voltage source - an overview'," 2014. [Online]. Available: https://www.sciencedirect.com/topics/engineering/ideal-voltage-source(lastvisitedon21/04/2020)

38. R. Teodorescu, M. Liserre, and P. Rodriguez, *Grid converters for photovoltaic and wind power systems.* John Wiley & Sons, 2011, vol. 29.

39. D. T. Feeders, "Ieee pes distribution system analysis subcommittee's, distribution test feeder working group," *ed*, 2013.

40. ——, "Ieee pes distribution system analysis subcommittee," *OnlineAvailable: http://www. ewh. ieee. org/soc/pes/dsaco m/testfeeders/index. html*, 2011.

41. A. M. Stanisavljević, V. A. Katić, B. P. Dumnić, and B. P. Popadić, "A brief overview of the distribution test grids with a distributed generation inclusion case study," *Serbian Journal of Electrical Engineering*, vol. 15, no. 1, pp. 115–129, 2018.

42. G. Leci and F. Cornelius, "Increasing grid capacity to connect renewable energies," 2016.

43. L. H. Kocewiak, *Harmonics in large offshore wind farms*. Department of Energy Technology, Aalborg University, 2012.

44. L. BeloquiLarumbe, Z. Qin, and P. Bauer, "Introduction to the analysis of harmonics and resonances in large offshore wind power plants," in *2018 IEEE 18th International Power Electronics and Motion Control Conference (PEMC)*. IEEE, 2018, pp. 393–400.

45. K. Cheepati and T. Prasad, "Importance of passive harmonic filters over active harmonic filters in power quality improvement under constant loading conditions," *IOSR J. Electr. Electron. Eng*, pp. 21–27, 2016.

46. L. Bianco, I. V. Djalalova, J. M. Wilczak, J. Cline, S. Calvert, E. Konopleva-Akish, C. Finley, and J. Freedman, "A wind energy ramp tool and metric for measuring the skill of numerical weather prediction models," *Weather and Forecasting*, vol. 31, no. 4, pp. 1137–1156, 2016.

47. K. T. Bradford, R. Carpenter, and B. Shaw, "Forecasting southern plains wind ramp events using the wrf model at 3-km," in *AMS Student Conference*, 2010.

48. ""large-scale wind energy slows down winds and reduces turbine efficiencies"," 2016. [Online]. Available: https://phys.org/news/2016-11-large-scale-energy-turbine-efficiencies.html(lastvisitedon29/07/2020)

49. A. Shukla, A. Das, and S. Anand, "Method to reduce harmonic voltage distortion and improve harmonic current sharing in an islanded ac microgrid," in *2019 IEEE International Conference on Industrial Technology (ICIT)*, 2019, pp. 498–503.

50. Yusran and A. Ikhsan, "Simulation of filter and load influence on single phase inverter against voltage and current harmonic," in *2019 2nd International Conference on High Voltage Engineering and Power Systems (ICHVEPS)*, 2019, pp. 1–4.

51. M. Costea, T. Leonida, and A. R. Andor, "Damping of harmonics by upstream propagation through the power grid," in *2019 International Conference on ENERGY and ENVIRONMENT (CIEM)*, 2019, pp. 209–213.

52. L. G. Mahiwal and J. G. Jamnani, "Analysis and mitigation of harmonics for standard ieee 13 bus test system using etap," in *2019 International Conference on Computing, Power and Communication Technologies (GUCON)*. IEEE, 2019, pp. 546–550.

53. M. Mitra, S. Chattopadhyay, and S. Sengupta, *Electric Power Quality (Power Systems)*. Springer Netherlands, 2011.

54. "Pes test feeder - ieee test feeders data," 1991. [Online]. Available: https://site.ieee.org/pes-testfeeders/resources/(lastvisitedon14/06/2020)